CFD simulation of flow through packed beds using the finite volume technique

Submitted by Matthew John Baker to the University of Exeter as a thesis for the degree of Doctor of Philosophy in Engineering in May 2011

I certify that all material in this thesis which is not my own work has been identified and that no material has previously been submitted and approved for the award of a degree by this or any other University.

Acknowledgements

And I would like to acknowledge my supervisor, Dr Gavin Tabor for his continuous help and understanding.

Abstract

When a disordered packed bed, or any heterogeneous media is studied using computational fluid dynamics, the tortuous task of generating a domain and creating a workable mesh presents a challenging issue to Engineers and Scientists. In this Thesis these challenges are addressed in the form of three studies in which both traditional and novel techniques are used to generate packed beds of spheres and cylinders for analysis using computational fluid dynamics, more specifically, the finite volume method. The first study uses a Monte-Carlo method to generate random particle locations for use with a traditional CAD-based meshing approach. Computational studies are performed and compared in detail with experimental equivalent beds. In the second study, where there is a need for actual, physical beds to be studied, magnetic-resonance-imaging is used coupled with a novel approach known as image based meshing. In parallel experimental studies are performed on the experimental bed and compared with computational data. In the third study, to overcome fidelity issues with the previous approaches, a physical packed bed is manufactured which is 100% geometrically faithful to its computational counterpart to provide a direct comparison. All three computational studies have shown promising results in comparison with the experimental data described in this Thesis, with the data of Reichelt (1972) and the semi-empirical correlation of Eisfeld & Schnitzlein (2001). All experiments and computational models were carried out by the author unless otherwise stated.

Contents

List of Figures

Publications

Baker, M. J., Young, P. G. Y., Tabor G. R. (2010) Image based meshing of packed beds of cylinders at low aspect ratios using 3d MRI coupled with computational fluid dynamics. Computers and Chemical Engineering. *doi* : 10.1016 j.compchemeng.2011.03.017

Baker, M. J., Tabor, G.R (2010) Computational analysis of transitional airflow through packed columns of spheres. Computers and Chemical Engineering vol 34. pp 878 - 885.

Hu, Z., Notarberardino, B., Baker, M., Tabor, G., Hao, L., Turner, I and Yang, L. (2009) On Modeling Bio-Scaffolds: Structural and Fluid Transport Characterization Based on 3-D Imaging Data.Tsinghua Science and Technology Vol 14. pp 20-23

Cox J, Abel R, Xuan VB, Cotton R, Young P, Baker M, Tabor G, Nickels T, Fluid flow in and around the olfactory organ of a hammerhead shark, Annual Meeting of the Society-for-Experimental-Biology, Glasgow, SCOTLAND, 28th Jun - 1st Jul 2009. COMPARATIVE BIOCHEMISTRY AND PHYSIOLOGY A-MOLECULAR INTEGRATIVE PHYSIOLOGY, vol. 153A, no. 2, 2009, S68-S68

Cox J, Tabor G, Baker M, Young P, Cotton R, Xuan VB, Holmes W, Three-dimensional structure and hydrodynamics of the nasal passageway of a hagfish, Annual Meeting of the Society-for-Experimental-Biology, Glasgow, SCOTLAND, 28th Jun - 1st Jul 2009. COMPARATIVE BIOCHEMISTRY AND PHYSIOLOGY A-MOLECULAR INTEGRATIVE PHYSIOLOGY, vol. 153A, no. 2, 2009, S125-S125

Nomeneclature

Sybmols

a_p	Specific particle surface area, S_p/v_p (m^{-1})
A	Cross sectional area of tube (m^2)
A_{ratio}	Aspect ratio $(A_{ratio} = D/d_p)$
A_w	Ergun semi-empirical coefficient (Eisfeld and Schnitzlein, 2001)
B_w	Ergun semi-empirical (Eisfeld and Schnitzlein, 2001)
d_p	Particle diameter (m)
D	Bed confining tube diameter (m)
E	Energy (J)
f	Fanning friction factor
F	Force (N)
g	Gravity $(9.81\ m/s/s)$
h	Height (m)
h_L	Head loss (m)
h_r	Distance moved (m)
H_{ratio}	Depth ratio (L/d_p)
k	Turbulent kinetic energy (J)
k_p	Permeability (m^2)
k_1	Coefficient (Eisfeld and Schnitzlein, 2001)
k_2	Coefficient (Eisfeld and Schnitzlein, 2001)
K_f	Kinetic factor
L	Packed bed length (m)
m	Mass flow rate (kg/s)

p	Probability
ΔP	Pressure drop (Pa)
Q	Volumetric flow rate (m^3/s)
r	Pipe radius (m)
R	Universal gas constant (8.314 $J/molK$)
R'	Gas constant for air (287 J/KgK)
Re	Pipe Reynolds number ($Re = \rho UC/\mu$)
Re_{dp}	Particle Reynolds number ($Re_{dp} = \rho U d_p/\mu$)
Re_D	Pipe diameter Reynolds number ($Re_D = \rho UD/\mu(1-\varepsilon)$)
Re_p	Packed bed Reynolds number ($Re_p = \rho U d_p/\mu(1-\varepsilon)$
$\Re$	Reynolds stresses
S	Source term
S_p	Particle surface area (m^2)
t	Time (s)
T	Temperature K)
u	Velocity (m/s)
U	Superficial Velocity (m/s)
U_i	Interstitial velocity/Pore velocity ($U_i = U/\varepsilon$)
v_p	Volume of particle (m^3)
V	Volume of confining container (m^3)
V_v	Volume of voids (m^3)
y	Distance of cell node from wall (m)
$y+$	Dimensionless distance of cell node from wall
α	Linear 'laminar' coefficient of packed bed and fluid properties

β	Non-linear 'turbulent' coefficient of packed bed and fluid properties
Γ	Turbulent diffusity
ℓ	Turbulent length scale (m)
ε_t	Turbulent kinetic energy dissapation
ε	Porosity (V_v/V)
ρ	Fluid density (kg/m^3)
μ	Fluid dynamic viscosity (Pa/s)
ν	Fluid kinematic viscosity (m^2/s)
ϕ	Dimensionless pressure drop $(\phi = \Delta P d_p/L\rho U^2)$
ϕ_e	Ensemble
σ	Route mean square (RMS)
τ	Tortuosity (L_0/L)
τ_0	Shear stress (Pa)
θ	Angle (rad)
ω	Turbulent frequency (Hz)

Chapter 1

Introduction

It is not surprising that man has been observing the motion of fluids for centuries. The Italian polymath Leonardo da Vinci drew some of the earliest sketches depicting the chaotic motion of fluids in his quest for a better scientific understanding. In the nineteenth-century, the physicist Osborne Reynolds conducted some of the first experiments through die injection, in which he observed and quantified the modes of fluid flow. Today, in the digital age, computational fluid dynamics (CFD) is a popular approach used to analyse the complex behaviour of a fluid. A computer, or more commonly computers are used to solve a large set of partial differential equations to describe the motion of a fluid. CFD's popularity has stemmed from the relatively low set-up cost and man-hours compared to a full empirical study, coupled with the generally accepted accuracy of CFD. In addition, the amount of data which can be extracted from computational methods is far greater than its empirical counterpart without considerable on-cost. In 1991 D. R. Chapman postulated that CFD was en-route to succeeding empirical methods and that

> "wind tunnels were destined to become cabinets for computers"

This postulation is plausible for many simple fluid flow problems, but for complex stochastic turbulent flows there is still no realistic model that provides a sufficient level of accuracy. What is more, creating a working domain for complex geometries with intricate curved surfaces can be challenging, if not near impossible for some cases. The focus of this work is to study methods of generating packed bed

models for analysis using computational fluid dynamics. A packed bed can be defined as "A fixed layer of small particles or objects arranged in a vessel to promote intimate contact between gases, vapors, liquids, solids, or various combinations thereof; used in catalysis, ion exchange, sand filtration, distillation, absorption, and mixing" (McGraw-Hill, 2003). The focus of this work is to analyse three different techniques, with particular focus on the drop in pressure caused by the media when a fluid percolates through the media. In addition, this work aims to study meshing techniques and associated fidelity issues with the generation of computational models in comparison to experimental beds. Ultimately this work leads to new correlations for pressure drop and porosity generated from the large quantity of empirical and computational data generated in this study.

The first method presents the case study of three disordered beds of spheres generated using a traditional CAD (computer-aided-design) based geometry defining approach. The beds are random unstructured and due to this, a Monte-Carlo approach (repeat random-sampling) is used to provide a coordinate location for each sphere comprising the bed. A computational domain is created using the coordinates of each particle in conjunction with a tertiary CAD package, AutoCAD. The computational model is then imported into the commercial finite volume meshing package, Gambit. Issues regarding meshing robustness are encountered using this technique in regard to a high level of cell skewness in attempting to represent particle contact points. Despite localised skewness issues a good computational data set was achieved. To validate the computational results, a comparable physical model is created for experimental investigation in which pressure drop per unit length is monitored. A physical representation cannot be accurately recreated due to the beds' stochastic disordered nature (each random pack will be different). In this case, physically equivalent beds are created and compared with computational data. An equivalent bed can be described as having the same dimensional characteristics, such as bed length, particle diameter and void volume, but may display a considerably different internal structure. Both computational and empirical measurements are compared with the correlation of Eisfeld & Schnitzlein (2001) and have shown promising results. Moreover, this technique provides a good engineering approximation in regard to modelling the pressure drop through random disordered beds. However, this technique

has proved limited in regard to successfully producing a workable computational model due to mesh construction issues associated with the interface of highly curved surfaces.

CAD based approaches coupled with an equivalent experimental bed have yielded positive results in regard to predicting the expected pressure drop caused by the media. However, in some cases it is desirable to compare the exact internal flow paths. This requires an identical experimental bed structure as the computational domain, something not provided in the CAD based-equivalent bed approach. To achieve this, non-invasive methods, such as magnetic resonance imaging (MRI) and computed-tomography, used in the field of diagnostic medicine have become a popular approach used by some researchers (Manz *et al.*, 1999; Sharma *et al.*, 2001; Sullivan *et al.*, 2005; Zhang *et al.*, 2006) to determine a packed bed's internal structure. MRI or CT are used to determine the internal structure from a grey-scale image, this is then segmented using a surface defining algorithm, then a traditional CAD based approach is used to create a workable mesh. Although possible, this method is tortuous and time consuming and often requires considerable user intervention and simplification of the flow geometry. To ameliorate this affect, the work described here uses MRI coupled with a technique known as image based meshing to recreate the internal bed structure and create a suitable mesh for analysis. The technique is applied to MRI scans of disordered packs of cylinders and spheres and the results have been shown to be promising in regard to predicting the expected pressure drop caused by the media. However, problems have arisen concerning geometric fidelity issues such as particle necking as a result of the scan resolution.

Based on the knowledge gained and the restrictions concerning fidelity, this Thesis moves onto replicating an exact geometry for experimental and computational analysis, where both experimental and computational beds are 100% geometrically faithful and can be realistically compared. The method described here utilises MacroPac and the Monte-Carlo algorithm to generate random stochastic beds of spheres, bi-distributed and weighted 50:50 by volume. A 3d model is created in a stereolithography (STL) file format from a simple C program suitable for import into the image-based surface defining and mesh creation software ScanCAD/ScanIP/ScanFE (Simpleware, Exeter UK). In parallel a computational

model is created from the mesh using rapid-prototyping RP, more specifically 3d printing (3dP), in which the computational model is geometrically faithful to the experimental. This method ameliorates problems associated with comparing computational results to equivalent beds and the associated problems with scanning physical beds and replicating them using a surface defining algorithm. This method produced the most promising results of the three methods in respect to the closeness of experimental and CFD and the correlation proposed by Eisfeld & Schnitzlein (2001).

The work as a whole has shown how three techniques can be applied to analyse the flow structure and pressure drop through packed beds. The first method has been shown to be relatively simple and efficient in respect to time, but the method is burdened by the problem of highly skewed elements jeopardising localised flow patterns. However it still provides a realistic engineering approximation for pressure drop per unit length. The method is also limited in comparing equivalent beds with the same dimensional characteristics, but different flow paths. The second method has been shown to, again, produce a reasonable engineering approximation in regard to pressure drop, but is severely limited by geometric fidelity issues concerning the necking of particles caused by inefficiencies in the scan resolution. In addition, the method is costly and time consuming and not a realistic approach for industry based applications. The final method, as far as the Author is aware, is the first application of rapid prototyping applied to create a geometrically faithful bed for direct comparison with CFD. The method is relatively costly, but due to its novel technique could used to investigate other phenomena which is not possible with traditional methods and technique stands on its own merits. In all three cases the results have yielded promising results and provide the reader with an interesting insight into the creation and analysis of packed beds using the three techniques.

Chapter 2

Literature Review

> "An ordinary man can surround himself with two thousand books and thenceforward have at least one place in the world in which it is possible to be happy"
>
> Augustine Birrell

2.1 Introduction

In this Thesis we are interested in the phenomena of gaseous fluid flow through packed beds and how the bed geometry affects the flow. In addition, we are interested in the techniques and methodologies by which this can be achieved with accuracy and precision and the possibility of a viable alternative to empirical techniques. In which case it is necessary to understand the previous literature concerning the study of packed beds. The literature concerning the flow through packed beds is vast and would constitute a whole thesis if discussed in its entirety. To make the review logical and coherent, the packed bed and its geometric properties are introduced followed by the physics of fluid flux through such media. A detailed review of the various correlations proposed to approximate pressure drop through a packed bed are then discussed, followed by literature concerning computational methods applied to packed beds.

2.2 Packed bed geometric properties

Packed beds have been used extensively in engineering processes such as filtration, heat and mass storage, industrial stripping and catalysis. A packed bed can be defined as a number of particles dumped into a container. The particles form a matrix like structure which contains voids or pores in which a fluid is free to percolate. A packed column is a specific case where the packed bed is confined inside a cylindrical tube. The packed column can either be fixed or fluidized. As the name suggests the particles in a fixed bed are static and fixed in position and unable to move. A fluidized bed is the phenomena when the particles are in motion, excited by the stream of fluid thus able to follow the random non-deterministic movement of the fluid. In this work we are only concerned with the study of fixed beds, their geometric properties and their influence on the flow.

2.2.1 Particle Equivalent Diameter

A packed bed consists of particulate matter which is influential in determining the properties of the bed in regard to the flow properties. The bed particles can be uniform in size and shape, such as mono-sized spheres, or can be irregular such as coal or gravel. In order to study a packed bed mathematically, the bed has to be described by a number of parameters. In the case of a bed particles, the parameter of interest is the particle diameter. When the bed particles are not spherical they are represented as an equivalent sphere of the same volume (Sissom & Pitts, 1972) which can be characterised by the equivalent diameter or by the sphericity (a particles deviation from a perfect sphere), ψ. When the particles are spherical the equivalent diameter simply reduces to the particle diameter. To get a mean representation of bed equivalent diameter, it is coupled with the bed surface area per unit volume giving the relationship

$$\frac{a_p}{(1-\varepsilon)} = \frac{\pi d_p^2}{\pi/6 d_p^3}$$

which re-arranging for d_p gives

$$d_p = \frac{6(1-\varepsilon)}{a_p}$$

where a_p is the specific particle surface area, S_p/v_p (m^{-1}) where S_p is the particle surface area and v_p is the particle volume. ε is the porosity, given as the volume of voids or pores (V_v), divided by the total volume, V $(\varepsilon = V_v/V)$. However the particle equivalent diameter does not completely eliminate the effect of the particle shape (Aris, 1957). For example, a particle may have the same equivalent diameter, but may be geometrically completely different, changing the flow pathways through the bed considerably. In the case of beds with varying diameter particles a mean average can be introduced. However, this does not give a realistic representation of the beds properties as the assumption is the bed packing will behave as if the bed particles are mono-sized. In reality, bed particles of varying sizes will pack more closely than mono-sized particles.

In this work we investigate the packing and flow phenomena of spheres and cylinders. A sphere can be described as an infinitely sided volume, or as a single continuous surface which is perfectly round. In reality a perfectly round sphere does not exist and the closest to being 'perfectly round' is Einsteins fused quartz gyroscope with a sphericity of less than 40 subatomic layers, which is considered by some as being the world's roundest object. The fused quartz gyroscope was manufactured to measure the effect of frame dragging and geodetic effect of space time form Einstein's 1916 general theory of relativity.

Cylinders are described by their length to width ration, l_c/w. A short stubby sphere would have a low length to width ratio, a long cylinder, would have a large length to width ratio.

2.2.2 Packing Regimes

In addition to the particle geometry, the arrangement in which they are ordered within the bed is highly influential in regard to the ease in which a fluid can pass through the media. In the case of random irregular size/shape particles (coal, gravel etc), the packing regime will always be random and unstructured

with no known mathematical description to describe the particles orientation and position. Beds can be loosely packed or densely packed, based on the number of particles packed into a known volume, and this is sometimes referred to as packing efficiency. In addition, the packing can be structured or random unstructured. If a packing regime is considered to be structured, the coordinates of each particle have a full mathematical description and constant respective porosities and packing densities.

The astronomer Johannes Kepler (1611) studied the packing of mono sized spheres to determine which was the most efficient way of packing in regard to packing densities and efficiency. He questioned, should the spheres be packed directly on top of one another, known as simple cubic packing, or should the sphere layers be staggered so the spheres on the second layer sit within the hollows formed by the first layer, known as face centred cubic packing. Kepler conjectured that face centre cubic packing was the densest possible packing scenario, but could not prove this mathematically.

For a simple cubic arrangement the packing density is $\rho = \pi/6$, approximately 0.52. For a face centred cubic arrangement the packing density is $\rho = \pi/3\sqrt{2}$ approximately 0.74. In addition, if the central coordinate of the first sphere in a pack is $0, 0$, then the next spheres centroid in the series will be one diameter (d_p) width away in the x, y and z directions. The relative ease in which simple

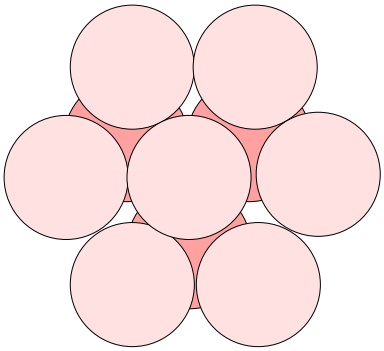

Figure 2.1: Close hexagonal packing of spheres

mathematical relations can be applied to describe the packing regime makes the

structured packing regimes appealing to many researchers (Dalman *et al.*, 1986; Delele *et al.*, 2008; Lloyd & Boehm, 1994; Logtenberg *et al.*, 1999).

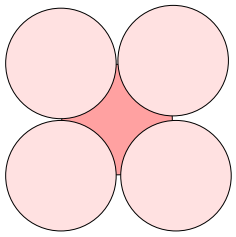

Figure 2.2: Face centred cubic packing of spheres

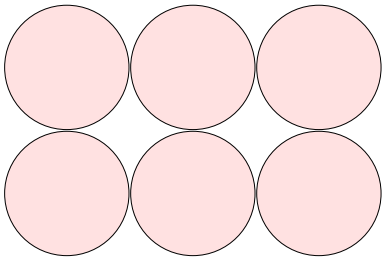

Figure 2.3: Simple cubic packing of spheres

When a packing regime is considered unstructured, the location of each particle is random and stochastic and there is no deterministic mathematical algorithm to describe the particle location. A unstructured pack can be created physically by simply dumping a number of particles into a container. However, due to the stochastic nature of unstructured packing, it is virtually impossible that an unstructured pack with the same disordered structure can be replicated. In the case of a few particles (< 5) there is a chance statistically that the same bed structure may be replicated. In the case of several thousand particles the chance of replicating a packed bed by dumping particles is near impossible. This phenomena has posed a problem to researchers when trying to separate different phenomena from the packing regime as the same bed structure cannot be replicated. This issue further poses a problem in respect to reinforcing CFD data with empiricism. Unstructured beds can be generated computationally, but there currently exist no

method in which they can be reproduced with geometric fidelity. The other option available to researchers is to create a random unstructured pack physically and use non-invasive methods, such as MRI or CT to create a computational model.

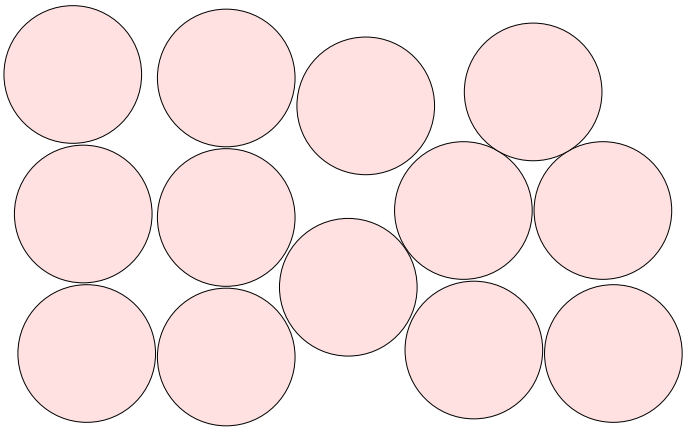

Figure 2.4: Random unstructured spherical pack

2.2.3 Aspect Ratio

In order to compare similar scenarios with varying dimensional values it is often desirable to use a dimensionless property. The primary dimensionless property used to characterise a packed bed is the ratio between the equivalent diameter (d_p) of the particle and the container diameter (D). This is referred to as the aspect ratio given as

$$A_{ratio} = \frac{D}{d_p}$$

Packed beds are categorised as being low or high aspect ratio; a tube of sand would be considered high aspect ratio, a tube snooker balls would be considered low aspect ratio. As we might expect, the velocity profile through the high aspect ratio bed would be fairly uniform across its profile and can be considered as a pseudo-homogeneous network of capillaries with uniform flow rates. The network of flow through a low aspect ratio bed would be highly disordered due to the varying sizes of the voids as a result of the inhomogeneities in the packing

leading to a variation in local porosity. The exact value at which a low aspect ratio

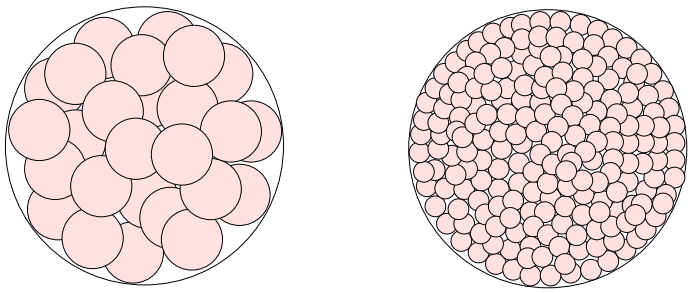

Figure 2.5: Left; Low aspect ratio bed. Right; High aspect ratio bed

bed becomes a high aspect ratio bed or vice versa is not well defined. However, $A_{ratio} = 50$ is often suggested as a reasonable value to distinguish between a low and high aspect ratio bed.

In addition to the aspect ratio, the bed length can be defined as the dimensionless bed depth ratio, which describes the ratio of bed depth to the particle equivalent diameter given as

$$H_{ratio} = \frac{L}{d_p} \tag{2.1}$$

2.2.4 Porosity

A packed bed can be described as a restriction or a partial blockage in a pipe which interacts with the fluid in some way. The ease with which the fluid can pass through the medium is determined by the volume of voids within the bed, V_v and is governed by the area available for the flow to pass. This can be represented in a dimensionless form as porosity (ε) or void fraction given as the volume of voids divided by the total volume.

$$\varepsilon = \frac{V_v}{V} \tag{2.2}$$

Because regular packings have a complete mathematical description their porosity can be represented by a simple geometric relation. For a face centred cubic pack this is given as

$$\varepsilon = 1 - \left(\frac{\pi}{6}\right)$$

and for close hexagonal as

$$\varepsilon = 1 - \left(\frac{\pi}{\sqrt{3}2}\right)$$

The porosity of most concern to packed beds is the bulk average porosity as described. We have discussed the fact that a high aspect ratio bed is random and disordered in structure, and due to this its porosity can vary quite considerably throughout the bed. Conversely, in a high aspect ratio bed there is little variation in porosity throughout the bed.

Due to the porosity's simple volume fraction relation, determining an experimental value for porosity is relatively simple. Water displacement is the traditional method, where the volume of the confining container (V) is measured. Water is added to the container filled with the particulate matter filling the void volume and as a result the volume of water entrained is equal to V_v. However, this method is susceptible to inaccuracies from entrained air and wetting issues associated with porous particles. Other methods are also possible, such as non-invasive methods such as magnetic resonance imaging and X-ray computed tomography (Mantle *et al.*, 2001; Nguyen *et al.*, 2005; Sederman *et al.*, 2001). However, these methods suffer from resolution issues resulting in questionable values of void volume, V_v.

Empirical correlations exist to predict porosity in disordered beds such as those of de Klerk (2003); Dixon (1988); Jeschar (1964) and Zou & Yu (1995). However, these approaches are regressions based on empirical data, rather than mathematical reasoning and can vary quite considerably.

2.2.5 The wall region

When particles such as spheres, are packed into a container, they usually pack together in a random disordered fashion (Fig 2.4). The particles directly adjacent to the confining wall will not pack as efficiently as those in the core of the bed due to the containers flat surface. As a result of this there is an increased porosity next to the wall in comparison to the bed core. This region of increased porosity

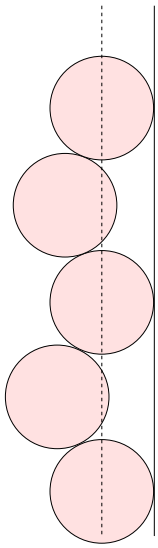

Figure 2.6: The wall region, to the right of the dashed line

is refers to as the wall region, whilst the region not affected by the confining wall is regarded as the core region. In very low aspect ratio beds ($1.2 < A_{ratio} < 3$), such as a cluster of a few spherical particles, the wall region is dominant across the whole bed. In high aspect ratio beds the wall region is still present, but statistically has no measurable effect on the motion of the fluid. In the case of spherical particles uniform in shape and size the wall region can be quantified as $d_p/2$ (Martin, 1978), which holds well in most cases. For other particles such as cylinders, the exact value can vary quite considerably due to the particles orientation and packing density, but a reasonable first assumption of the wall region thickness would to employ the assumption made by Martin (1978).

2.3 The Physics of Flow

The nature of the flow through packed beds is complex and notoriously difficult to study due to the medias opaque, disordered characteristics. In a high aspect ratio bed the flow is disordered but statistically can be considered homogeneous due to the relatively uniform size of the voids. In a low aspect ratio bed the bed structure is considerably more disordered and interconnecting large voids increase velocity channelling. In some cases an individual flow path can be observed known as the pathway of mainstream velocity in which the majority of the fluid flux is being channelled as a result of the inhomogeneities in the packing.

However, a single flow path may not guaranteed and may change transiently and polyfurcate into other regions. Complicating matters further, the wall region is likely to be highly influential. We know that in a low aspect ratio bed, at the wall the porosity is likely to be considerably higher, therefore this becomes the pathway of least resistance and increased channelling can be observed. The effect of the wall region has spurred much debate, especially in regard to the resistance to the flow caused by the medium. In high velocity flow the increased porosity at the wall provides less resistance to the flow therefore the fluid flux is transferred through the bed in an easier fashion (Foumeny *et al.*, 1993; Stanek, 1994). In low velocity flow, the increased surface area results in an increase in the frictional forces exerted on the flow, thus resulting in increased resistance as observed by Mehta & Hawley (1969).

The velocity profile may also attribute to the affect of the wall region. The 1/7 power law turbulent velocity profile associated with high speed flow ($Re < 1500$) allows more fluid flux across the cross sectional area allowing more fluid to be channelled into the wall region (the boundary layer thickness is much less in a turbulent regime) in constrast to the parabolic velocity profile associated with fully developed 'low speed' laminar flow ($Re < 1500$)where the boundary layer thickness is much greater.

The carriage of flow through a porous medium obeys the same relationships as for basic fluid mechanics. The volume of fluid per unit time or fluid flux transported through the bed is described by the volumetric flow rate, Q (m^3/s). This is related to the superficial velocity, U, from simple dimensional reasoning

in the form of

$$U = \frac{Q}{A} \tag{2.3}$$

where A (m^2) is the cross sectional area of the pipe. The superficial velocity is termed 'superficial' as it is the velocity that would be present in the absence of the media. For instance, a flow measuring device placed immediately before the media would measure the superficial velocity.

Another term to used describe the velocity is the interstitial velocity, U_i, which is the average velocity within the pores. This takes into account the bed porosity through the relation

$$U_i = \frac{U}{\varepsilon} \tag{2.4}$$

where ε is the porosity. This forms the average pore velocity, as there is no guarantee of homogeneity within the pores in a disordered bed and it is derived from the global property of average porosity.

2.3.1 Flow Regimes and Turbulence

The flow of a fluid can be characterised by a selection of dimensionless numbers, such as the Froude number, Strouhol number, Prandtl number, but none of which are of more importance to this work than the dimensionless number proposed by Reynolds (1883). The Reynolds number is characterised by the ratio of the inertial and viscous forces and is defined as

$$Re = \frac{\rho U C}{\mu} \tag{2.5}$$

where ρ is the fluid density (kg/m^3), U is the velocity (m/s) (for packed beds the superficial velocity), μ is the dynamic viscosity ($Pa.s$) and C is an appropriate scaling length (Reynolds, 1883). In the case of pipes the scaling length would simply be the diameter, in the case of aerofoils the chord length. In fact, any sensible scaling length can be used providing consistency is followed when matching the Reynolds number for equivalent experiments. Alternatively, we can define the Reynolds number as

$$Re = \frac{U D}{\nu} \tag{2.6}$$

where the density and dynamic viscosity is replaced by a single function known as the kinematic viscosity ν (m^2/s), given as the ratio of the dynamic viscosity and the density, $\nu = \mu/\rho$. Reynolds (1883) conducted a series of experiments in which he injected dye into a clear glass pipe carrying water. Reynolds (1883) observed the motion of the dye and concluded that at low velocities the fluid shears in a laminated fashion and the streak-line remains unbroken (stream-flow). At high velocities the streak-line is broken and disperses and mixes into the fluid in a sinuous fashion. Today, we categorize the modes of flow observed by Reynolds (1883) as being either laminar, transitional or turbulent.

Figure 2.7: Laminar flow represented by streamlines

Laminar flow is the motion of a fluid where fluid layers shear over each other in a orderly parallel (laminated) fashion as shown in figure 2.7. Viscosity effects are dominant and the flow exhibits no instabilities and no naturally induced vortices. In the case of pipe flow, the shear stresses and strains as a result of the fluids interaction with the pipe wall produce a parabolic velocity profile. If the Reynolds number is increased, laminar flow develops into a transitional regime. The lamination has now become unstable and bursts of chaotic behaviour (turbulence) is observed, which is then damped out by viscous effects. If the Reynolds number is further increased the unstable bursts of chaos become more frequent ultimately breaking up the lamination into a full turbulent flow regime.

Turbulent flow is chaotic with random fluctuations in velocity and formation of vortices (Eddies) which are random in space, time (Landahl & Mollo-Christensen, 1986) and of varying frequencies. Thus, the flow is highly rotational, diffusive and dissipative and it is impossible to derive an complete model of the phenomena. The largest vortices are associated with low frequency fluctuations in which the size is governed by the confining geometry. They gain their kinetic energy from viscous stresses and strains from the fluids interaction with its surroundings. The

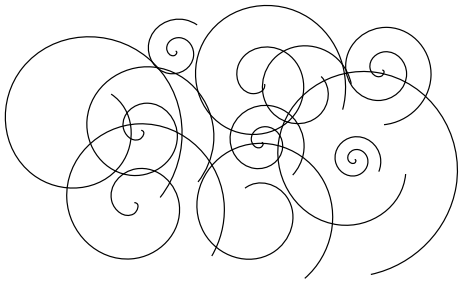

Figure 2.8: Turbulent flow

large vortices break up into smaller vortices in which kinetic energy is dissipated, referred to as the energy cascade (Lien & Leschziner, 1994). The smaller vortices break up further into the smallest possible eddies which are viscosity dependant and governed by the Kolmogorov length scale $(\nu/\varepsilon_t)^{0.25}$ and represent high frequency turbulence, where ν is the kinematic viscosity and $\nu$is the average rate of energy dissipation per unit mass. The transition from small vortices to the smallest possible vortices is where the majority of the kinetic energy is dissipated in the form of heat and less so, sound energy. A poetic description of the turbulent cascade was described by Lewis Fry Richardson's adaptation of the poet and author, Jonathan Swifts "Ad infinitum" (A flea hath a smaller flea) with

> "Great whirls have little whirls, which feed on their velocity. And little whirls have lesser whirls, and so in to viscosity."

We often think of vortices as being helical or spiral. In the free-stream this may often be the case, but the fluids interaction with its surroundings can often distort the shape of the vortex due to shear stresses and strains from the fluid itself or the wall region.

As the viscosity is the main contributor to the damping of vortices in turbulent flow, turbulence is more prevalent in low viscosity flow such as air. Laminar flow is more prevalent in high viscosity flows, such as oil or polymers.

We can use the original equation proposed by Reynolds (1883) to make an engineering approximation to the likely mode of the fluid flow. The low Reynolds Stokes flow regime usually exists when $Re << 1$. The critical Reynolds number where transition occurs from laminar to turbulent is often quoted as $Re_{crit} = 2000$

or more commonly $Re_{crit} = 2300$ (White, 2003) for circular pipe flow based on the pipe diameter as the suitable scaling length. However this approach of one single value for the onset of turbulence in misleading. A more realistic approach is to suggest a range of values where Laminar flow usually exists in a pipe below $Re = 2300$, transitional as $Re = 2300 - 4000$ and a complete turbulent regime has formed by $Re > 4000$ (Cengel & Cimbala, 2006). It must be noted that a common misinterpretation is to use this value for all cases of fluid flow. In fact, this value is only applicable for pipe flow and does not hold for open channels, square ducts where there are other empirically defined critical values. It is impossible to have an exact value for the transition between laminar and turbulent flow due to surface roughness and disturbances in the flow, not accommodated by the Reynolds number. The only conclusive approach to determine if a flow is laminar or turbulent is through flow visualisation, or a more modern semi-empirical, optical technique to give a visual indication of turbulent vortices and unsteady flow effects. But even then, such as in the case of wake regions behind bluff bodies, there can be true stochastic turbulence co-existing with deterministic unsteady behaviour.

Optical methods rely on a direct line of sight, which is not possible in a opaque porous medium. However, optical methods such as laser Doppler anemometry (LDA) and particle image velocimetry have been attempted Calis *et al.* (2001); McGreavy *et al.* (1986); Yevseyev *et al.* (1991). LDA uses a laser to illuminate a seeded flow of (a flow containing small particles) coupled with a high resolution video camera. It uses the Doppler shift to determine the particles velocity.

Similar to LDA, PIV requires a seeded flow, a camera and a laser. The laser illuminates the flow in a series of pulses allowing the particles to be tracked by successive high frequency images taken by the camera. From the movement of the particles the software is able to produce realistic velocity vectors (direction and magnitude), providing there is a sufficient number of particles in the flow and they have a density similar to the fluid. Although the same limitations, such as direct line of sight are applicable to PIV and LDA as traditional visualisation methods, some attempts have been made using these techniques to study packed beds. McGreavy *et al.* (1986) adopted LDA to analyse the internal flow structure through a packed bed. LDA has also been adopted by Calis *et al.* (2001) to

analyse the flow structure in fixed beds of $A_{ratio} = 1.47$ and 2. Yevseyev *et al.* (1991) also use LDA to analyse the internal flow structure in a bed of regular arrangement, and show the formation of vortices in the voids. They describe this as turbulence, however it is difficult to conclude from their results whether they are analysing true stochastic turbulence or deterministic periodic vortex structures and recirculation. Attempts have been made with the use of optics and refractive index matched transparent beds Giese *et al.* (1998); Hassan (2008). This is limited by the temperature dependant refracted indices and can therefore only be used for studies at the near wall region (Gotz *et al.*, 2002).

2.3.2 Packed beds Reynolds Numbers

As with pipe flow, the flow through packed beds can also be loosely characterised by the Reynolds number, but this is complicated further by the existence of several forms of Reynolds number, based on different parameters and length scales and each with unique critical values for the onset of turbulence. In many applications of packed beds the Reynolds number is defined as

$$Re_{dp} = \frac{\rho U d_p}{\mu} \tag{2.7}$$

where the scaling length is simply the particle equivalent diameter, and this is therefore known as the particle Reynolds number. We can see that this equation is solely dependant on the properties of the fluid and the particle diameter and makes no reference to the bed porosity, ε. Experimentation has shown that a bed can be loosely packed or densely packed and this can be represented by a large or small value of porosity respectively. Based on this equation and empiricism a new set of values for critical flow are formed, based on the particle Reynolds number where the flow can be characterised as laminar ($Re_{dp} < 10$), transitional ($10 < Re_{dp} < 300$) or turbulent ($Re_{dp} > 300$) (Ziolkowska & Ziolkowska, 1988). However, these experiments were conducted primarily using dye injection, and although the use of dye injection is a well established and accurate method of determining the onset of turbulence in pipe flow or open channel flow, problems arise when applying the technique to porous media. For a completely laminar,

steady flow a stream of dye will remain to follow the path-line/streamline. For a turbulent flow the streak-line will break up due to the random and chaotic formation of vortices. Due to the geometry of a packed bed, a large pore converging to a small pore will dampen out any large scale vortices formed within the bed, in which case re-lamination may occur. With the use of dye injection once the streak-line has broken up, there is no way it can return to a streak line and therefore any re-lamination will remain undetected and the flow will appear turbulent throughout the bed, or at least post-streak-line separation. Attempts have been made to determine turbulent spectra within the void space of a cubic arrangement using hot-wire anemometers (Tsotas, 2002a) who report no vortex shedding from behind spherical particles. Their experimental technique relies on the use of hot-wire anemometers positioned in the bed voids to determine both the instantaneous velocity and the root-mean-square (RMS) of the velocity fluctuations. However, (Tsotas, 2002a) describe no margins of uncertainty or response time. Hot-wire anemometers rely on Newton's law of cooling to determine the velocity and it is probable that the resolution of the response time is not sufficient to describe the highest frequency turbulent events. Scheidegger (1960) reviewed a considerable amount of research where critical values were quantified and came up with the conclusion that it is impossible to define a single critical value for the onset of turbulence due to discrepancies between the results reported (Ziolkowska & Ziolkowska, 1988). Furthermore, most empirical methods struggle to distinguish between true stochastic turbulence and deterministic unsteady behaviour.

In some cases, even when all the particles in a packed bed are uniform in size and shape, the pore volume may still vary due to the heterogeneous nature of a random packing of spheres. In this case there is a strong possibility that all three states of flow will exist within the internal structure. We already know that the ease in which flow can pass through a porous medium is strongly dependant on porosity, in which case the packed beds Reynolds number is defined as

$$Re_p = \frac{\rho U d_p}{\mu(1-\varepsilon)} \tag{2.8}$$

which is simply the particle Reynolds number modified by the dimensionless packing fraction $(1-\varepsilon)$. This form of Reynolds number is also seen in some literature with the particle diameter (d_p) replaced with the confining pipe diameter, D, given as

$$Re_D = \frac{\rho U D}{\mu(1-\varepsilon)} \tag{2.9}$$

Due to the addition of porosity the packed beds Reynolds number is particularly useful for comparing beds of different porosities. The Reynolds number, due to its dimensionless form can be applied to set the limitations of various correlations. Bear (1972) suggest that Darcy's law is only valid providing the particle Reynold's number is in the region of $1 < Re_{dp} < 10$. A lesser used form is the modified Reynolds number proposed by Eisfeld & Schnitzlein (2001), given as

$$Re' = Re_p(1-\varepsilon) \tag{2.10}$$

which is simply the particle Reynolds number multiplied by the packing fraction. The packing fraction and porosity are both dimensionless entities, in which case their position in the equation is irrelevant, only modification of perceived values is needed for the onset of turbulence.

When applying the Reynolds number to a packed bed, it must be kept in mind that the Reynolds number is a global entity or bed average quantity. When the bed flow patterns and geometric properties are fairly uniform, such as a high aspect ratio bed (e.g a tube full of sand) the average Reynolds number will give a realistic average representation of all the flow. Conversely, for a high aspect ratio bed with a strong disordered geometry and a highly influential wall region, the Reynolds number is likely to vary considerably. The Reynolds number relies on an appropriate scaling length and velocity to ensure dimensional correctness and or the addition of porosity, which in itself is an average quantity. Analysing the bed on a macro-scale we know that the porosity can vary considerably, especially at the near wall region. As a function of porosity the velocity may vary throughout the bed due to flow channelling and the changing paths of mainstream velocity. Due to these effects the bed Reynolds number is likely to vary considerably throughout the media. Based on this assumption, the flow may be laminar in certain areas of the bed but also exhibit true stochastic turbulence in other

locations as well as periodic burst of unsteady behaviour which are damped out by the viscous effects. In the case of a low aspect ratio bed it is unlikely that a packed bed displays full turbulence throughout. Conversely, a very high aspect ratio bed ($A_{ratio} > 500$) is likely to display no turbulence due to the pore size being smaller than the smallest turbulent structures, governed by the Kolmogorov length scale.

2.3.3 Pressure drop

We have discussed the fact that a packed column can be considered as a partial blockage constrained by a pipe. Due to the blockage a back pressure is formed or a pressure drop (ΔP) due to the ease in which the fluid can pass through the medium and is given the SI units Pascals (Pa) or Newtons per metre squared (N/m^2). This is usually measure experimentally using a differential fluid column manometer or pressure transducers located before and after the bed. In liquids it may be appropriate to describe the pressure drop as a head-loss related to the pressure drop by

$$h_L = \frac{\Delta P}{\rho g} \tag{2.11}$$

In some cases a sign convention is used ($+/-$), to distinguish between a drop in pressure and an increase in pressure. The pressure drop can be described as a function of the bed properties and the properties of the fluid as

$$\Delta P = f(\varepsilon, \tau, d_p, D, L, Re) \tag{2.12}$$

Theoretical and empirical correlations have been derived to link these parameters in the form of a pressure drop equation. One of the most influential bed parameters concerning the pressure drop is the bed porosity, ε. Coupled with porosity and bed length is tortuosity, τ. Tortuosity as its name suggest is how indirect the route of a fluid particle from the bed entrance to the bed exit and is given as

$$\tau = \frac{L_0}{L} \tag{2.13}$$

where L is the bed length and L_0 is the route of the fluid particle. However, determining an accurate value of bed tortuosity is nearly impossible due to the opaque nature of a packed bed. A bed can have identical geometric values, such as porosity, aspect ratio and particle diameter but the tortuosity can vary considerably. If we imagine two packed beds, each containing one hundred identical spheres, with the same value of porosity, aspect ratio. Consider two scenarios (figure 2.9); the first scenario the spheres are packed inside the bed in such a way that they are in a simple-cubic formation; in the second scenario they are random and disordered. In the first scenario there is little resistance to the flow as most of the fluid particles and channelled through the voids. In the second scenario the fluid particles are obstructed by the media and there is no obvious route for the particles to travel. The second bed is considered 'more tortuous' than the first.

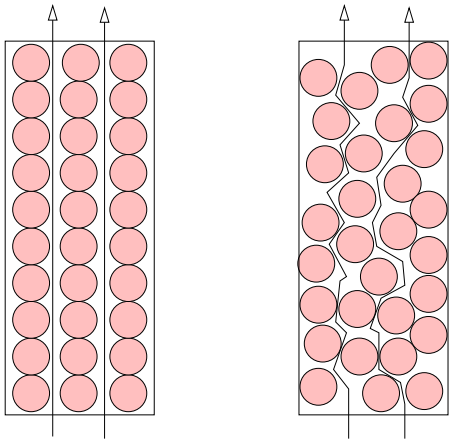

Figure 2.9: Tortuosity. Left; simple cubic arrangement (low tortuosity). Right; a random disordered pack (highly tortuous).

In regard to high aspect ratio beds the bed inhomogeneities, such as the effect of the confining wall have a considerable effect on the pressure drop and are coupled with the effect of local porosity. The effect of the confining wall on the pressure drop has caused much debate. The work of Mehta & Hawley (1969) suggests an increase in pressure drop due to the effect of the additional wall friction in low aspect ratio beds ($7 < A_{ratio} < 91, Re_{d_p} < 10$). This research is

particularly controversial as all other research presents the opposite effect. The work was restricted to a low Reynolds regime ($Re_{dp} < 10$) where it could be argued that the wall friction is dominant and the coefficient of drag is less dependant on particle geometry. More likely this is just a misinterpretation of data (Eisfeld & Schnitzlein, 2001). Stanek (1994) and Foumeny *et al.* (1993) suggest that the homogeneity's as a result of the increased porosity at the container wall reduce the pressure drop due to flow channelling. However, there is still a lack of conclusive evidence to prove or disprove either theory.

2.4 Theoretical and Experimental Correlations

In many applications of packed beds, the effect which is of most importance to Scientist and Engineers is the pressure drop caused by the presence of the media. The most conclusive way to determine pressure drop through a packed bed is to undertake an individual experimental investigation for every specific case. This would entail creating a suitable geometry and forcing a fluid through the media by means of a pumping system, with a manometer tapping at the extremities to measure the pressure drop. Although possible, this would be tortuous and too time consuming for most industrial engineering applications. In the digital age CFD has become a viable alternative to empirical methods, however it can be relatively time consuming when defining a complex disordered geometry, in addition, more information will be generated than is required in most industrial applications. Data such as instantaneous pressure and velocity fields can be extracted along with a considerable amount of other data associated with the motion of a fluid.

Where an engineering approximation is solely required, a simple mathematical relation is used to approximate the pressure drop. These relations have been developed by Scientist and Engineers over the past three centuries. Generally the theoretical approximations treat the media as a bulk or gross entity limiting the amount of information that can be extracted. However, serve their purpose from simplicity and efficiency.

2.4.1 Flow Models

Flow models usually represent a mathematical correlation in the form of a regression around an experimental study or based on a theoretical postulation or understanding (e.g based on dimensional analysis). Some correlations can be a blend of both e.g based on a theoretical understanding but with an empirical coefficient to adjust the data. The following section focuses on flow models and the fundamental assumptions underlying the development of these equations, such as flow characterisation and limitations and subsequent failures of these models. Here, rather than starting with the earliest models to predict pressure drop through a porous medium and proceeding chronologically through time, a path many authors have chosen to take, we shall begin with the Reynolds hypothesis which describes the pressure drop per unit length relation given as

$$\frac{\Delta P}{L} = \alpha u + \beta u^2 \tag{2.14}$$

where α and β are empirical coefficients dependant on the fluid properties, the bed geometry and friction (Hassanizadeh & Gray, 1987), and u is the fluid velocity. Unsteady flow effects can be further added to the equation by the addition of $c\partial u/\partial t$, representing the change in velocity with respect to time.

$$\frac{\Delta P}{L} = \alpha u + \beta u^2 + c\frac{\partial u}{\partial t} \tag{2.15}$$

Reynolds hypothesis is generally considered in two distinct parts, where αu is the laminar and hence linear element and βu^2 is considered the non-linear turbulent element of the equation. It is generally sufficient to consider the flow to be steady state, hence in most cases the term $c\partial u/\partial t$ is negligible.

Nearly all models proposed to describe pressure drop per unit length can be traced back to the Reynolds hypothesis with the coefficients (α and β) quantified. These coefficients are either quantified empirically or through certain analytical assumptions. We know a packed bed is comprised of a series of inter-connecting voids and loosely behave as a series of varying length pipes. Due to this, in most cases a pipe flow analogy can be applied, known as the theoretical or fictitious tubes model. In this case, the laminar (α) and turbulent (β) elements can be

regarded as being equivalent to the Hagen-Poisselle relationship and the Darcy-Weisbach equation respectively to describe pressure drop through a pipe. The Hagen-Poiselle relationship is described as

$$\frac{\Delta P}{L} = \frac{8\mu}{R_h^2} u \tag{2.16}$$

and the Darcy-Weisbach by

$$\frac{\Delta P}{L} = f\left(\frac{L}{D}\right)\frac{1}{2g}u^2 \tag{2.17}$$

The Hagen-Poiselle equation is a simple relation which specifically describes pressure drop through a smooth straight pipe in a laminar, parabolic flow regime. The term R is the hydraulic radius, which for round pipes is described as the ratio of the cross sectional area over the whetted perimeter (for a full pipe this would be $R/2$). The Darcy-Weisbach equation is applicable for both turbulent or laminar flow regimes by the adjustment of the friction factor, f, and accommodates variables such as wall roughness, which as we have discussed can induce unsteady behaviour. For a laminar flow regime in a smooth pipe the friction factor, f, can be simply described as $f = 16/Re$ (Hagen-Poisselle relation). For turbulent or laminar flow, accounting for wall roughness the Moody diagram can be used in conjunction with the pipe Reynolds number to find a suitable value of f. This technique for determining pressure drop through a straight pipe is well established and relies on just a few variables. Determining suitable values for a packed bed is dependant on many variable which are not easily determined with the current methods available. Throughout this Thesis, for numerical simplicity the U.S style of the Darcy-Weisbach equation is adopted omitting the multiplication factor 4. Combining both the Hagen-Poiselle relationship and Darcy-Weisbach equation yields

$$\frac{\Delta P}{L} = \frac{8\mu}{R_h^2} u + f\left(\frac{L}{D}\right)\frac{1}{2g}u^2 \tag{2.18}$$

In most cases, the Hagen-Poiselle relationship forms the bases for the linear (laminar) models and the Darcy-Weisbach equation for the non-linear (turbulent) models. These two equations have satisfied all the dimensional characteristics to

describe pressure drop through a single tube in a packed bed, but alone do not model the drop in pressure well. The next section describes the development of this equation to model a series of tubes of varying lengths.

When comparing pressure drop through packed beds from literature it is often desirable to present the pressure drop in its dimensionless form, ϕ, which allows packed beds of different properties to be compared.

$$\phi = \frac{\Delta P d_p}{L \rho U^2} \tag{2.19}$$

This allows beds of different particle diameters and lengths to be compared. This form also takes into account fluid properties such as density, however, does not consider the fluid viscosity. Further more, this relation as described above does not take into account bed porosity (ε), which is highly influential on the ease with which a fluid can pass through the media. This however, is taken into account to some extent by the particle diameter. We have discussed that the pressure drop per unit length ($\Delta P/L$) in the laminar regime is linear and the turbulent regime the pressure drop per unit length is a quadratic trend increasing with the Reynolds number. When using the dimensionless pressure drop, ϕ, the U^2 is on the bottom of the equation implying that the dimensionless pressure drop decreases as a function of the Reynolds number.

2.4.2 Linear models

The earliest theoretical explanation for the phenomena of flow through porous media (including packed beds) is Darcy's law (Darcy, 1856) determined by empiricism, re-enforced with simple dimensional analysis. Darcy's law is a linear law, analogous to Ohm's law of resistance, Fourier's law of heat conduction and Fick's law of diffusion (Dullen, 1992) all of which are globally known as linear transport equations. Darcy type equations assume the flow regime through the porous medium to be Hagen-Poiseuille flow and therefore can only be applied to low Reynold's number conditions. Hagen Poiseuille flow is described as the flow through a cylindrical pipe and assumes the flow to be incompressible, viscous and laminar, in which case a complete solution to the Navier-Stokes equations is

possible. For a sufficiently slow, steady, unidirectional, Newtonian flow, Darcy (1856) defined the pressure drop-velocity relation as

$$\frac{\Delta P}{L} = -\frac{\mu u}{k_p} \tag{2.20}$$

where L is the bed length, μ is the dynamic viscosity of the fluid, u is the fluid velocity and k_p is the permeability. The minus sign simply distinguishes between a drop in pressure and an increase in pressure. The permeability is the property which describes the ease in which a fluid can percolate through it and can be described as the medias hydraulic conductivity. Darcy's law can be described as the linear element of the Reynolds hypothesis with the coefficient quantified as $\alpha = \mu/k_p$. Brinkman (1947) used the equation of Darcy (1856) and added a term for viscous shear. Neale & Nader (1974) suggest that due to the additional viscous shear term, the equation proposed by Brinkman (1947) is compatible with boundary layers within a porous medium. Brinkman (1947) extended Darcy's law to give

$$\nabla P = -\frac{\mu u}{k} + \mu' \nabla u \tag{2.21}$$

Blake (1922) modified the equation of Darcy (1856) with the addition of the superficial velocity, $U = u\varepsilon$ (The Depuit-Forcheimer relation). The superficial velocity is the velocity that would pertain if the fluid occupied the duct on its own without the presence of the media. Blake (1922) also quantified permeability (k_p) based on an empirical approach, with the addition of the hydraulic radius, R_h giving

$$k = \frac{R_h^2 \varepsilon}{k_2} \tag{2.22}$$

The hydraulic radius is satisfactory for a square duct or open channel where the cross section remains constant, but for a packed bed an average is introduced based on the volume to surface area ratio. We know that the volume available to the flow is the void volume, V_v and is related to the porosity by $\varepsilon = V_v/V$. The whetted surface area per unit volume is $a_w = a_p/V$ and combining this with the porosity gives the packed bed hydraulic radius given as

$$R_h = \frac{\varepsilon}{a_w} \tag{2.23}$$

substituting in terms of the equivalent diameter (d_P gives

$$R_h = \frac{d_p \varepsilon}{6(1-\varepsilon)} \tag{2.24}$$

and this forms the basis for the theoretical tubes models. Some of the earliest research carried out using this arrangement was by Blake (1922) and Kozeny & Sitzber (1927). To incorporate a higher range of Reynolds numbers using the equation of Blake (1922), Kozeny modelled a packed bed as a bundle of parallel small diameter tubes (Kozeny & Sitzber, 1927; Strigle, 1994) and hence the pressure drop can be related to Hagen-Poiselle flow. The Hagen-Poiselle relation (U.S) is given as

$$\frac{\Delta P}{L} = \frac{\mu U}{\frac{1}{2} R_h^2} \tag{2.25}$$

Making the assumption that a packed bed can be made up of a bundle of parallel theoretical tubes, the hydraulic radius can be substituted into the Hagen-Poiselle relation, with the addition of the superficial velocity $U = u\varepsilon$ giving

$$\frac{\Delta P}{L} = 72 \frac{U \mu L (1-\varepsilon)^2}{d_p \varepsilon^3} \tag{2.26}$$

This assumption relies on all the tubes being equal in length. In reality, packed beds are complex and tortuous, with interconnecting flow channels having no uniform geometry in a bed of randomly dumped particles (Strigle, 1994). As a result the fluid takes a longer path than simply the length of the theoretical tube. Carman (1937) then applied the work of Kozeny & Sitzber (1927) to experimentally determine pressure drop through packed beds and concluded that the bed length should be multiplied by a constant (25/12) to account for the extra length (Tortuosity) (Bird *et al.*, 1960) and as a result produced the Carman-Kozeny equation (Carman, 1938; Strigle, 1994). However, the value of (25/12) is not a constant and is heavily dependant on the bed tortuousity. This equation is sometimes referred to as the Blake-Kozeny equation. These designations are often interchanged between Blake-Kozeny and Carman-Kozeny (Middleman, 1998).

$$\frac{\Delta P}{L} = \frac{150 \mu \left(1-\varepsilon\right)^2 U}{\varepsilon^3 d_P^2} \tag{2.27}$$

In many applications of packed beds where the flow is characterised as being turbulent; the Carman-Kozeny equation does not hold where there are high losses in kinetic energy $Re_p > 10$ (Strigle, 1994), in which case the non-linear element, βU^2 needs to be quantified.

2.4.3 Non-linear models

Non-linear models are based on quantifying a suitable value for β in the Reynolds hypothesis. We know that for laminar flow Blake (1922) and Kozeny & Sitzber (1927) modelled the pressure drop by the pipe flow assumption and the theoretical tubes model and applied the Hagen-Poisselle relationship for laminar flow. We know from elementary fluid mechanics that the Darcy-Weisbach equation describes the pressure drop through a straight pipe in turbulent conditions

$$\Delta P = f\left(\frac{L}{D}\right)\frac{U^2}{2g} \tag{2.28}$$

Burke & Plummer (1928) used the Darcy-Weisbach relation, and by substituting superficial velocity and the hydraulic radius for a packed bed deduced the term to form

$$\Delta P = 3/2f\left(\frac{L}{d_p}\right)\frac{U^2(1-\varepsilon)}{2\varepsilon^3} \tag{2.29}$$

From extensive empirical investigations Burke & Plummer (1928) concluded that for turbulent flow through a packed bed the friction factor could be described as $3f/2 = 3.50$. Substituting this back into equation 2.30

$$\Delta P = 1.75\left(\frac{L}{d_p}\right)\frac{U^2(1-\varepsilon)}{\varepsilon^3} \tag{2.30}$$

Bird *et al.* (1960) suggest that the Burke-Plummer equation is only valid for flow Reynolds numbers greater than $Re_p = 1000$.

Ergun (1952) took the equations of Carman (1937) and Burke & Plummer (1928) and added these together producing a mathematical portmanteau to model both laminar and turbulent flow, which completely satisfies the linear and non-linear terms in Reynolds hypothesis, by theoretical tubes and inclusive of an

empirical coefficient.

$$\frac{\Delta P}{L} = \frac{150\mu\left(1-\varepsilon\right)^2}{\varepsilon^3 d_P^2}U + \frac{1.75\left(1-\varepsilon\right)\rho}{\varepsilon^3 d_P}U^2 \tag{2.31}$$

Although the Ergun equation satisfies Reynold's hypothesis, the coefficients are based around the empirical data of Carman (1937) and Burke & Plummer (1928) which are mostly high aspect ratio. Foumeny *et al.* (1993) suggest that when the aspect ratio is < 50, wall effects cause the Ergun equation to yield a poor result. In addition Hicks (1970) studied the equations of pressure drop and subsequently concluded that the Ergun equation is limited to $Re_{dp}/(1-\varepsilon) < 500$ and (Handley & Heggs, 1968) coefficients for the Ergun equation to $1000 < Re_p/(1-\varepsilon) < 5000$. Choi *et al.* (2008) suggests that for low Reynolds numbers ($Re_p/(1-\varepsilon) < 10$) the Ergun equation tends to underpredict the pressure drop and in the larger Reynolds regime ($Re/(1-\varepsilon) > 10$ the Ergun equation over predicts the pressure drop in comparison to experimental results.

The numerical coefficients of the Ergun equation have been the subject of much discussion, with conflicting observations. The coefficient values are usually given as 150 and 1.75 (Ergun, 1952). From empirical data Leva (1959) suggested alternative coefficients of 200 and 1.75, with MacDonald *et al.* (1979) recommending coefficients in the range of 180 and $1.8 - 4.0$. In addition Handley & Heggs (1968) suggest values of 1.24 and 368. Du Prieur and Woudberg state that the coefficients are severely dependant on the interstitial physical flow conditions that vary considerably between different types of structure (Plessis & Woudberg, 2008). Investigation into the coefficients (Plessis & Woudberg, 2008) further suggest that tuning the Ergun coefficients is not recommendable due to its resemblance to a 'fudge factor' approach to which the coefficients are adjusted to fit every new application. In reality is is possible that these coefficients are unique to the individual bed being analysed, in which case it is almost impossible to create a set of coefficients to fit all cases perfectly. On the contrary, there have been arguments to suggest that 1.75 and 150 are not constants but depend on the Reynolds number, particle shape, size and porosity (Handley & Heggs, 1968; Hicks, 1970). Research carried out by Rehder (1990) suggests that the parameters that have the most influence on the result of the Ergun equation are the porosity

and the superficial velocity, where the superficial velocity causes the theoretical pressure drop to increase or decrease, whereas the porosity causes the gradient of the theoretical curve to vary in magnitude.

2.4.4 Wall correction models

In the case of low aspect ratio beds ($A_{ratio} < 50$), where the particle diameter is not sufficiently smaller than the tube diameter, the correlations discussed so far do not model experimental data well. Choi *et al.* (2008) suggest that when the bed diameter (D) is not significantly larger than the particle diameter (d_P), the flow maldistributions and wall friction are not negligible. In these cases an assembly of models have been devised known as wall correction models, in many cases based on an existing correlation which is corrected to take into account the wall region. The theoretical tube models such as Ergun & Orning (1949), Burke & Plummer (1928) and (Kozeny & Sitzber, 1927) assume the porosity to be uniform across the bed, such as the case of an infinite packing, which neglects the wall region and ultimately leads to the breakdown of these equations at low aspect ratios.

Gibilaro (2004) proposes a simple model for the effect of the container wall based on the application of a two zone flow model applied to the Ergun equation. The bed is separated into two regions, where the bulk or core region is the central region unaffected by the wall, and the wall region is the region directly adjacent to the wall usually taken as a distance $d_p/2$ (Martin, 1978). Gibilaro (2004) replace the function of superficial velocity (U) with a corrected average superficial velocity, bulk velocity (U_B) or fluid flux defined as

$$U_B = \frac{U_S}{2.06 - 1.06(\frac{D/d_P - 1}{D/d_P})^2} \tag{2.32}$$

In addition, porosity (ε) is replaced with a bulk porosity (ε_B) which is the porosity in the bulk region excluding any effects of the wall region. This equation models pressure drop relatively well at low Reynolds regimes but deviates away from the experimental results quickly as the Reynolds number increases.

Reichelt (1972) proposed a correlation to determine dimensionless pressure drop based on the Ergun equation with the addition of two coefficients accounting for the effect of the confining wall region and the porosity effect at high Reynolds numbers caused by the wall region (Eisfeld & Schnitzlein, 2001). The equation proposed by Reichelt (1972) is based on the hydraulic radius theory and is given in the form

$$\phi = \frac{K_1 A_W^2}{Re_{dp}} \frac{(1-\varepsilon)}{\varepsilon^3} + \frac{A_W}{B_W} \frac{1-\varepsilon}{\varepsilon^3} \tag{2.33}$$

where K_1 is a coefficient. The wall correction terms are given as

$$A_W = 1 + \frac{2}{3(D/d_p)(1-\varepsilon)} \tag{2.34}$$

and

$$B_w = \left[k_1 \left(\frac{d_p}{D} \right)^2 + k_2 \right]^2 \tag{2.35}$$

Using the equation proposed by Reichelt (1972), Eisfeld & Schnitzlein (2001) devised a semi-empirical approach. Their method utilises the correlation proposed by (Reichelt, 1972) with the modification of the coefficients to a regression fitted to 2300 data points from 23 different research articles. Some of the work carried out by Leva (1959) is purposely omitted from the study due to their inconsistency with the other experimental data (Eisfeld & Schnitzlein, 2001; Wagstaff & Nirmaier, 1995). Their correlation resulted in several communications (Tsotas, 2002b) regarding their failure to recognise the dual effects of increased wall friction and flow maldistributions at the container wall. Tsotas (2002b) argued that the two effects could be studied separately by the extended Brinkman equations and cannot be accounted for by the correlations proposed by Eisfeld & Schnitzlein (2001). There is little weight to this argument as the equation of Eisfeld & Schnitzlein (2001) is derived from a range of the empirical data which correctly encompasses all of the various effects of flow channelling and increased wall friction in the range of experimental methods. However the effects of flow channelling and increased wall friction cannot be separated from the data. What is more, their model is intended to give an empirical approximation for dimensionless pressure drop, which is a bulk value, and is not intended to study increased wall friction and flow distributions. However, the increased wall friction and flow

inhomogeneities may account for the large spread of data at high Reynolds numbers. Eisfeld & Schnitzlein (2001) conducted quite an extensive survey comparing the data with other empirical correlations. In most cases the route-mean-square deviations of the data surveyed compared to other correlations is low ($\sigma < 0.3$) (Ergun, 1952; MacDonald *et al.*, 1979; Reichelt, 1972), but in some cases it can be as high as $\sigma > 0.7$ (Foscolo *et al.*, 1983; Foumeny *et al.*, 1993; O'Neill & Benyahia, 1997).

Choi *et al.* (2008) propose a correlation which recognises the increased wall friction and the increased porosity as a result of the confining wall to predict pressure drop per unit length at wide range of Reynolds numbers ($Re = 10^2 - 10^3$). They modified the original equation proposed by Ergun (1952) to take into account the effect of the confining wall.

$$\frac{\Delta P}{L} = \frac{150(1-\varepsilon)^2 \mu U M^2}{\varepsilon d_p^2} + \frac{1.75(1-\varepsilon)\rho M U^2}{\varepsilon^3 d_p} \tag{2.36}$$

where M is defined as

$$M = 1 + \frac{2d_p}{3D(1-\varepsilon)} \tag{2.37}$$

The correlation fits the data of some research with some degree of accuracy ($\sigma < 10$) (Handley & Heggs, 1968; Mehta & Hawley, 1969), but fits the experimental data of Foumeny *et al.* (1993) with less accuracy ($\sigma > 25$). On the assumption the data has been collected competently, this reinforces the theory that there is no single correlation that can model every specific case with a good deal of accuracy. A creative correlation which is difficult to categorize is the correlation proposed by Fried & Idelchik (1989). The model determines pressure drop based around the packing angle, where the bed porosity, ε is given as

$$\varepsilon = 1 - \frac{\pi}{6(1 - cos\theta)(\sqrt{1 + 2\cos\theta})} \tag{2.38}$$

Fried & Idelchik (1989) modify the Reynolds number to produce

$$Re = \frac{0.45 U_{up} d\rho}{\mu(1-\varepsilon)\sqrt{\varepsilon}} \tag{2.39}$$

Subsequently, using these the parameters the pressure drop per unit length becomes

$$\frac{\Delta P}{L} = \frac{1.53}{\varepsilon^{4.2} d}\left(\frac{30}{Re} + \frac{3}{Re^{0.7}}\right)\frac{\rho U^2 up}{2} \tag{2.40}$$

This method is only valid for packing angles between $\theta = 60° - 80°$ (Hexagonal close packing and a simple cubic lattice), is limited to porosity ranges between 0.26 and 0.48, and does not accurately model random, disordered packing.

2.5 Computational literature

The previous section discusses the development of correlations based on theoretical and experimental approaches to predict the drop in pressure across a packed bed or porous medium. Experimental and theoretical approaches in many cases can give a good indication of pressure drop, but do not allow quantitative analysis of the flow pattern analysis within the bed. Flow models assume the media to be a homogeneous bulk or gross entity and neglects the complex internal flow structure of the media. Due to this, the pressure drop models are considerably more effective in high aspect ratio beds which can be considered as a homogeneous continuous medium. The most realistic and extensively used approach to analyse the motion of a fluid within a complex, heterogeneous structure is to use computational fluid dynamics (CFD) to solve the motion of a fluid mathematically from a set of governing equations. CFD can be broken down into two basic approaches; continuum approaches (Finite Element and Finite Volume) and the lattice-Boltzman method. The lattice-Boltzmann method solves the discrete Boltzmann equations which describe the motion of individual fictitious particles coupled with a collision model for a dilute gas. In a dilute gas, molecules move around as free particles apart from when they collide with other particles. This method makes use of certain parts of the Boltzmann equation coupled with a collision model to describe the particle motion and collision events. The linkage with the finite volume method is under particular assumptions the Boltzmann equation can be used to derive a form of the Navier-Stokes equations.The finite element and finite volume methods solve the Navier-Stokes equations by integrating the equations over a mesh of finite elements or volumes. The equations

are coupled and non-linear and contain unknowns in which finite difference equations are substituted for the properties of the flow, which are solved using an iterative method. Once a solution has been generated, properties of the flow can be extracted for each individual cell or element for analysis.

CFD techniques are well defined and have established themselves as an accurate representation of fluid behaviour. The major constraint with any CFD technique applied to a complex media is defining a suitable computational geometry for the flow domain in which the fluid motion can be analysed. In order to solve the governing equations used in a CFD solver, the flow domain has to be suitable discretized into small volumes or elements leading to the solution of a partial differential equation. This process is referred to as meshing or grid generation. If a suitable grid or mesh is not produced, geometric fidelity issues occur with respect to the representation of the computational domain. Moreover, if a mesh of suitable quality is not created, instabilities occur when trying to solve the governing equations.

Primarily there are four techniques for describing the geometry with relevance to packed beds. The first is to produce a structured bed. Because the bed is structured the location of each particle can be easily described by simple mathematics coupled with an appropriate coordinate system. This can be used in conjunction with CAD software or created directly in a mesh generation program such as GAMBIT (Fluent Inc). Secondly, we know a structured bed is repeating, therefore its geometry does not change through the bed and the flow characteristics are not likely to vary. Using this assumption and mesh generation software a simple unit cell approach can be adopted. One or more unit cells (voids) can be modelled using CFD and the data extracted and collated to produce a representation of a full scale model. This method vastly reduces computational expenditure, but in some cases does not take into account the small scale flow characteristics that would be achieved by modelling a full bed. This method is not suitable for highly disordered geometries where the flow patterns vary considerably through the bed. However, does provide a reasonable engineering approximation in regard to a pressure drop approximation in structured beds. Thirdly, where unstructured, random beds are required for study a non-deterministic object packing algorithm is needed to generate the locations of each

of the particles. This can then be used in conjunction with CAD software and a suitable meshing program to generate a workable computational domain. Finally, where an actual physical beds available for study, non-invasive methods such as magnetic resonance imaging (MRI) and computed tomography (CT) can be used with geometry defining software to recreate a bed for computational analysis and direct comparison.

Once the geometry has been defined using one of the four major techniques discussed, the geometry must be suitably discretized so that the bounding equations can be suitably integrated. Grids or meshes are constructed from a matrix of elements or cells and in nearly all cases these are tetrahedral, hexahedral or polyhedral which are all constructed from a series of connecting flat surfaces. Packed beds often contain spherical media, where a sphere is a round continuously sided volume and cannot be represented as fully smooth by a series of flat surfaces but rather is represented as a geodetic sphere. Further more, when spheres are in contact with each other they produce an infinitely small contact point which is difficult for a mesh generation software's discretization algorithm to fully describe at this stage. This phenomena has become one of the major constraints when analysing packed beds using CFD approaches. Some Researchers have used novel methods to overcome these constraints which are discussed in the following section. The constraints and limitations concerning CFD approaches are discussed in detail in Chapter 3.

2.5.1 Structured Bed Approaches

In most applications of CFD to packed beds the ratio of particle to tube diameter (aspect ratio) is low. This is attributed to the complex geometries associated with high aspect ratio beds and the vast number of cells required to realistically represent the flow domain. This follows a simple relationship; the larger the number of cells, the more computer power needed to realistically solve the problem in a suitable time frame. A sphere is also an infinitely sided object, so in theory to fully represent a sphere an infinite number of cells is required, which of course is not possible. In which case it has to be represented by a finite number of cells. The more cells the closer the sphere is to a true sphere.

Naturally, in the early days of computing the only beds possible to practically analyse were those of low aspect ratios in cases with only a couple of spherical particles in 2-dimensions and structured formation, with steady laminar flow. Spheres and a structured array are chosen due to their simple mathematical description in respect to location and geometry. It is debatable if this can be classified as a packed bed or simply a cluster of spherical particles. This alone raises the question, when is it reasonable to suggest a cluster of spheres has become a packed bed? Furthermore, is one continuous layer of spheres a packed bed, or does it require 2, 3 or 4? In many cases where CFD has been applied to packed beds spherical particles are chosen due to the possible regular packing regimes, which can easily be described mathematically, such as face centred cubic (FCC), or close hexagonal (CHP). These arrangements are equivelent to the stacking patterns of oranges. If the reader is interested in the flow through oranges, complete with crate, the reader should consult Delele *et al.* (2008). The advantage of using spheres is they only require a single coordinate, e.g Cartesian or polar, and single value of radius, with this data a complete description of both the location and geometry of the particle can be determined. However, this is often outweighed by the complications produced by particle contact points and the fact a sphere is a continuously sided object which cannot be meshed retaining its geometric fidelity.

The earliest work demonstrating the application of CFD to packed beds, is that of Dalman *et al.* (1986). They use a velocity-pressure formulation of the 2d Navier-Stokes equations solved numerically using a finite element technique to analyse the flow past two spheres. Dalman *et al.* (1986) investigated laminar flow with Reynolds numbers up to $Re = 200$, with Prandtl number of 0.72 and 7.0 for a range of sphere sizes and separations, where the Prandtl number is defined as the ratio of dissipation and conductance in the form $P_r = \mu c_p/k$, where c_p is the heat capacity ratio and k is the conductivity. Although the packing possibilities are limited using this approach, the work gave a valuable insight into flow structure through packed bed and demonstrated the formation of eddies between the bed particles (Taskin, 2007) indicating regions of poor heat transfer. The work of Dalman *et al.* (1986) is probably the first investigation into the flow structure within internal bed voids. With all early work, one of the main difficulties is

producing a workable mesh. Where two spheres touch elements are often highly skewed with poor aspect ratios. Dalman *et al.* (1986) report no particle contact points points between the spheres and the particles are not in contact with each other, ammeliorating the problem of degenerate elements at the particle contact points.

Eight years after Dalman *et al.* (1986), Lloyd & Boehm (1994) studied flow and heat transfer around a linear array of 8 spheres in 2d using the finite element package FIDAP. Lloyd & Boehm (1994) use Reynolds numbers of 40, 80 and 120 with Prandtl numbers ranging from 0.73-7.3. This work was a considerable advancement from that of Dalman *et al.* (1986) due to the number of particles being analysed. They investigated the effect of sphere spacing on the particle drag forces and concluded that the heat transfer from the particles to the fluid decreased as the particle spacing increased.

Derx & Dixon (1996) performed possibly one of the earliest 3-dimensional calculations on a bed of three spheres. As with the work of Dalman *et al.* (1986) no contact points are reported between the particles. Logtenberg & Dixon (1998) modelled a 3-dimensional bed of 8 spheres in the form of two layers of four spheres perpendicular to the flow with low aspect ratios of 2.43. They use the commercial CFD code FLOTRAN to investigate fluid flow heat transfer using air for Reynolds number of $Re = 9 - 1450$. Logtenberg *et al.* (1999) modelled a bed of ten spheres with aspect ratios of $A_{ratio} = 2.43$ using a FEM. Similar to the earlier work of Lloyd & Boehm (1994) they focus on heat transfer and fluid flow, focusing on wall-particle contact points. Unlike Dalman *et al.* (1986) and Logtenberg & Dixon (1998) they emulate the contacts between the spheres by leaving small gaps between the particles set to zero velocity on the assumption that there is a stagnation zone at the particle contact points. With the early work described so far, the major limiting factor in regard to producing realistic flow patterns is the small number of particles being analysed. As computers advanced and computational power became more readily available, the number of particles being modelled grew considerably and progressed to studies in 3-dimensions.

Dixon & Nijemeisland (2002) use the finite volume technique to model small clusters of 44 structured spheres with aspect ratios, $A_{ratio} = 2$ and $A_{ratio} = 4$ and Reynolds numbers of $Re = 373 - 1922$. They use a mesh constructed

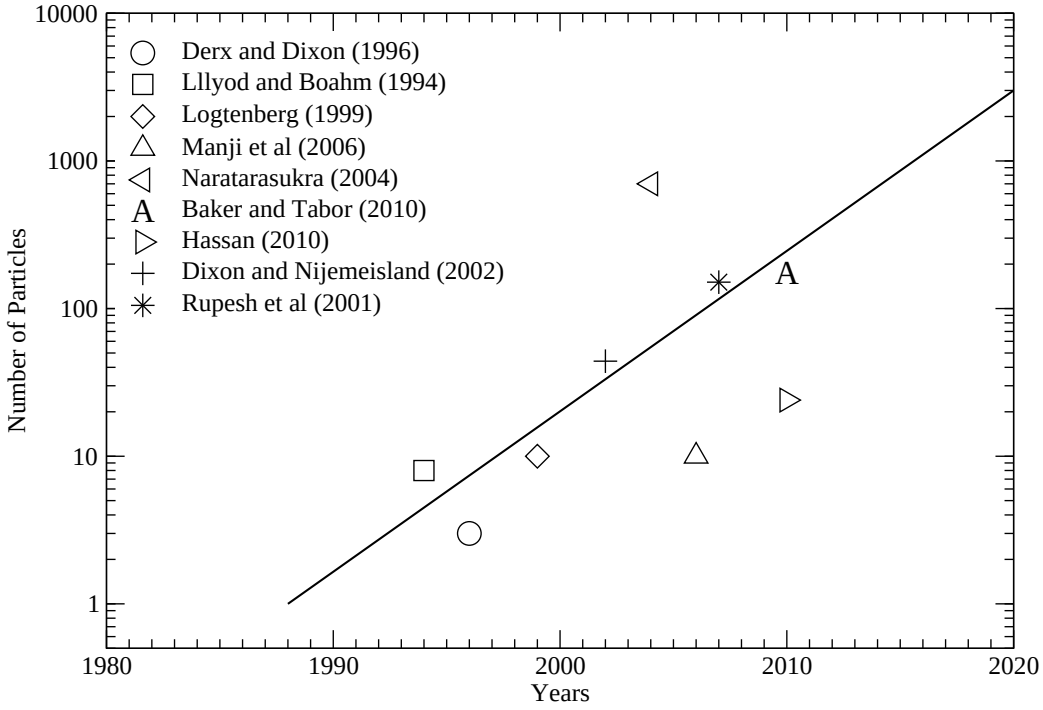

Figure 2.10: Number of particles as a function of date in years

of tetrahedrons, unstructured in nature, where a suitable mesh density (based on a mesh refinement study) is conducted on single spherical particle instead of the whole domain. They also correctly address the issue of particle contact points and refine the mesh further in the region. As expected with meshing curved geometries with zero spacing the mesh exhibits high levels of skewness and degenerate elements. However, in the case of the higher aspect ratio bed ($A_{ratio} = 4$) the mesh is too coarse to determine an accurate flow field. However, the work does produce convincing results for aspect ratios ($A_{ratio} = 2$) and show vorticity and recirculation in the voids.

Guardo *et al.* (2007) studied the effect of turbulence models in packed beds for

modelling wall to fluid heat transfer in a regular pack in a cylindrical container. They use the commercial code Fluent to study a range of Reynolds numbers between $127 < Re < 912$ and obtained values for pressure drop. They implement the $k-\varepsilon$ (Standard, RNG, Realizeable), Spalart-Allmaras and the $k-\omega$ turbulence models and compared the the pressure drop from the expected behaviour of the Ergun equation. The pressure drop calculations produced by the turbulence models show good agreement with the Ergun equation. However, Guardo *et al.* (2007) use an aspect ratio of $A_{ratio} = 3.923$ which is low aspect ratio bed and we know the Ergun equation does not yield a good result (Foumeny *et al.*, 1993) for $A_{ratio} < 50$. In addition the Spalart-Allmaras turbulence model is designed to be applied without wall functions, in which case the mesh must be fine enough to resolve the flow right down to the viscous sub layer. The mesh volumes are not discussed, but from figures published it looks plausible that this is not the case. A thesis defended by Guardo (2007) focuses on flow around spherical particles in a cubic array based on the geometry of Suekane *et al.* (2003) using the finite volume technique. To avoid problems associated with degenerate mesh elements around particle contacts, each of the particle diameters are enlarged by 1%. Correlations are compared to magnetic resonance velocimetry on the same geometry.

Even today, it is still not yet possible to perform a 3-D simulation of a full-size industrial scale fixed bed reactor (Freund *et al.*, 2005). Once the full internal micro-scale flow of a full size packed bed reactor can be accurately modelled, the possibilities for further research in the field of CFD of packed bed reactors is limited to the application of new techniques and approaches in which the process of delivering a model is made more efficient.

Manjhi *et al.* (2006) examine regular packings of small numbers of spheres (< 10) in a cylindrical tube using lattice Boltzmann techniques, and are able to produce convincing visualisations of the micro-structural flow in these highly simplified geometries. Attempts have also been made to blend numerical simulations on simplified geometries with empirical data (Tobís, 2008). A unit-cell approximation makes the calculation reasonably tractable. However for random, unstructured, packed beds the true geometry is complex and tortuous, and a single unit cell may not be considered representative. Instead a larger section of the bed must be simulated, large enough to contain a significant and representative

diversity of micro-structure and thus hopefully large enough to be considered representative of the micro-structural flow.

Rupesh & Joshi (2008) study low aspect ratio ($A_{ratio} = 5$) fixed beds of 151 spherical particles arranged in 8 layers in a cubic orientation. They monitor drag coefficients and pressure drop at pipe Reynolds numbers of $Re_{d_p} = 0.1 - 10,000$. They state 'for simplicity' that the inlet velocity profile is kept flat. This is suitable for a turbulent regime due to its closeness to the 1/7 power law. However, using a flat velocity profile for a creeping regime (Stokes flow) is questionable due to the likelyhood of the existence of a parabolic profile. Furthermore, Rupesh & Joshi (2008) neglect to state whether the velocity inlet has been adjusted to form U_{avg} based on the volumetric flow rate. Rupesh & Joshi (2008) discuss increased pressure drop due to wall friction in the creeping flow regime and reduced pressure due to wall channelling in the turbulent regime based on their computational results. Using CFD alone to make this statement is questionable due to the way in which the $k - \varepsilon$ model and standard laminar solvers are treating the wall region in regard to suitable $y+$ values and inlet profile. In addition Rupesh & Joshi (2008) give no indication of $y+$ values at the near wall region nor is there any attempt at a mesh refinement study to indicate the meshes independence from the solution.

A rather more unusual approach is adopted by Narataruksa *et al.* (2004). They use the package COMSOL MULTIPHYSICS to analyse the the flow structure in a pack bed with and without a static mixer with inlet Reynolds numbers (based on pipe diameter) of $Re = 2.31$. 700 hundred catalyst particles are packed into a cylindrical container in a cubic arrangement with considerable gaps between the particles ensuring consistency in element size. A simple arrangement such as this and an incompressible steady-state creeping flow regime, solver stability and convergence is virtually guaranteed. However, due to the structured packing regime the particles do not completely fill the container resulting in large gaps around the bed leading to a dominant near wall region. Narataruksa *et al.* (2004) use a mesh sizes of 168450 and 241471 cells, which are incredibly coarse for a bed containing such a large number of particles, in addition the domain is not subjected to a mesh indeterminacy study, in which case they cannot guarantee the mesh is not effecting the overall solution. To put this into perspective, in the

work of Baker & Tabor (2010), 174 particles are studied, and when the domain is subjected to a mesh refinement, the pressure drop ceased to be affected by the mesh after 1,168,328 cells. Narataruksa *et al.* (2004) are monitoring the direction and the magnitude of the flow in addition to the pressure drop which is considerably more sensitive. Although, this argument could be rebutted in the sense that this is a creeping flow regime and the direction and the magnitude of the flow is likely to be fairly constant and the particles have no contact points. Even so, a mesh this course cannot attempt to en-capture the boundary layer or model any effects in the near wall region. What is more, Narataruksa *et al.* (2004) compare their results with the Blake-Kozeny equation. We know the Blake-Kozeny equation is a theoretical tube model and assumes the porosity to be uniform across the bed, a continuously packed medium and high aspect ratio. In the work of Narataruksa *et al.* (2004) the aspect ratio is low ($A_{ratio} = 12.31$) and therefore the wall region will be dominant nullifying the the application of the Blake-Kozeny equation. Moreover, in this specific case the particles do not fill the whole container, in which case the magnitude of wall dominance will increase. A more suitable equation to compare the results of Narataruksa *et al.* (2004) would be a wall correction model such as Eisfeld & Schnitzlein (2001) or Reichelt (1972).

Finally, Hassan (2008) use Large Eddy Simulation to study flow in pebble gas cooled reactors in a cubic array of 24 spheres. They initially conduct studies using a zero equation turbulence model due to its speed and robustness, moving on to the implementation of a LES solver. They also attempt to use PIV with a matched refractive index fluid to derive experimental results. They report complex flow structures near the particle contact points where the size and frequency of turbulent events increase with the Reynolds number. Hassan (2008) correctly bring to light the issues associated with two touching spheres and use the CFD solver CFX-5 due to its function regarding its method of treating zero spacing by creating a common point on the vertices of a plane (Hassan, 2008). They use a Delaunay based algorithm to generate a mesh of 1.7 million tetrahedral elements.

2.5.2 Simple Unit Cell Approaches

An additional major constraint when applying a CFD approach to a packed bed of many particles, is the relatively large meshes which are produced and the limitations in computational power. One possible approach to ameliorate this is to assume a regular structure to the bed which can be reproduced using a simple unit cell (Hellström & Lundström, 2006). This differs from a structured bed approach in that only one or two pores are studied and the flow is assumed to be the same in all the other pores contained within the bed, rather then studying bed as a whole. An example of this was presented by Tóbis (2000) using a simple cubic unit cell and comparing against theoretical expectations and experiments on 6 similar structured beds. Tóbis (2000) uses the finite volume code Fluent and the standard $k-\varepsilon$, Spalart and Almaras and the Reynolds Stress turbulence models to investigate flow around the media and frictional resistance. The work of Tóbis (2000), as expected, indicates large discrepancies when compared to the Ergun constants, probably due to the Ergun constants being specific to high aspect ratio beds ($A_{ratio} < 50$). Regardless of the Ergun constants, the experimental and computational data presented in the work of Tóbis (2000) compares well. Gunjal *et al.* (2005) conducted a similar study by employing a single unit-cell approach of an array of spheres encompassing simple cubical, 1-D rhombohedral, 3-D rhombohedral and face centred cubic structures, coupled with CFD and investigate the interstitial flow in the void space. A similar approach was used by Calis *et al.* (2001) to model a limited subset of bed geometries known as composite structured packed beds; instead of a single unit cell they represented the bed in terms of a single linear row of spheres with appropriate boundary conditions. This considerably reduces the computational effort required in contrast to modelling a full packed bed, however, it is plausible that this technique does not give a realistic representation of the full flow structure.

2.5.3 Random unstructured Beds

In most applications of packed beds, the geometry is disordered and unstructured. We have discussed the non-deterministic nature of unstructured bed geometries and no deterministic mathematical relation will describe them. In such

cases the geometry must be defined via some form of randomised object packing algorithm. Zeiser *et al.* (2001) were probably the first to actually model a random unstructured by using CFD. They used a Monte-Carlo method to generate a random-unstructured bed of particles. An example of which is the code MacroPac (Evans, 1988; Rowe *et al.*, 2005), which uses a Monte Carlo approach to explore packing space. Zeiser *et al.* (2001) then apply the Lattice-Boltzmann method to model the expected behaviour of the fluid in a reacting, viscous flow regime. They report velocity channelling close to the wall region and were in good agreement with observations from experiment. Caulkin *et al.* (2007) describe the code DigiPac, where the objects to be packed are represented as assemblages of voxels in space which are allowed to move one grid spacing at a time within a cubic lattice; their resulting motion allows them to explore every possible packing space. The work of Caulkin *et al.* (2008) provides an interesting review of the viability of the digital packing algorithm DigiPac to predict bed structure. They use the Lattice-Boltzmann technique to investigate flow structure and velocity distribution within beds of mono-sized spheres, equilateral cylinders and raschig rings with aspect ratios of $A_{ratio} = 6.1, 8.3$ and 5.0 respectively. They compare results from LBM with experimental data empirically derived from non-invasive and non-destructive measuring techniques. Zeiser *et al.* (2002) apply Lattice Boltzmann techniques to solve the flow in a packed column with the addition of a parabolic velocity profile and a fixed static pressure at the outlet. Their aspect ratio is low ($A_{ratio} = 3$) so wall effects are dominant in their flow; however they are able to investigate in some detail the micro-structural flow in the bed. They also report that discretization of the spherical objects leads to a significant error, most probably due to the block structured lattice and in this case they conduct a detailed mesh refinement study. They controversially report that the Lattice-Boltzmann method can produce results equally as accurate as the finite volume method but with much coarser grids. Pan *et al.* (2006) apply Lattice Boltzmann techniques to both a simple cubic arrangement unit cell model and also to a random bed; the focus of their paper is comparing different variants of the Lattice Boltzmann technique rather than experimental validation. However, there are still unresolved computational concerns with LBM due to its restrictions to a limited class of mesh, there are also no reasons to suggest the LBM method

outperforms traditional Navier-Stokes based solvers (Tabor *et al.*, 2008). Magnico (2003) uses the finite volume techniques applied to a somewhat larger bed (several hundred particles and A_{ratio} of $5-7$) but quite a low Reynolds number (between 20 and 200) eliminating the need for a turbulence model.

Jafari *et al.* (2008) use the finite volume technique and the commercial code Fluent to analyse a packed bed reactor of several hundred particles. This work is particularly significant in the field due to the range of turbulence models applied. They compare Large Eddy simulations (LES) with Reynolds stress models and compare the steady-state incompressible Navier-Stokes equations as an alternative to a turbulence model. They conclude that the steady-state Navier-Stokes equations model flow well through a packed bed of spheres and hold well even into the lower end of the turbulent regime. In addition they use a combination of C++ programming with a code obtained from MatLab to create a journal file for the the CAD based meshing program GAMBIT as described by Zamankhan *et al.* (1999) which uses a random number generator to carefully position a 3d array of non-overlapping spheres. However, it can be observed that their spherical particles merge significantly at the inter-particulate contact points as a product of the mesh resolution which is a common problem. In the case of complex spherical geometries an 'all or nothing' situation arises from the fact that producing a successful mesh involves making the particles 'non-contact' or making the particulate contact points unrealistically large. This can be achieved by either enlarging or reducing the sphere diameters. In regard to analysing the flow patterns and pressure drop, either method can be conclusively argued as being more accurate than the other. This also presents an issue when using this technique in regard to dermining an accurate value of porosity from the mesh volume. Atmakidis & Kenig (2009) analyse the wall effect on the pressure drop in packed beds with moderate aspect ratios in the laminar flow region. They use the finite volume CFD solver, CFX. They analyse both regular and irregular packed beds of spheres generated using the ballistic deposition method combined with a Monte-Carlo approach to produce a random packing. Due to meshing issues, each particle is shrunk by 2% to avoid skewed elements at the inter-particulate contact points. This technique changes the flow geometry considerably, however it significantly reduces problems associated with mesh skewness and in addition

reduces particle merging and contact points additionally affecting the geometry. It is arguable whether the benefits of having a good mesh outweigh the effects of changing the flow geometry which has already been modified to some extent by the discretization in the mesh creation algorithm. However, Atmakidis & Kenig (2009) do conduct an extensive mesh refinement study where the local void velocity is analysed and their mesh contains over 30,000,000 cells. Atmakidis & Kenig (2009) report increased velocity channelling at the near wall region where the porosity is greater than that of the core region and channelling in random packs is not as structured as channelling in regular packs. Although their results are low aspect ratio, they compare their data with the expected results of Carman (1938), Ergun (1952), Reichelt (1972) and Zavoronkov *et al.* (1979).

2.5.4 Scanned Geometries

Methods discussed in the previous section focus on the creation of artificial beds either by a simple mathematical relationship, i.e a regular pack, or certain random sampling algorithms for disordered packs (Monte-Carlo simulations). These methods are limited to the creation of artificial beds and their comparison with structured or equivalent beds, which we already know may the same in regard to properties such as porosity, particle diameter etc, but may display a different internal structure. Methods have been developed to recreate actual physical beds and reproduce them in a computational form. One method which has been used extensively in the analysis of packed beds and porous media is magnetic resonance imaging (MRI). The acronym MRI is generally used as an alternative to NMR (Nuclear magnetic resonance) due to its inclusion of the word nuclear; due to the Cold war and the Chernobyl disaster, patients lacked confidence in the safety of the technique. MRI is used extensively in medicine for diagnostic purposes, but its use is becoming more widespread in determining random disordered geometries due to its non-invasive properties.

MRI techniques work by exciting hydrogen atoms. The human body is comprised of soft tissue, which contains water molecules. Water is comprised of two protons of hydrogen, H_2 and one of oxygen, O forming H_2O. A proton has a magnetic moment (a torque which is exerted due to its magnetic field) and when the

protons contained within the water molecules are influenced by a magnetic flux some of their moments align with the direction of the moment of the magnetic source. In the case of MRI, the scanner uses a radio frequency to produce an electromagnetic field (Callaghan., 1994). As the intensity and frequency is modulated more or less water protons spin up. When the field is turned off, the spin states relax. As a result of the difference in kinetic energy a photon is released, which is detected by the scanner and processed for analysis. This technique provides not only non-invasive visualisation of structures but also has a functional ability, providing limited flow visualisation. However, functional MRI techniques are limited to relatively low pipe Reynolds number, $Re < 200$ (Guardo, 2007) and the resolution is not sufficient to visualise the smaller turbulent structures.

Another non-invasive technique, not as widely used in the analysis of porous media is X-ray computed-tomography (CT, CAT scanning), which has been applied by Tabor *et al.* (2007, 2008). CT uses a different approach than MRI in which the sample is bombarded with an X-Ray source. The source rotates around the sample and an X-Ray detector, such as a scintillator tube, is positioned on the other side which detects the strength of the radioactive flux passed through the sample which can be interpreted and an image produced.

Non-invasive methods have proved valuable in both medicine and research in the field of porous media research, however there is still much improvement needed to the technique regarding fidelity issues and improvement to the relatively coarse resolution. The scan data often contains artifacts caused by motion in the scan or in the case of CT insufficient X-ray penetration (Herman., 2009).

What is of most interest in regard to this Thesis is determining a suitable geometry for computational analysis using MRI. With both MRI and CT, signals are analysed using a Fourier transform in which pixelated grey-scale 2-dimensional slices are produced forming a stack of images representative of the signal strength. Using the stack of grey-scale images, 3-dimensional surfaces can be extracted using a surface generation algorithm, such as morphological thinning or image based meshing. Alternatively, instead of creating surfaces from the grey-scale image, the image can be used, coupled with location defining algorithms to determine the locations of spherical particles (Aste *et al.*, 2004; Richard *et al.*, 2003; Seidler *et al.*, 2000).

In general, the use of non-invasive techniques applied to packed beds can be broken down into two approaches, firstly a non-invasive technique is used to determine the complex packed bed geometry and flow is modelled through the structure using CFD (Sullivan *et al.*, 2005), secondly the non-invasive method is used to not only determine the geometry but also to analyse the flow structure using MRV (magnetic resonance velocimetry). CT can be used to determine the complex structure, but is limited by its non-functionality and therefore flow distributions cannot be monitored in this way.

Manz *et al.* (1999), have applied the Lattice Boltzmann method based on an MRI visualisation of a packed bed simulated for Reynolds numbers $0.4 < Re < 0.77$ (i.e. in the creeping flow regime). They use 3d MRI and MRI velocimetry (MRV) to characterise the structure of the inter-particle void space and three components of velocity within the voids and compare this with the Lattice Boltzmann simulations. In both these cases the volume of interest for computational simulation is determined directly from the 3d MRI data by partitioning the void volume from the particles, and in both cases the Lattice Boltzmann method is used to perform the calculations. The equations are solved on a highly-structured lattice which has a 1-to-1 correspondence with the voxels of the MRI scan. The resulting method is very fast and efficient, but the structured lattice means that complex boundaries are pixelated. They compare the micro-structural flow from the Lattice Boltzmann simulation with detailed measurements from the MRI, but do not compare macroscopic parameters of the bed such as overall pressure drop. Johns *et al.* (2000) use MRI to analyse a similar flow regime of flow through packed beds of spherical particles in a creeping flow regime. They use an in house algorithm based on a variant of the morphological thinning technique. When applied to non-invasive methods the morphological thinning technique is a way of surface generation by means of the removal of certain foreground pixels (erosion) from the stack of grey-scale slices generating a skeletal structure from which a 3d surface can be generated (Johns *et al.*, 2000).

Sharma *et al.* (2001) have applied magnetic resonance imaging to investigate bed voidage, pressure drop and bed density in packed bed reactors. They conclude that in all cases, analysis of MRI data results in voidage values which are consistently higher than values determined from water substitution. Ren *et al.*

(2005) also use MRI coupled with velocity encoding and pulsed-field-gradient nuclear magnetic resonance (PFG-NMR) to investigate the flow structure within packed beds of cylinders and spheres with aspect ratios of $A_{ratio} = 1.4 - 32$. They conclude that radial flow structure follows an oscillatory pattern not too dissimilar to the radial porosity, reinforcing the link between porosity and interstitial velocity. In addition they concluded that the velocity in the near wall region can be up to four times the average bed velocity indicating the distinct variance in radial velocity in low aspect ratio beds.

Zhang *et al.* (2006) couple non-invasive methods with a digital packing algorithm for a packed bed of cylinders. They use the code DigiPac which combines both Monte-Carlo methods and Discrete element methods and compare this with beds analysed using micro-CT. Their algorithm allows the reconstruction of each particle with respect to its location and orientation calculated from the micro-tomography scan. Their method ameliorates fidelity issues in regard to scan resolution and signal attenuation.

2.6 Literature Review Discussion

The previous research discussed in this chapter all strives towards a common goal, which is, 'to be able to realistically model a packed bed'. Theoretical correlations attempt to model pressure drop, usually from a blend of a theoretical assumption and empirical data. However, the amount of data which can be extracted is limited. In a high aspect ratio bed, which can be considered homogeneous and isotropic these correlations, based around classic theoretical tube models, describe the pressure drop well. Whereas with low aspect ratio beds, which we know are highly disordered and heterogeneous, the majority of models do not model pressure drop well due to each case being 'individual' with its own specific bed characteristics and geometric properties. A packed bed can even have the same dimensionless quantities, but the internal structure can be considerably different affecting the flow paths and pressure drop considerably.

Many of the theoretical correlations which are intended for low aspect ratio beds try to homogenise the effects of the individual bed structure which in reality is un-homogonizeable. An example of this is the correlation proposed by Eisfeld

& Schnitzlein (2001). The wide array of data on which the statistical model is based attempts to accommodate every individual packed bed geometric case at any given Reynolds number. In reality the regression does not give a realistic value of dimensionless pressure drop for empirical data at the extremities of the data set and the spread of data can be up to one order of magnitude. Although unrealistic, each low aspect ratio bed should have its own coefficients based around the beds structural properties, failing that, beds should at least be grouped into some sort of categories for unique coefficients to be assigned. A pragmatic solution for a Scientist or Engineer is to choose a correlation which is based on the bed properties closest to the one in which the dimensional pressure drop is desired.

When more data needs to be extracted than solely pressure drop, computational methods can be applied usually in the form of computational fluid dynamics. The computational methods described in this Chapter vary considerably but are all burdened with the same issues regarding definition of the geometry and creating a workable domain for computational analysis. Linked to this are certain trade-offs e.g does a large bed with a coarse mesh provide a better representation of the flow phenomena than a fine mesh with a small number of spheres? Geometric fidelity issues also arise with comparing computational beds with experimental beds. Beds can be analysed in two ways, artificially i.e computationally; or physically and then scanned to create a computational model. The computational work containing analysis of artificially created beds is usually limited to spherical media due to the relative simplicity of a sphere location and orientation being provided by a single coordinate. In the case of spherical structured beds the domain can be defined by a simple mathematical description, however the particle contact points produce issues regarding meshing the infinitesimally small contact points and this leads to highly degenerate meshes. Attempts have been made to ameliorate this phenomena by reducing the particle volumes leaving a constant gap between particles, losing geometric faithfulness. Conversely, particle volumes have been enlarged leading to a definable contact area. In addition, simple unit cell approaches also reduce this phenomena. The one advantage of using a simple unit-cell or a structured bed approach is an experimental replica can be produced with relative simplicity in which computational data can verified

through empirical measurements using methods such as PIV or LDA. However, these experimental techniques are burdened by their own limitations.

In most real world applications of packed beds, the beds are random and disordered and cannot be analysed using structured bed approaches. In which case a non-deterministic random sampling program can be used to define the location of each particle centroid. However, issues arise using this technique regarding meshing the particle contact points and the technique is still burdened with geometric fidelity issues as a result of the mesh resolution.

The one issue with creating a random-unstructured bed computationally is the problem of reinforcing the data with empirical measurements on a geometrically faithful bed. A structured bed can be easily recreated experimentally with fidelity, however, issues arise when applying the same to random disordered beds. To compare computational random beds with experimental, an equivalent bed can be created with the same dimensional characteristics (aspect ratio, porosity), but for a randomly dumped bed of particles to have the same internal geometry as a computationally generated bed is near impossible. An equivalent bed allows typical pressure drop to be analysed with quite some accuracy, but the internal flow distributions can not be compared using this technique.

As an alternative to creating an artificial bed and comparing the data with equivalent beds a physical, experimental bed can be scanned using a non-invasive technique and reproduced computationally using surface creation software. However, this method is severely limited by the coarse scan resolution. The bed is often faithful in respect to the flow paths and broad geometry, but where particles touch certain fidelity issues can arise. Due to the scan resolution and magnetic susceptibility induced artifacts, particles merge forming necking between particles altering the bed porosity significantly.

The the author's knowledge, none of the approaches described in the literature provide an experimental geometry which is 100% geometrically faithful and thus for which the pressure drop can be compared in detail.

Chapter 3

Computational Fluid Dynamics

"If a man's wit be wandering, let him study the mathematics"

Francis Bacon

3.1 Introduction

Computational fluid dynamics, as the name suggests, is the use of a computer or computers to solve problems associated with the motion of a fluid. This is achieved in most cases by generating an approximate solution of a partial differential equation (PDE). We know that both ordinary differential (ODE) equations and partial differential equations have unknown variables which are strongly dependent on each other with no obvious, simple mathematical solution. The routes of computational fluid dynamics can be traced back to developing numerical techniques for the solution of ODEs and PDEs, ultimately leading to techniques for determining approximate solutions to the Navier-Stokes equations. Initially, finite difference (FD) approximations were the first to evolve due to their relative simplicity (Guardo, 2007). In this method a grid is created and the derivatives in the PDE are replaced with a finite difference scheme (such as Forward, Backward or central differencing) which then turns the PDE into a linear algebraic description for solution. The major constraint with this method is that before the invention of the digital calculator all calculations would have to be done by hand and even the most rudimentary linear problems involving relatively simple lapla-

cian operators would be tortuous to solve iteratively (Guardo, 2007; Richardson, 1910). Ritz (1910) developed a method for solving problems associated with elastic deformation using a method involving approximation of a potential function in terms of trial functions with undetermined coefficients, where the unknowns coefficients are determined by minimizing the potential function (Guardo, 2007). Courant (1943) further improved this technique by discretization of the control volume into triangles. Using the concepts introduced by Courant (1943), Clough (1960) developed the first complete finite element method. With the invention of the microprocessor in the 1950's these techniques were soon being solved via computer such as the work of Hess & Smith (1967), where primitive computer calculations are used to calculate the potential flow function around arbitrary bodies.

What is debatably considered to be the first numerical model which makes use of a discretized control volume and a finite difference approximation was proposed by Richardson (1910). Richardson used this method to analytically predict the weather forecast, an attempt which ultimately ended in failure (Guardo, 2007; Richardson, 1910). The first successful solution was achieved by Thom (1933) for flow past a cylinder at low velocities. The method is particularly useful for hyperbolic, parabolic conservation equations [such as the Navier-Stokes equations].

Two principle methods exist today, the continuum methods (FV and FE) and the lattice-Boltzmann method. There is much debate as to which method is most suitable for porous media flow. Vidal *et al.* (2010) suggest that discretization of the Navier-Stokes equations using the finite volume method has proved limited when analysing flow in complex geometries. As a result Vidal *et al.* (2010) suggest the Lattice-Boltzmann method is the preferred method of choice for many researchers (Nourgaliev *et al.*, 2003; Succi, 2001). Their argument is based on the ease of discretizing complex geometries by means of a simple structured lattice/grid, where the two phases are encoded with Boolean reasoning. However, the special regular uniform lattice used by LBM is limited in regard to fitting complex geometries with highly curved surfaces such as packed beds. Vidal *et al.* (2010) further argue that the inherent locality of its scheme make parallelisation straightforward and simple and in contrast to the finite volume method, the lattice-Boltzmann method requires less computational effort. This may be

the case for a simple laminar flow scenario, but Taskin (2007) suggests that a turbulence simulation using the lattice-Boltzmann method is considerably more expensive than the FV methods. However, Taskin (2007) neglect to mention whether this is compared to a direct-numerical simulation, large-eddy-simulation or a Reynolds average based model with a suitable closure term. As a rebuttal to the arguments of Vidal *et al.* (2010), if the finite volume technique was applied to a primitive, block structured lattice, as in the case of the lattice-Boltzmann method, one might ask the question 'would there be any difference in the computational expense?'. The relatively high computational expense associated with the FVM is primarily due to solving the governing equations for the complex unstructured meshing options which are availible in the FV method for meshing highly curved surfaces.

Al-Jahmany *et al.* (2009) compare the LBM and finite volume method over a backwards facing step. Al-Jahmany *et al.* (2009) et al conclude that in this case the LB method is in good agreement with the FV method. However their study is limited to a backwards facing step in which a block-structured lattice-can be constructed with ease. If the same test was applied to a complex-highly curved geometry it is likely that the LB method would not perform as well.

Many computational fluid dynamics solvers such as Fluent, have a built in porous medium solver, where a porous volume (3d) or porous jump (2d) can be inserted in a flow geometry to model the effect of the porous medium. These porous medium solvers to not calculate the micro-structural flow but more the effect on the porous medium has on the external flow and treat the media volume as a bulk or gross entity with homogeneous properties. They also rely on empirically based coefficients such as inputs for Darcy's Law or the Ergun equation to calculate the pressure drop caused by the media. Although limited, their use is mainly focused on the flow effects of the porous media on the flow domain, which constitutes a relatively small element of geometry. In contrast, the work presented here aims to simulate the microstructural flow, and could be used to determine the coefficients for such porous media models.

3.2 The Finite Volume Method in CFD

A CFD code using the finite volume method is based around the solution of the governing flow equations (Navier-Stokes). The solver achieves this by integrating the flow equations over the entire flow domain. The unknown properties of the flow are replaced with finite difference approximations which are approximated iteratively with a guess and correct procedure. To write a CFD code to deliver a solution for every new fluid flow case would be time consuming and unforgiving. Due to this, general commercial CFD codes have evolved, such as Fluent, CFX and OpenFoam. They provide user friendly GUIs (graphical user interfaces) to allow the user to utilize an in built code with a variety of problem solving facilities to deliver a solution for problems associated with fluid flow, heat transfer etc. To describe the whole process can be long winded, so for simplicity, the process of generating a solution to a fluid problem using a general CFD code is described in three stages; the pre-processor, the solver and the post-processor.

3.3 The pre-processor

The first step involved in the pre-processor stage is to define a suitable geometry in which the fluid flow problem is to be analysed. Defining the geometry can be achieved by replicating a known geometry through computer aided design (CAD) in the case of relatively simple geometries. For more complex natural geometries the geometries may be probed using a non-invasive technique, such as MRI or CT coupled with some sort of geometry defining algorithm. Once the geometry has been created a suitable mesh can be constructed. A mesh can be described as a volume which has been discretized into a series of smaller volumes or elements. This can be straight forward in the case of simple geometries, but more challenging in highly disordered media such as a packed beds or porous mediums. Once a workable mesh has been created, additional known quantities of the fluid are defined such as density, viscosity and turbulent quantities. Boundary conditions are applied to cell faces in the form of a flux adjacent to an inlet/exit or wall such as temperature, pressure, velocity profile etc. This can be argued as being

the most crucial stage in the development of a solution, as the determination of a realistic answer is highly dependent on the global mesh quality.

3.3.1 Mesh structure

Cells which make up the mesh come in a variety of shapes and sizes applicable to specific cases. Usually cells are tetrahedral or cubic, although recently polyhedral cells have been used. We can classify grids or meshes as being either structured or un-structured (Fig 3.1). What makes a grid structured is that each of its cells can be ordered in respect to their indices (usually i, j, k or $1, 2, 3$). In the case of a irregular, disordered packed bed the use of a structured grid would be near on impossible due to the complex geometry and the representation of spherical particles. In addition, it would be impossible to trace a single line through the bed in order for the bed to be ordered by its indices due to the obstruction of the media. Unstructured grids the cells are not ordered in respect to their indices but with some other fashion specified within the CFD code. Most modern CFD solvers, such as Fluent, CFX, can handle both structured and unstructured grids. There is no difference in the accuracy between structured and unstructured grids. However, Structured codes have the advantage that the cell adressing is simpler and less costly; then the code runs faster. However, structured grids are limited to fairly rudimentary geometries. Hybrid grids also exist in which the mesh can be block structured in regions of open space and then become unstructured in areas of complex geometrical restriction. A Mesh can also be categorised as being coarse or fine. A coarse mesh would contain a relatively low cell density per unit volume with large cells, whereas are a fine mesh would contain a densely populated flow domain with cell small volumes.

—

3.3.2 Traditional CAD mesh generation

Traditional mesh generation methods use a CAD based approach, in which CAD program is used to define a geometry. The geometry can be created in tertiary CAD software, such as AutoCAD or SolidWorks and then imported into a commercial meshing package, such as ANSYS Gambit in a suitable file format (STL,

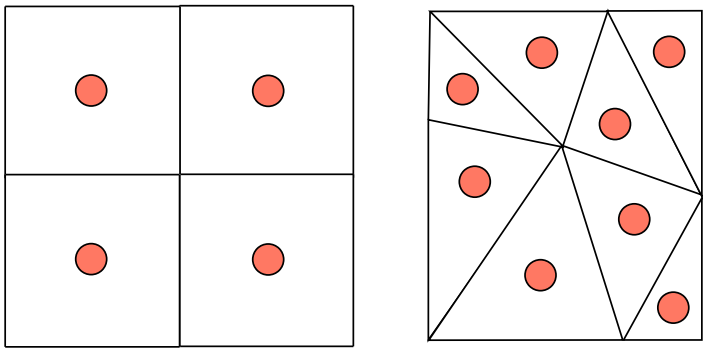

Figure 3.1: Left; Structured grid, Right; unstructured grid

ACIS, IGES). Alternatively, some commercial meshing software, such as Gambit have a built-in CAD interface which allows the control volume and the bounding surfaces to be created in the software directly, to avoid file format conflictions. Once the control volume and surfaces have been defined, volume discretizations are created from the bounding surfaces using meshing algorithms such as advancing front (AF), Delaunay triangulation (DT) , octree etc. CAD based approaches work well for simple geometries, but complications arise in their application in converting non-invasive image data into a suitable mesh for analysis and often require considerable user intervention and appreciable simplification of the model geometry (Antiga *et al.*, 2002; Cebral & Loehner, 2001; Young *et al.*, 2008). The user intervention usually requires an 'intermediate step' in which the image data is converted into suitable surfaces in form of a CAD geometry which can then be imported into commercial meshing software. This 'intermediate step' often results in the process being time consuming and unrobust (Young *et al.*, 2008). If a workable mesh can be created, it often contains highly skewed and degenerate elements.

The advancing front method of mesh creation originally proposed by van Phai (1982), requires an initial discretization of the domain surface into triangles. A layer of nodes is then offset from the surface creating the first layer of nodes and

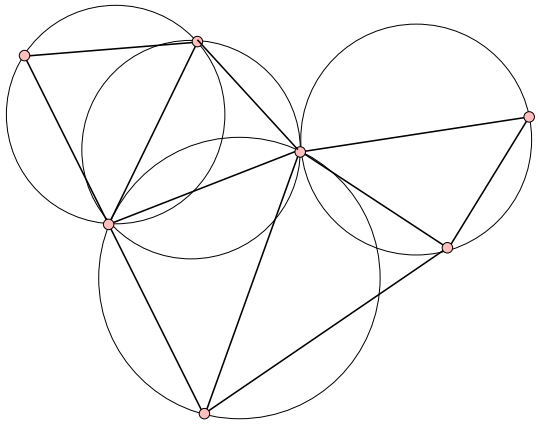

Figure 3.2: Delaunay triangulation of a series of points

tetrahedral volumes. The next layer then 'piggy backs' off the first layer of nodes creating the second layer of tetrahedral cells (Young *et al.*, 2008). However, this method is unrobust when creating meshes where either the initial surface triangulation is poor or where there is insufficient room for advancement.

The Delaunay mesh algorithm or Delaunay tetrahedralizations is the most commonly used and is based on the Delaunay triangulation criterion proposed by Delaunay (1934) or 'empty sphere theory'. In 2d, a Delaunay triangulation is a way of joining a collection points in which groups of three points are joined which fall on the circumference of a circle as shown in 3.2 and this ensures that no point falls within the boundary of another circle. This method can be gereralised to 3d using spheres and tetrahedrons.

The octree meshing algorithm developed by Shepard *et al.* (1988) is a meshing strategy based on cubic cells being recursively subdivided into smaller cells. The octree method does not originate from an existing surface mesh, such as Delaunay or advancing front, but adapts the grid to account for the surface. The cubes that intersect the surface are subdivided and tetrahedral elements are formed to body fit the surface the surface.

3.3.3 Image based mesh generation

Image based meshing (voxel based IBM) is a method of surface extraction from an image, usually a grey-scale image slice from a scanned image extracted from MRI, CT or another non-invasive technique, in which a computational mesh is created for computational fluid dynamics or finite element analysis. It is not solely a meshing algorithm such as Delaunay or Octree but encompasses the whole process of surface extraction and mesh creation (Young *et al.*, 2008).

Non-invasive techniques, create a 3-dimensional image by taking a series of 2-dimensional grey-scale-voxelised slices through the sample, known as a stack. These are often stored in a unique format specific to medicine known as DICOM (Digital Imaging and Communications in Medicine). The stack of slices can be imported into image based meshing software such as ScanIP (Simpleware, Exeter UK) in which the VOI can be segmented by a method of simple thresholding. Thresholding is one of of the simplest forms of image segmentation techniques and relies on the 0-256 grey-scale. A threshold value is set by the user (between 0 and 256) all of the pixels with a value below the threshold are considered background pixels and all pixels above the threshold are treated as the image (or vice-versa) binarising the image into two or possibly more masks. In the case of packed beds an image, ideally would be completely binary, consisting of the particulate matter and the void volume allow simple accurate segmentation between the media. In addition to the voxel based IBM is CAD-based IBM; a CAD surface is identified and extracted for for meshing using (pre-existing) meshers.

One disadvantage with this approach is the uniformity in mesh density. In open expanses contained within the geometry where the flow is unlikely to have any special features, the density of the mesh is likely to be too fine resulting in a considerable amount of unnecessary computational effort. However, viewed from another angle the mesh is perfectly structured in these regions meaning relative efficiency in calculation considering the high amount of computational effort. Recent research (Young *et al.*, 2008) has shown that the number of cells can be greatly reduced in the effected areas using an octree decimation scheme.

Image based meshing provides increased robustness in creating meshes in the most tortuous of geometries which traditional Delaunay based approaches would

find near impossible without user intervention and considerable manual simplification of the geometry.

3.3.4 Mesh quality analysis

Regardless of the type of mesh it is paramount that the mesh is significantly fine enough and of a sufficient quality not to compromise the solution. To ensure this is the case it is desirable to conduct a mesh refinement. A mesh refinement study consists of a mesh being constructed in the desired geometry and a flow problem simulated. A suitable parameter is monitored, usually the parameter of interest such as lift, drag pressure drop etc. The mesh is continuously refined and in most cases the answer will change. The mesh is refined further until eventually the answer will stabilise and subsequent refinement will yield a similar answer with no significant change. In a turbulent time dependent flow, transient effects may cause the solution to vary even after a mesh is considered independent. In some highly complex geometries the created mesh may be already fine enough and in which case as the mesh is refined the solution will remain stable. The IBM approach can be problemistic in that the geometry itself may change with refinement. Over refinement may also be an issue; turbulence models have restrictions on cell sizes in the wall region in regard to suitable $y+$ values. The $y+$ value is the dimensionless wall distance; this is given as the frictional velocity ($u*$) multiplied by the cell node disctance from the wall (y), as a ratio of the kinematic viscosity (ν).

An argument surrounding a mesh refinement study is which property should be monitored to determine whether the mesh is independent of the solution. For example, the mesh being analysed may have been found to independent of the global properties (e.g pressure drop, lift and drag), but is still not fine enough to be independent of the local properties of the flow. In the case of packed beds, the pressure drop is highly dependent on the flow geometry. The bed contains many small pores, in which case a workable mesh is likely to be already sufficiently fine to constitute an independent mesh. Any further refinement is not likely to affect the global property of pressure drop (the property being monitored) but may affect local properties such as recirculation. A pragmatic approach is to

monitor the desired property of the flow to be determined, once this has stabilised, regardless of the other flow properties, the mesh can be considered sufficiently independent from the solution at least for the problem in question.

A mesh refinement study ensures the mesh is fine enough not to be affecting the solution. However, the cells must be of a sufficient quality not to affect the solution. One measure of the cell quality is the skewness which is described by its deviation from a 'perfect cell'. Cells which are significantly skewed (slithers) can lead to solution instability and convergence problems.

In the case of some complex geometries such as packed beds skewed elements are more or less unavoidable due to the curved surfaces and infinitesimally small contact points observed in spherical beds. Some packages provide a skewness compensation algorithm, such as Fluent with the PISO algorithm and additionally the facility to merge skewed elements with neighbouring cells to create a single polyhedral element from a number of degenerate tetrahedrons. Various

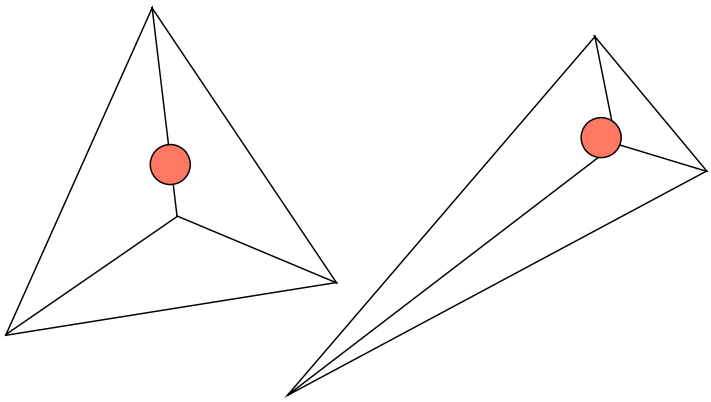

Figure 3.3: Left; perfect tetrahedral cell, Right; highly skewed degenerate cell

metrics of skewness are available. One approach is to use the equiangle skewness based on the angle deviation method given as

$$E_{ang} = max\left[\frac{\theta_{max} - \theta_{equal}}{180 - \theta_{equal}}, \frac{\theta_{max} - \theta_{equal}}{\theta_{equal}}\right] \tag{3.1}$$

where θ_{min} and θ_{max} are the respectively the maximum and minimum angles between any two edges of the cell, and θ_{equal} is the ideal angle for an equilateral (perfect) cell. In which case an equilateral "perfect cell" will have a skewness of 0 (Cengel & Cimbala, 2006). This method can be applied to any mesh structure or cell type.

Another approach is to use the dimensionless form of equivolume skew (E_V). The cell equivolume skew uses the volume deviation method given in the form

$$E_V = \frac{V_O - V_C}{V_O} \tag{3.2}$$

where the V_O is the optimal cell size of an equilateral cell with the same circumradii and V_C is the cell size. The equivolume skew method only applies to tetrahedral and triangular elements. In both cases, the cell equivolume/equiangle skew of 0 indicates a 'perfect' cell and 1 indicates a highly skewed, completely degenerate element.

Another parameter widely recognised in the field is known as the cell squish index (CSk_{index}). The cell squish index uses the dot-product (scalar products) of each vector pointing from the centroid (the node location) of the cell to each of the cell faces and the face area vector associated with each face given as

$$CSk_{index} = max\left[1 - \frac{\underline{A_i}.\underline{r}_{c0/xfi}}{|\underline{A_i}||\underline{r}_{c0/xfi}|}\right] \tag{3.3}$$

where $\underline{A_i}$ are the cell face area vectors and $\underline{r}_{c0/xfi}$ are the vectors connecting the cell centre to the respective face centre. The closer the CSk_{index} value is to 1, the more degenerate the cell.

All of the mesh quality assessment methods described here are bulk quantities. Statistically a mesh can appear good quality i.e 97% of the cells have a squish index of less than 5, but the 3% degenerate cells lead to convergence problems and instability in the solution. Meshing a random un-structured packed bed is particularly difficult, not only from its disordered structure, but additionally because is contains many spherical particles with many contact points. We know that a sphere is an infinitely sided volume and therefore touches with a neighbouring sphere at an infinitely small contact point. In which case the adopted

meshing algorithm has to compensate by either producing a slithered element, or increasing the contact point to the minimal cell size. (Young *et al.*, 2008) compared the EVoMaC method (ScanIP, ScanFE) to the Delaunay triangulation approach used in Ansys Gambit, using Fluent's mesh verification tool and showed that for an open cell foam the EVoMaC method displayed a considerably better quality mesh in regard to the cell squish index. Cavendish *et al.* (1985) suggest that the Delaunay mesh generation technique is prone to creating highly skewed (slivered) elements.

3.4 The solver

In the FV method the solver is considered as the calculation process that ultimately leads to a solution of the transport equations. The first step in the process is to integrate the equations over all of the finite volumes contained within the mesh. Finite difference approximations (interpolations) are then substituted for terms in the transport equations representing the flow variables. The resulting approximations are then solved using an iterative 'guess and correct' procedure.

The transport equation is a PDE which describes the transport phenomena of properties such as heat, mass, momentum transfer, turbulence etc. The general incompressible, time dependent transport equation is described as

$$\rho\left[\frac{\partial \phi_e}{\partial t} + \nabla.\phi_e \underline{u}\right] = \nabla.\Gamma\nabla\underline{\phi_e} + S_{\phi_e} \tag{3.4}$$

here, ρ is the fluid density and is a constant as we are dealing with incompressible flow, ϕ_e is some conservative property of the fluid and S_{ϕ_e} is a sink term. Integrating this across the control volume gives

$$\int_{cv} \rho\frac{\partial \phi_e}{\partial t}dV + \int_{cv} \rho\nabla.\phi_e\underline{u}dV = \int_{cv} \nabla.\Gamma\nabla\underline{\phi_e}dV + \int_{cv} S_{\phi_e}dV \tag{3.5}$$

Gauss' theorem (divergence theorem) is used to convert the spatial derivative term $\nabla.(\underline{\phi_t}\ \underline{u})$ into a surface integral of the flux across the cell faces, which converts the governing equations into a set of difference equations which can be

solved numerically. Guass's theorem is given as

$$\int_{cv} \nabla \underline{a} dV = \int_A \underline{n}.\underline{a} dA \tag{3.6}$$

applying this to 3.5

$$\frac{\partial \phi}{\partial t}\left(\int_{cv} \rho \underline{u} dV \right) + \int_A \rho \underline{n}.\phi \underline{u} dA = \int_A n.\Gamma \nabla \phi dA + \int_{cv} S_\phi dV \tag{3.7}$$

In time dependent problems a further integration is required over a small interval of $t + \Delta t$ resulting in

$$\int_{\Delta t} \frac{\partial \phi}{\partial t} + \left(\int_{cv} \rho \underline{u} dV dt \right) + \int_{\Delta t} \int_A \rho \underline{n}.\phi \underline{u} dA dt = \int_{\Delta t} \int_A n.\Gamma \nabla \phi dA dt + \int_{\Delta t} \int_{cv} S_\phi dV dt \tag{3.8}$$

Finite difference approximations are substituted in for the flow variables in the integrated transport equation to convert the integrals into algebraic equations. These difference approximations can include backwards differencing, central differencing and upwind schemes and combinations and variants depending on the level of precision desired. The algebraic equations are then solved using an iterative 'guess and correct' procedure. The guess and correct algorithms are given appropriate acronyms, such as SIMPLE, PISO, SIMPLEC etc. Initially the velocity field approximation is determined by solving the momentum equation, and the pressure gradient is used from the previous iteration to determine the pressure distribution forming "the guess" in the procedure. The momentum equation is rearranged to form a Poisson equation for the pressure (the pressure equation) which can be solved to update the guessed pressure, and the velocities are corrected to form a new set of conservative fluxes as depicted in Fig 3.4. The SIMPLE algorithm (semi-implicit method for linked equations) is one example of the guess and correct procedure for the calculation of pressure developed by S.V.Patankar & D.B.Spalding (1972). The procedure formulated as a result of two unknowns and in which case the pressure cannot be calculated until the velocity is determined and the velocity cannot be calculated until the pressure is determined. Due to this, one is guessed and the other is then corrected. The acronym PISO, meaning Pressure Implicit with Splitting of Operators or the

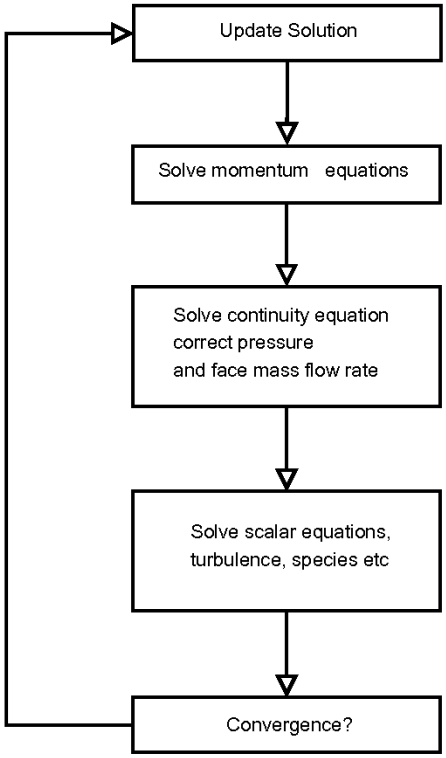

Figure 3.4: Iterative loop

'PISO loop', involves a single predictor step and two corrector steps (Versteeg & Malalasekera, 1995). The PISO algorithm is therefore a more advanced SIMPLE algorithm with the inclusion of an extra corrector step for enhancement (Versteeg & Malalasekera, 1995). The SIMPLEC and PIMPLE algorithms are derivatives of SIMPLE and PISO tuned for specific cases.

3.4.1 The Navier-Stokes Equations

The Navier-Stokes equations are the principal equations used in the finite volume method. They form a set of deterministic non-linear, second order, partial differential equations and are the governing equations of a Newtonian fluid which may be a liquid or a gas (Drazin & Riley, 2006). The Navier-Stokes equations can essentially be broken down into three fundamental principles which include,

the conservation of mass, the conservation of momentum (Newton's second law) and the conservation of energy (Douglas *et al.*, 2005) i.e the first law of thermodynamics.

The Navier-Stokes equations were deduced by Stokes (1846, 1880) from a selection of hypothesis and postulations of Navier (1827); Poisson (1831); Saint-Venant (1843) and Stokes (1845) leading to a rational derivation of the equations that we are familiar with today (Drazin & Riley, 2006). For an incompressible laminar flow (stream-flow) the Navier-Stokes equations are described by, the equations can be written in the differential Eulerian form,

$$\nabla.\underline{u} = 0 \tag{3.9}$$

$$\rho\left[\frac{\partial u}{\partial t} + \nabla.\underline{uu}\right] = -\nabla p + \mu\nabla^2\underline{u} + F \tag{3.10}$$

where $\partial u/\partial t$ is unsteady acceleration, $\nabla.uu$ is convective or advective term, and $-\nabla p$ is the pressure gradient. For a steady incompressible fluid, $\partial u/\partial t$ and $\frac{\partial \rho}{\partial t}$ are omitted from the equation to eliminate fluctuations in velocity due to time and change in density with respect to time yielding

$$\nabla.\underline{u} = 0 \tag{3.11}$$

$$\rho\nabla.\underline{u} = -\nabla p + \mu\nabla^2\underline{u} + F \tag{3.12}$$

A flow can be considered incompressible if $\Delta P < 5\%$ and the flow velocity is less than $100m/s$ in air ($M < 0.3$) (Cengel & Cimbala, 2006). Only a hand full of exact solutions exist for the Navier-Stokes equations, such as Stokes Boundary layer, the Taylor Green vortex, Hagen Poiselle flow (laminar, steady flow through a circular pipe) and Couette flow (the flow between two flat plates). In many cases exact solutions only exist due to certain assumptions and terms being considered as negligible. It could be argued that no terms in the equation can equate to exactly zero. For example, unsteady effects could be so minute ($\partial U/\partial t << 0$) that they are unmeasurable and therefore a flow could be assumed to be steady-state.

In complex geometries such as flow through packed beds, the 3d Navier stokes

equations have no exact solution (as with most cases), when solving the equations computationally the iterative nature does there is no guarantee that an exact answer will exist. However, formulations do exist to model the permeability of porous media deduced from the Navier-Stokes equations, such as the work of (Azzam & Dullien, 1976). This assumes the medium to be homogeneous. Similarly, Whitaker (1996) show that the Darcy's Law with the Forcheimer correction can be deduced using volume averaging from the Navier-Stokes equations.

3.4.2 Modelling turbulence

> "[Turbulence], the invention of the Devil on the 7th day of creation".
> Bradshaw (1994)

We have discussed that turbulence is pseudo-random, stochastic and unsteady in nature and notoriously difficult to model. We use the term pseudo-random because the turbulent eddies are deterministic but the occurrences are random. In many engineering flows we are not interested in the turbulent structure itself or occurrences, but more so the location of turbulence, the intensity and its effects on the surroundings. To study the turbulent structure itself requires a direct numerical simulation (DNS). A DNS approach allows the complete (approximate) solution of the Navier-Stokes equations without an additional turbulence modelling. The mesh is fine enough to attempt to en-capture the smallest unsteady turbulent vortices (governed by the Kolmogorov length scale) and the smallest turbulent frequencies and events. A DNS approach is by far the most accurate way to model a full turbulent regime as it can resolve a time dependent vortex structure, but the computational expense increases steeply with respect the Reynolds number (Tennekes & Lumley, 1972). Although DNS represents an accurate representation of turbulence, it is impossible for any model to completely replicate the exact time dependent turbulent structure at a discrete point in time due to the random, stochastic nature of turbulence. Ferziger & Perić (1996) highlight the limitations on computer power by suggesting that in a flow domain of $0.1m^2$ in a high Reynolds regime, might contain vortices as small as $100\mu m$ in size and would require a computational mesh of around 1×10^{12} to be able to capture the smallest turbulent structures. In addition Ferziger & Perić

(1996) suggest limitations on the time-step as the fastest events take place around 10kHz, in which case a time-step of around $100\mu m$ would be needed. Speziale (1991) (although dated) stated that a DNS approach on a simple turbulent pipe at a Reynolds number of 500000 would require a supercomputer that is 10 million times more powerful than the fastest supercomputer availible at the time. Even with the non-linear growth of computing technology it is still not expected that a full DNS approach could be possible for analysing a whole aircraft for several decades (Cengel & Cimbala, 2006). With relevance to this work, DNS has been applied to flow through porous media (Morais *et al.*, 1970), however, this was used to model a steady-state, laminar non-Newtonian fluid, which requires substantially less computational power than a DNS approach on a fully turbulent, compressible, time dependent flow.

As an alternative to a DNS approach, an averaging procedure can be applied to the Navier-Stokes equations by decomposition of the flow variables in which various models are formulated to model the effect of turbulence. This averaging can either be space filtered, such as large eddy simulation (LES) or ensemble-averaged, such as the Reynolds averaged Navier-Stokes (RANS) equations. The averaged Navier-Stokes equations do not model the exact turbulent structure, but give an indication of the location of turbulence and its intensity. Ferziger & Perić (1996) suggest that due to the complex nature of turbulence, it is improbable that the turbulence model will represent all turbulent flow and in which case should be considered as an engineering approximation.

The RANS approach is the most widely used in industry. In commercial engineering the ultimate goal is to make money, now and in the future. To do this using CFD, a good job is not only a job which is accurate with a suitable level of precision, but also takes a reasonable amount of time to make it cost effective. The exact mathematics concerned with turbulence is too complex to be implemented and would produce far more information than what is required for most engineering flows. A turbulence model is applied to simplify the mathematics. Turbulence models can be separated into two classifications. The first are the classical models and based on the averaged Reynolds equations, the second are based on space-filtered averaging such as Large-Eddy Simulation. A RANS based

approach is far cheaper than LES or a DNS approach and provides a suitable level of accuracy for most industrial engineering flows.

3.4.3 Reynolds-Averaged Navier-Stokes (RANS)

In many engineering flows the motion is turbulent and unsteady. A full time dependent solution of the Navier-Stokes for a high Reynolds flow regime in complex geometries is not likely to occur in the near future. In which case certain assumptions can be made about the flow to give a realistic engineering approximation accounting for the effect of turbulence rather than the turbulent structure itself. This is achieved by averaging out any unsteady behaviour forming the Reynolds averaged Navier-Stokes (RANS) equations. The Reynolds average method relies on averaging out all of the unsteadiness within the flow and considers all unsteadiness is a result of turbulence. If we imagine a plot of a turbulent flow velocity, u, we can decompose this into a mean component ($\widehat{u}$) and fluctuation around this mean (u')

$$u = \widehat{u} + u' \tag{3.13}$$

The same decomposition can also be applied to an ensemble of the other flow properties. Now every flow variable can be written in the form of the sum of the time averaged value, $\widehat{\phi}$ and fluctuating value around the mean, $\widehat{\phi}'$

$$\phi(t) = \widehat{\phi} + \phi' \tag{3.14}$$

The requirement is to define what is meant by this average. One convenient approach is to define the time average;

$$\widehat{\phi} = \frac{1}{\Delta t}\int (t)dt \tag{3.15}$$

where t is the averaging interval. The averaging interval must be considerably larger than the frequency of the fluctuations in order to capture a significant number of events. The flow variable can be now expressed as

$$\widehat{\phi'} = \frac{1}{\Delta t}\int \phi'(t)dt \equiv 0 \tag{3.16}$$

From these basic equations a set of rules can be derived and applied to the Navier-Stokes equations. The rules are applied to the unsteady accellerative term, the pressure term and divergence of stress term, the flow is incompressible so no averaging is applied to the density, ρ. Re-writing this for for simplicity in all x, y and z components yields the x, y and z-momentum equations in the form of

$$\rho\left[\frac{\partial u_x}{\partial t} + \nabla.\underline{\widehat{u}_x}\,\underline{\widehat{u}} + \nabla.\widehat{u'_x\underline{u'_x}}\right] = -\frac{\partial \widehat{p}}{\partial x} + \mu\nabla^2\,\widehat{u}_x \tag{3.17}$$

$$\rho\left[\frac{\partial u_y}{\partial t} + \nabla.\underline{\widehat{u}_y}\,\underline{\widehat{u}} + \nabla.\widehat{u'_y\underline{u'_y}}\right] = -\frac{\partial \widehat{p}}{\partial y} + \mu\nabla^2\,\widehat{u}_y \tag{3.18}$$

$$\rho\left[\frac{\partial u_z}{\partial t} + \nabla.\underline{\widehat{u}_z}\,\underline{\widehat{u}} + \nabla.\widehat{u'_x\underline{u'_x}}\right] = -\frac{\partial \widehat{p}}{\partial z} + \mu\nabla^2\,\widehat{u}_z \tag{3.19}$$

writing out with a single operator for x, y and z components gives the RANS equations

$$\rho\left[\frac{\partial u}{\partial t} + \nabla.\underline{\widehat{u}}\,\underline{\widehat{u}} + \Re\right] = -\nabla p + \mu\nabla^2.\underline{\widehat{u}} \tag{3.20}$$

where the fluctuating component $\nabla.\widehat{\underline{u'_x}\underline{u'}}, \nabla.\widehat{\underline{u'_y}\underline{u'}}$ and $\nabla.\widehat{\underline{u'_z}\underline{u'}}$ have now become the Reynolds stresses, $\Re$. Writing these in their partial differential form gives

$$\Re_x = \left[-\frac{\partial \widehat{u'^2_x}}{\partial x} - \frac{\partial \widehat{u'_x u'_y}}{\partial y} - \frac{\partial \widehat{u'}_x u'_z}{\partial z}\right] \tag{3.21}$$

$$\Re_y = \left[-\frac{\partial \widehat{u'_x u'_y}}{\partial x} - \frac{\partial \widehat{u'^2_y}}{\partial y} - \frac{\partial \widehat{u'_y u'_z}}{\partial z}\right] \tag{3.22}$$

$$\Re_z = \left[-\frac{\partial \widehat{u'_x u'_z}}{\partial x} - \frac{\partial \widehat{u'_y u'_z}}{\partial y} - \frac{\partial \widehat{u'^2_z}}{\partial z}\right] \tag{3.23}$$

As a result, three normal stresses and three shear stresses are produced (Reynolds Stresses)

$$\tau_{xx} = -\rho u'^2_x \qquad \tau_{yy} = -\rho u'^2_y \qquad \tau_{zz} = -\rho u'^2_z \tag{3.24}$$

$$\tau_{xy} = \tau_{yx} = -\rho\widehat{u'_x u'_y} \qquad \tau_{xz} = \tau_{zx} = -\rho\widehat{-u'_x u'_z} \qquad \tau_{zy} = \tau_{yz} = -\rho\widehat{u'_x u'_y} \tag{3.25}$$

The momentum equations are a set of equations containing four unknown quantities, u_x, u_y, u_z and p. The additional term $\Re$ represents turbulence where the fluctuating terms have been averaged out by the averaging procedure. In which case any turbulent fluctuations will be presented as an average around the mean flow. As a result of the averaging procedure the Reynolds stresses have themselves also generated six other additional unknowns. In order to close the equations a turbulence model is introduced.

3.4.4 Turbulence models for RANS

In this work, we refer to a turbulence model as a closure term for the RANS equations based on certain assumptions of the flow. Because turbulence is chaotic and stochastic, turbulence models are grossly simplified and therefore should be considered as an engineering approximation. There are no general purpose turbulence models for every situation, however models such as the $k - \varepsilon_t$ and $k - \omega$ are the closest to what can be considered 'general purpose' due to their stability and general good behaviour in most cases. In the majority of cases turbulence models are specialised and are optimised for a particular type of flow and therefore must be chosen carefully.

> "All [turbulence] models are wrong, but some models are useful"
> George. P. E. Box

In choosing a suitable closure term user must weigh up the implications of a particular turbulence model, usually influenced by the Reynolds number, the flow geometry, cost implications and desirable properties which need to be extracted from the solution.

A brief example comparing different solvers in porous media can be found in the work of Kuwahara *et al.* (2006). They compare LES with the low Reynolds number $k - \varepsilon$ model applied to turbulent flow through packed beds of cylinders. LES and $k - \varepsilon$ are in good agreement with each other when analysing the flow structure from plots of velocity vectors but show a surprising difference in respect to the production of turbulent kinetic energy. According to Kuwahara *et al.* (2006), the $k - \varepsilon$ coupled with the effective velocity formulation is renowned for over estimating turbulent kinetic energy around a stagnation point.

Turbulence models can be separated into two classifications. The first are the classical models and based on the averaged Reynolds equations, the second are based on space-filtered averaging such as Large-Eddy Simulation. The classical models are traditionally the most widely used in engineering purposes, such as the mixing length model, the $k-\varepsilon$ and the $k-\omega$ models. These are all based around Newton's theory that there is an analogy between the viscous stresses and Reynold's stresses on the mean flow (Landahl & Mollo-Christensen, 1986). Newton's law of viscosity states that the viscous forces are linearly proportional to the fluids rate of deformation, analogous to Hooke's law of stress and strain. For an incompressible Newtonian fluid, written in Einstein index notation gives

$$\tau_{ij} = \mu_{ij} = \mu\left(\frac{\partial u_i}{\partial x_j} + \frac{\partial u_j}{\partial x_i}\right) \tag{3.26}$$

A turbulent vortex will decay unless there is a shear stress present, such as flow passing a cavity. And as stated in Newton's law of viscosity as the turbulent stress increases the turbulent rate of deformation also increases. What is described as being the earliest turbulence model is that of French mathematician Bousinesq (1877). Bousinesq (1877) hypothesised that the Reynolds stress terms are linked to the mean rate in deformation, suggesting that turbulence could be modelled as a laminar flow with enhancement of the viscosity (Landahl & Mollo-Christensen, 1986) giving

$$\tau_{ij} = -\rho\widehat{\underline{u}_i'}\widehat{\underline{u}_j'} = \mu_t\left(\frac{\partial\,\widehat{u}_i}{\partial x_j} + \frac{\partial\,\widehat{u}_j}{\partial x_i}\right) \tag{3.27}$$

where μ_t is the eddy viscosity or turbulent viscosity and assumed to be constant. The eddy viscosity is not a property of the fluid but a fictional viscosity based on dimensional reasoning to account for turbulence. The Boussinesq hypothesis on its own is not enough to model turbulence unless its values are known. From equation 3.27 we can see that turbulent momentum transport is proportional to the mean gradients in velocity and hence the transport of turbulence is given to be proportional to the gradient of the mean value of the transport quantity

$$-\widehat{\rho\underline{u}_i'\underline{\phi}_j'} = \Gamma_t\frac{\partial\phi}{\partial x_i} \tag{3.28}$$

where Γ_t is turbulent diffusivity. This forms the basis of the Prandtl mixing length model as discussed in the succeeding section. Because a turbulent vortex is damped by viscous effects, the turbulent diffusivity, Γ_t is likely to be close to the value of turbulent viscosity, μ_t giving the Prandtl-Schmidt relation

$$\sigma_t = \frac{\mu_t}{\Gamma_t} \tag{3.29}$$

experiments have shown that in most cases the Prandtl/Smhmidt relation is nearly a constant (Versteeg & Malalasekera, 1995).

3.4.5 Two equation models

A two equation model is an eddy viscosity model which has two additional transport equations to account turbulent properties in the flow. Here, the most common two equation turbulence models are discussed, the $k-\varepsilon$ and the $k-\omega$ model. In both cases, k accounts for the turbulent kinetic energy and ε_t and ω are dissipative terms which describe the turbulent scales. Due to the complex mathematical description of the two linked equations, these models require significantly more computational effort than a mixing length model, but are still significantly computationally cheaper in comparison to a DNS approach.

3.4.5.1 The $k-\varepsilon_t$ model

Here the general $k-\varepsilon_t$ model is discussed, in reality $k-\varepsilon_t$ is a family of models where specific adaptations have been implemented for it to model specific cases such as Launder, Chien etc. As its name implies, the $k-\varepsilon_t$ equation is described by two transport equations, the first is turbulent kinetic energy (k) is described by the PDE

$$\frac{\partial}{\partial t}(\rho\kappa) + \nabla.(\rho\kappa u_i) = \nabla.\left[\left(\mu + \frac{\mu_t}{\sigma_\kappa}\right)\frac{\partial \kappa}{\partial x_j}\right] + P_\kappa + P_b - \rho\varepsilon_t - Y - M + S_\kappa \tag{3.30}$$

and dissipation, ε by

$$\frac{\partial}{\partial t}(\rho\varepsilon_t) + \nabla.(\rho\varepsilon_t u_i) = \nabla.\left[\left(\mu + \frac{\mu_t}{\sigma_\kappa}\right)\frac{\partial\varepsilon_t}{\partial x_j}\right] + C_{1\varepsilon}\frac{\varepsilon}{\kappa}(P_\kappa + C_{3\varepsilon}P_b) - C_{2\varepsilon-t}\rho\frac{\varepsilon_t^2}{\kappa} + S_{\varepsilon_t} \tag{3.31}$$

where

$$P_\kappa = \mu_t S^2 \tag{3.32}$$

S is defined as the mean rate of strain given as

$$S = \left[2S_{ij}S_{ij}\right]^{1/2} \tag{3.33}$$

where the empirical numerical constants are given as $C_{1\varepsilon_t} = 1.44$, $C_{2\varepsilon_t} = 1.92$, $C_\mu = 0.09$, $\sigma_\kappa = 1.0$ and $\sigma_{\varepsilon_t} = 1.3$ derived from a wide range of experimental data on air and water. However, these coefficients are only valid for fully turbulent flows (Menter, 1993).

As with the one equation models, the turbulent viscosity is described on dimensional grounds as

$$\mu_t = C\rho\vartheta\ell = \rho C_\mu\frac{\kappa^2}{\varepsilon_t}$$

the velocity scale and the length scales are related to the kinetic energy and dissipation in the form

$$\vartheta = \sqrt{k} \qquad \ell = \frac{k^{3/2}}{\varepsilon_t} \tag{3.34}$$

We can see from this that the turbulent viscosity is only calculated from a single length scale and in which case the turbulent diffusion is only based on the calculated length scale. In reality all length scales throughout the spectrum contribute to turbulent diffusion.

The $k-\varepsilon_t$ model is considered "the initial port of call" in respect to it being the most widely applied and considered the most validated turbulence model. Although it models most industrial flows well, it performs poorly in cases such as some unconfined flows, flows with curved boundary conditions and fully developed flows in non-circular ducts (Versteeg & Malalasekera, 1995). In addition, the assumption with the $k-\varepsilon_t$ is the effects of the molecular viscosity are negligible and therefore the flow is considered to be fully turbulent.

3.4.5.2 The $k-\omega$ model

Another popular two equation model is the low Reynolds 'Standard' $k-\omega$ model proposed by Wilcox (1993). In this work the Author describes this model as the 'Standard' $k-\omega$ model to avoid any conflicts with other $k-\omega$ turbulence models. We have seen from the $k-\epsilon_t$ model that ε is the variable in which the length scale is formed. From dimensional analysis a length scale can also be determined from turbulent frequency in the case of the standard $k-\omega$ model $\omega = \epsilon_t/k$ (T^{-1} e.g Hz). ω has a number of advantages, the foremost being that $\omega \to 0$ at the wall and ω is derived from scratch. As a result the $k-\omega$ model is substantially more accurate than the $k-\epsilon_t$ model in the thin near wall layers and for confined flows. However, the model is particularly sensitive to free stream values in unconfined aerodynamic flows, which has prevented the model from becoming a replacement to the $k-\varepsilon_t$ model (Menter *et al.*, 2003). The standard k and ω are modelled by the following set of partial differential equations

$$\frac{\partial}{\partial t}(\rho\kappa) + \frac{\partial}{\partial x_i}(\rho\kappa u_i) = \nabla.\left[\Gamma_\kappa \frac{\partial_\Gamma}{\partial x_j}\right] + G_\kappa - Y - \kappa + S_\kappa \tag{3.35}$$

and

$$\frac{\partial}{\partial t}(\rho\omega) + \frac{\partial}{\partial x_i}(\rho\omega u_i) = \nabla.\left(\Gamma_\omega \frac{\partial_\Gamma}{\partial x_j}\right) + G_\omega - Y - \omega + S_\omega \tag{3.36}$$

where G_κ is turbulent kinetic energy generation as a result of the average gradients in velocity, G_ω is the specific dissipation rate. Γ_κ and Γ_ω are the effective diffusivity. S_κ and S_ω are source terms. Y_κ and Y_ω represent the turbulent dissipation of κ and ω.

3.4.5.3 The $k-\omega$ SST model

A sibling to the standard $k-\omega$ model is the SST $k-\omega$ model proposed by Menter (1993) which is an adaptation of the standard $k-\omega$ model with an additional shear stress transport (SST) term. The SST model was developed due to traditional models, such as the $k-\varepsilon_t$ having difficulties in describing an accurate description of boundary layer separation on aerofoils with adverse pressure gradients (Menter, 1993; Menter *et al.*, 2003) and problems associated with unconfined flows. To overcome the sensitivity of the standard $k-\omega$ model

in free stream flow Menter (1993) blended both the $k-\omega$ and $k-\varepsilon_t$ by combining the enhanced wall treatment of the $k-\omega$ model and the $k-\varepsilon$ models relatively high Reynolds features in the free stream. Thus, implementing the $k-\omega$ model in the boundary layer enables the model to be directly usable all the way down to the viscous sub-layer and eliminates sensitivity issues associated with the $k-\omega$ model (Menter *et al.*, 2003); the SST $k-\omega$ model switches between ω for the near wall and ϵ_t in the free stream. The governing equations to describe the SST $k-\omega$ model are given as

$$\frac{\partial}{\partial t}(\rho k) + \nabla.(\rho k \underline{\widehat{u}}) = \nabla.(\Gamma_\kappa \nabla k) + G_\kappa - Y - \kappa + S_\kappa \tag{3.37}$$

and

$$\frac{\partial}{\partial t}(\rho \omega) + \nabla.(\rho \omega \underline{\widehat{u}}) = \nabla.(\Gamma_\omega \nabla \omega) + G_\omega - Y - \omega + S_\omega \tag{3.38}$$

The k equation from the $k-\omega$ model is combined with a modified ω equation, which is a reformation of the ϵ_t equation and not the same as the standard ω equation; this includes the addition of a cross diffusion term added to equation 3.38 where the diffusive term is defined as

$$D_\omega = 2(1-F_1)\rho\sigma_{\omega,2}\frac{1}{\omega}\nabla k.\nabla\omega \tag{3.39}$$

where the closure coefficients F_1 is the first blending function defined as

$$F_1 = \tanh\left[\min\left[\max\left(\frac{\sqrt{k}}{\beta^*\omega y}, \frac{500\nu}{y^2\omega}\right), \frac{4\sigma_{\omega 2}k}{CD_{k\omega}y^2}\right]\right]^4 \tag{3.40}$$

In the $k-\varepsilon_t$ model, F_1 is equal to zero away from the surface. The $k-\omega$ model switches this to 1 inside the boundary layer (Menter *et al.*, 2003). and

$$CD_{kw} = \max\left(2\rho\sigma_{\omega 2}\frac{1}{\omega}\frac{\partial k}{\partial x_i}\frac{\partial \omega}{\partial x_i}, 10^{-10}\right) \tag{3.41}$$

where y is the distance to the nearest wall. The turbulent eddy viscosity is defined as

$$\nu_t = \frac{a_1 k}{\max(a_1\omega, SF_2)} \tag{3.42}$$

F_2 forms the second blending function defined as

$$F_2 = \tanh\left[\max\left(\frac{2\sqrt{k}}{\beta^*\omega y}, \frac{500\nu}{y^2\omega}\right)\right]^2 \tag{3.43}$$

In the SST model a production limiter is introduced to prevent the build up of turbulence within stagnation zones (Menter *et al.*, 2003).

$$P_k = \min\left(\tau_{ij}\frac{\partial \widehat{u}_i}{\partial_{xj}}, 10\beta^* k\omega\right) \tag{3.44}$$

3.5 The Philosophy of CFD

There are two main approaches to analyse a fluid flow problem. The traditional approach is to conduct a series of experiments on an actual physical model in a wind tunnel or water flume. As an alternative, computational fluid dynamics can be used to solve a set of bounding equations across a computational representation of a model. An experimental investigation is perfectly credible on its own, providing the experiment has been set up competently and any uncertainty justified by the researcher. However, the amount of data which can easily be extracted and on-costs is limiting its sole use in modern engineering analysis. CFD is well established and has proved to yield accurate results, but there is still a certain level of scepticism amongst empirical purists, namely due to turbulence. The acronym is occasionally disparagingly described as 'colours for directors'. This is attributed to a CFD solver delivering an approximate solution to a set of equations, whether the boundary conditions are correct or incorrect the solver may still run and produce an output, correct or incorrect. The computer is 'unintelligent' and cannot distinguish between a realistic or unrealistic solution. In some cases the boundary conditions may be correct but an unrealistic output is being generated due to an inappropriate turbulence model, a poor mesh/grid or other pre-processing issue.

CFD, much the same as an experimental investigation requires a competent user, with experience of the underlying physics of flow to produce a realistic output. He or She can then make quantitative decision as to the accuracy of the

answer generated, just the same as an experimental investigation. CFD can therefore be classed as computational empiricism, with many of the same underlying philosophies as traditional empiricism.

Experimental methods lend their use to determining global properties, lift, drag, pressure drop etc. Time dependent phenomena and small scale analysis is often challenging and expensive with traditional experimental approaches. CFD lends itself to not only determining global properties, but in addition small scale time-dependent flow characteristics can be extracted with relative ease. To satisfy empirical purists and computational sceptics, CFD and experimental methods can complement each other. If a fluid problem is analysed both with CFD and an experimental study is undertaken and the global properties are similar, it is a realistic assumption to suggest that the local properties extracted from the CFD are likely to be credible. Thus, CFD is always best reinforced with experimental data where possible. If not, it should be compared with a well established theoretical correlation known to give a realistic answer. The combination of CFD, experimental data and a well established theoretical correlation where the data matches well forms a powerful argument to the credibility of the data. We may never know the exact real answer, but what we can say is that the real answer falls somewhere within the limits of the three engineering approximations.

Chapter 4

On creating packed beds using Monte-Carlo and traditional CAD based approach

> "In theory, there is no difference between theory and practice. But in practice, there is" Anonymous computer scientist

4.1 Introduction

In this chapter the finite volume method is applied to investigate the pressure drop and flow structure of isothermal airflow through randomly packed beds of spheres with aspect ratios of 7.14, 6.25 and 4.54 (14mm, 16mm and 22mm). The results determined from the 14mm spherical media and have also presented in Baker & Tabor (2010). The geometry in these cases is created using a Monte-Carlo algorithm to achieve a random unstructured pack. The 3-dimensional computational models are then suitably discretized into meshes using Fluent's grid generation package, GAMBIT. In parallel, equivalent beds are created which match the characteristics of the computational beds. The beds are termed "equivalent beds" in regard to their dimensional characteristics being the same, but with a different internal structure and hence a different inter-connecting network of voids. The turbulence model used for closing the RANS equations is the SST $k-\omega$ model proposed by Menter (1994). Experimental studies are carried out and compared

to the correlation of Eisfeld & Schnitzlein (2001) and to the experimental data of Reichelt (1972). When studying complex geometries particle contact points have always presented an issue in regard to mesh quality. The problem of contacts is ameliorated to some extent by Dalman *et al.* (1986); Lloyd & Boehm (1994); Logtenberg & Dixon (1998) who leave small gaps between the particles and assume zero velocity at the contact point assuming that the contact point is within the boundary layer. Atmakidis & Kenig (2009) shrink the particles by 2% to avoid stability issues with skewed elements at contact points. In contrast Guardo (2007) use a structured cubic array but increase the particle volume by 1% to avoid convergence problems. Due to the structured cubic array and the increase in diameter the particles now merge with all contact points uniform in size and shape allowing a suitable mesh elements size to be set. Jafari *et al.* (2008) compare a space filtered LES approach with the Reynolds Stress model and a steady-state solver. They use the commercial code FLUENT coupled with its mesher, GAMBIT. They use a random number generator to carefully position each of the spherical particles. They compare the models in some detail, as with many model comparisons statistically analysing a few different beds cannot give a realistic confidence level to conclusively say whether one models turbulence in a particular media than the other.

The work presented here is similar to that of Atmakidis & Kenig (2009), only the spheres have not been shrunk by 2% and therefore retain their geometric fidelity to the original Monte-Carlo pack. Here we are interested in the two equation SST $k-\omega$ model and its behaviour in modelling flow in packed beds which is expected to be transitional to mildly turbulent in nature. The contact points remain unchanged and are meshed regardless, leaving the mesh geometrically faithful to the CAD model and the skewness compensated by the PISO solver. All the computational results are compared with experimental equivalent beds.

4.2 Experimental Setup

The experimental setup used in this work requires methods for measuring values of pressure difference ΔP, and volumetric flow rate (Q) and hence average velocity (U), and is based on the setup of Tóbis (2000), with the addition of two pressure

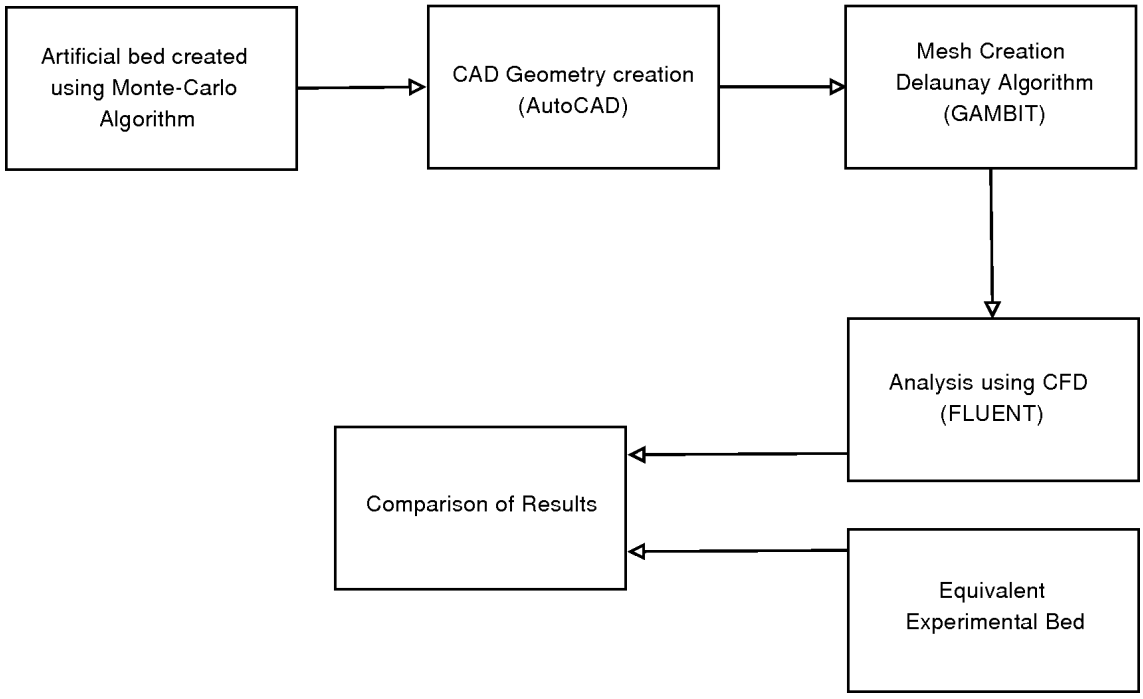

Figure 4.1: Chapter 4 methodology flow diagram

taps into the bed at 0.1 m vertical intervals, as shown in 4.2. These pressure tappings are added to provide an average pressure across the profile and eliminate the risk of velocity streams affecting the pressure reading. To keep all particles as uniform as possible 14mm, 16mm and 22mm marbles were used due to their consistency in diameter and the fact that they are hydraulically smooth. The packed bed was supported by a fine wire mesh screen enclosed in a 100 mm diameter Perspex column, with a length of 300 mm. Air was forced through the bed using a centrifugal pump. Volumetric flow rate Q, and hence average velocity U, was measured by measuring a differential pressure (ΔP) across a plate orifice manufactured from Perspex. The plate orifice method is use to measure the volumetric flow rate of a fluid. The orifice causes a vena-contracta to be formed by the pipe constriction and as the fluid velocity increases through the constriction there is a resulting decrease in pressure. Using Benoulli's princple the volumetric flow rate can be determined from this differential pressure and additional properties of the fluid. An experimental value for the flow coefficient C_f of the plate orifice was calibrated against a velocity profile, determined by hot-wire anemometers.

The plate orifice method was chosen over that of a Pitot-Darcy static tube, because the Pitot-Darcy static tube only determines the velocity at its immediate location, meaning that a full flow profile using this method would require many readings to be taken in different locations across the pipe section, then averaged to reduce error. The plate orifice is simply an application of Bernoulli's theory, the conservation of mass and the flow geometry. The pipe constriction causes a vena-contracta to be formed and from the differential pressure and Bernoulli's hypothesis the volumetric flow rate can be determined. One disadvantage of using a plate orifice is that there is a significant pressure drop immediately after the orifice; to reduce this, a Venturi meter could be used as an alternative, where the drop in pressure due to the device is less significant. In addition other complications are also documented regarding the use of reciprocating pumps. Where the pump cycle frequency is close to the natural frequency of orifice, results have shown a discrepancy of up to 40% as a result of the shedding of vortices from the lip of the orifice (Cengel & Cimbala, 2006). However, due to the low cost and ease of manufacture, along with general accuracy and ease of calibration, the benefits

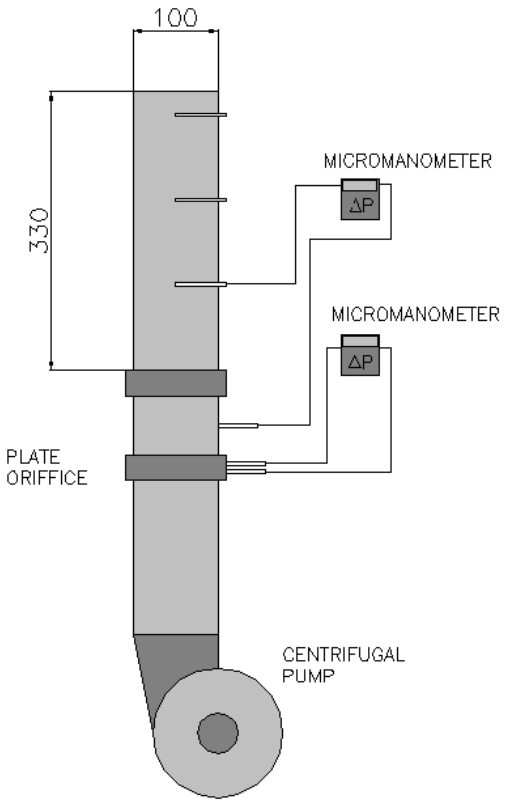

Figure 4.2: Experimental setup

of using a plate orifice outweigh the disadvantages. The header region before the bed was of sufficient length for the flow profile to be assumed as fully developed. Calculating the velocity from the volumetric flow rate ($Q = UA$) enables the average velocity across the profile to be calculated.

Differential pressures were taken from immediately before the bed (0.0) and at 0.1 m intervals. To validate the total pressure drop, differential pressure was recorded between intervals and added together, then compared with total pressure drop. An accurate value of air density was determined by using a barometer to determine atmospheric pressure p and a k type thermocouple placed in the flow to determine flow temperature T. This was used in conjunction with the specific gas constant for air $R = 287$ J/kgK, resulting in an air density of 1.117 kg/m^3 ($PV = MRT$) which matches closely to the standard density of dry air at $T =$ 300K, which is 1.177 kg/m^3 (Rogers & Mayhew, 1982).

An accurate value of porosity is also needed to describe the bed. Here three methods are used. Firstly, the classic method of water substitution is used. This method is reasonably accurate, but problems occur with porous particles and the wetting properties of water. In this case the medium is glass and so this is not likely to present a problem. In addition this method can also suffer from entrained air. To compensate for this a surfactant is used (washing up liquid) coupled with a vacuum chamber to remove any air. In comparison, MacroPac provides a method for determining porosity. Secondly, we know the overall volume of domain occupied, the size of the header and exhaust region and the mesh volume. In which case the porosity can be determined by simple volume diameter relations.

4.3 Computational Packing of Spheres

We have discussed the issues regarding unstructured beds and as a result a considerable amount of research has been carried out on the carriage of flow through regular beds (Atmakidis & Kenig, 2009; Dalman *et al.*, 1986; Tóbis, 2000) or a simple unit cell approach (Hellström & Lundström, 2006). This is because the discretization of a regular bed into a suitable domain for computational analysis is far easier due to homogeneity in pore sizes. However, in reality many industrial packed beds are not regular but random, unstructured and disordered, which

cannot be quantified by any deterministic mathematical formulae, but more described by the probability that an event may happen. In many cases Monte-Carlo methods are used where a solution from a deterministic algorithm is not possible. A Monte-Carlo approach does not relate to a specific algorithm, but a class of non-deterministic algorithms based on random sampling.

To implement this in this work, the particle packing simulation program MacroPac (Intelligensys, UK) was used to generate packed beds of spheres of the same diameter as those used for the real experiment. In MacroPac the Monte Carlo method is used to pack the spheres to the densest packing possible, by simulated shaking of the column and packing medium. A full scale discussion about Monte-Carlo algorithms and their mathematics are beyond the scope of this work. Here a Monte-Carlo algorithm is simply used as a tool to generate unstructured, random beds of particles. Here, the basic underlying physics used by MacroPac is explained as follows. The probability that a particle moves in the z-axis is

$$p = e^{-\frac{\Delta E}{R.T}} \tag{4.1}$$

ΔE is the change in potential energy when the object moves against a force in the -z direction. We know change in potential energy is given as

$$\Delta E = mg\Delta h \tag{4.2}$$

In the simulation the probability that a particle moves up

$$p = e^{m_r \Delta h_r K_f} \tag{4.3}$$

where m_r is the unit of mass and Δh_r is the distance moved. m_r and Δh_r are defined by the objects mass density relationship, $m = \rho V$ and boundary dimension parameters. K_f is the kinetic factor given as

$$K_f = \frac{m_f h_f g}{R.T} \tag{4.4}$$

The kinetic factor is also related to the amount of shaking; more shaking will produce a lower kinetic factor as more particles may move up due to the shake.

To avoid any experimental discrepancies, the container geometry used as an input parameter for MacroPac was identical to that of the experiment.

Having generated these computational beds, the coordinates of the sphere centres were exported to the CAD package AutoCAD and used to regenerate the packed spheres in ACIS format for export to the automatic meshing program Gambit. Figures 4.4, 4.3 and 4.5 show a view of the spheres in the bed displayed in Fluent. Although relatively simple, using this technique there is scope to produce much larger beds of spherical media, the only limitation is the large amount of computational power required in mesh generation and computational simulation.

MacroPac provides an inbuilt function by which bed porosities can be determined (where the exact method is discussed in the final chapter of this Thesis). Here the results produced for the bed porosity

Properties	ε (Experimental)	ε (MacroPac)
14mm spheres	0.48	0.50
16mm spheres	0.49	0.49
22mm spheres	0.52	0.54

Table 4.1: Porosity for packed beds determined both from MacroPac and experiment

4.4 Computational domain

The complex geometrical properties of random packed beds makes it extremely difficult to produce a workable mesh for this case. Even once a mesh has been produced the quality is often dubious containing non-positive volumes and highly skewed elements (slithers), which often lead to simulation divergence and instability. Due to this the discussion presented here has evolved from the following quote

> "Mesh quality concerns the characteristics of a mesh that permit a particular numerical PDE simulation to be efficiently performed, with

> fidelity to the underlying physics, and with the accuracy required for the problem"
>
> Patrick M. Knupp

Using traditional mesh quality analysis techniques, such as equivolume/equiangle skew cell squish index etc, the mesh can appear well within the limits of what is considered to be a good quality mesh due to the skewness averaging applied by the formula. A mesh can often contain a few highly slithered elements which can often go undetected until an un-expected solution divergence occurs.

In this work creation of the mesh of cells is done using Ansys Gambit, a general-purpose program with a variety of automatic meshing strategies based on a Delaunay algorithm for unstructured grids. Here the domain was meshed using the Tet/hybrid and TGrid options; this generates meshes comprised predominantly of tetrahedral cells but including other cells (prismatic and hexahedral) where necessary. Surfaces were not meshed separately and so were automatically meshed as triangles.

Properties	Cells	Faces	Nodes
14mm spheres	1168328	2456980	248950
16mm spheres	1447289	2991148	286421
22mm spheres	1235204	2542209	240310

Table 4.2: Mesh data

Each mesh is then partitioned by its principal axes into 4 segments to allow paralisation of the domain to reduce simulation time. Each segment is computed on a node, where each node consists of 1 quad core 2.6GHz processor with 8Gb of RAM. To reach an overall solution required between 4 and 8 hours computer time.

To capture the full effects of viscous drag on the micro-structural flow the mesh must significantly fine enough. In which case it is necessary to conduct a mesh convergence study (mesh indeterminacy study), by increasing the number of mesh elements and monitoring the same parameter of the flow, in this case the area weighted average pressure at the outlet.

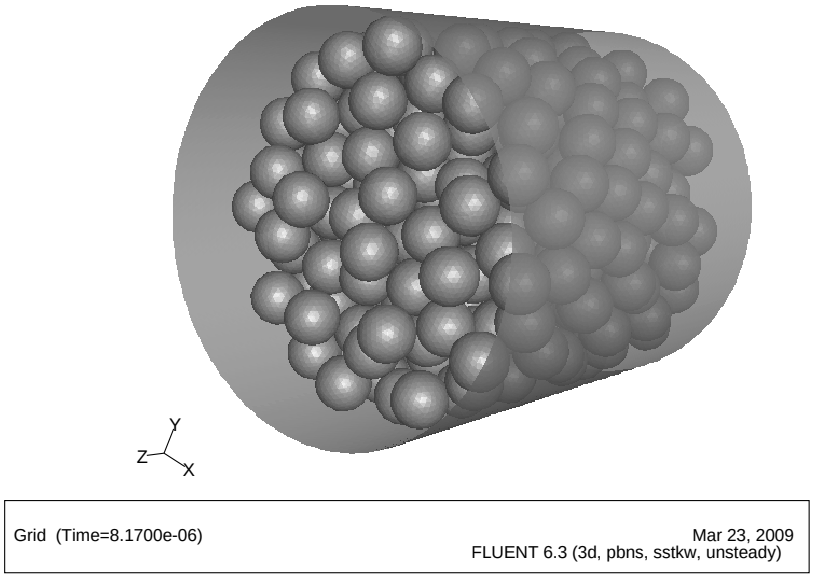

Figure 4.3: Computational domain for 14mm spheres

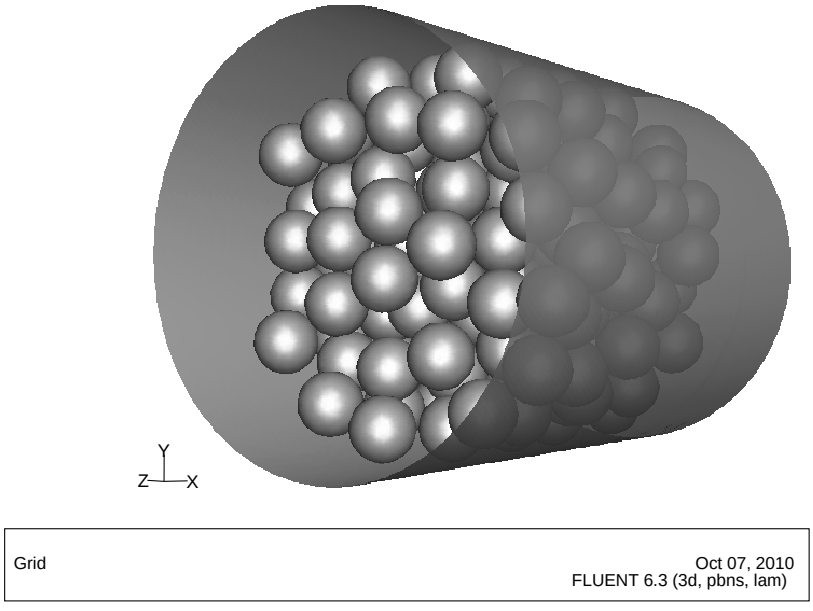

Figure 4.4: Computational domain for 16mm spheres

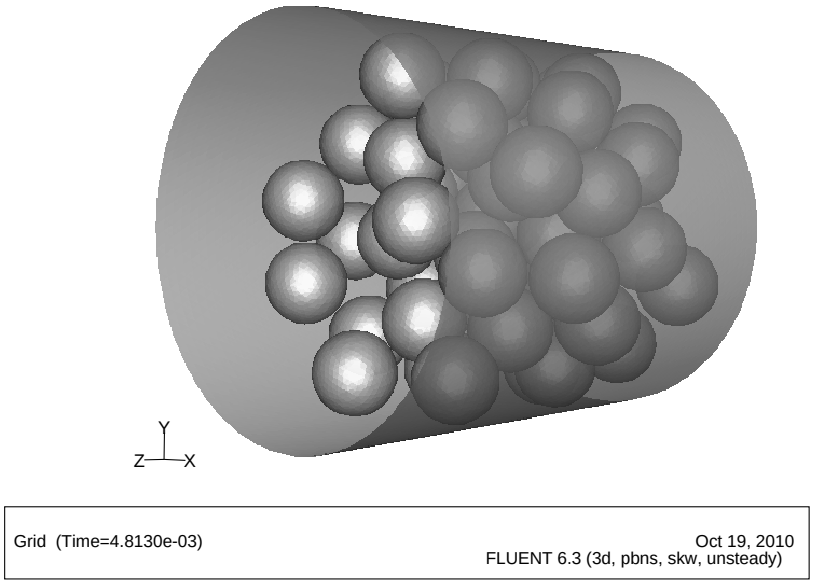

Figure 4.5: Computational domain for 22mm spheres

In this case the study (figure 4.6) concluded that the results did not significantly change after 1168328 cells, a mesh finer than this would yield no advantage in producing more accurate results and would be computationally more expensive. Due to the complex nature of the geometry the meshing algorithm used in Gambit can have problems producing a working mesh at certain size intervals in respect to the range in void sizes and particle contact points. The points on the graph represent meshes for which computational analysis was possible. In this case the quality of the mesh is analysed using the dimensionless form of equivolume skew (E_V). In both cases, the cell equivolume/equiangle skew of 0, indicates a 'perfect' cell and 1 would indicate a highly skewed, completely degenerate el-

Properties	Max Cell vol	Min Cell vol	Max face area	Min face area	Mesh Volume
14mm	1.834×10^{-9}	5.208×10^{-12}	3.14×10^{-6}	1.987×10^{-8}	5.796×10^{-4}
16mm	1.886×10^{-9}	7.39×10^{-12}	3.410×10^{-6}	1.519×10^{-7}	8.23×10^{-4}
22mm	1.752×10^{-9}	3.188×10^{-11}	3.275×10^{-6}	1.446×10^{7}	6.797×10^{-4}

Table 4.3: Mesh data

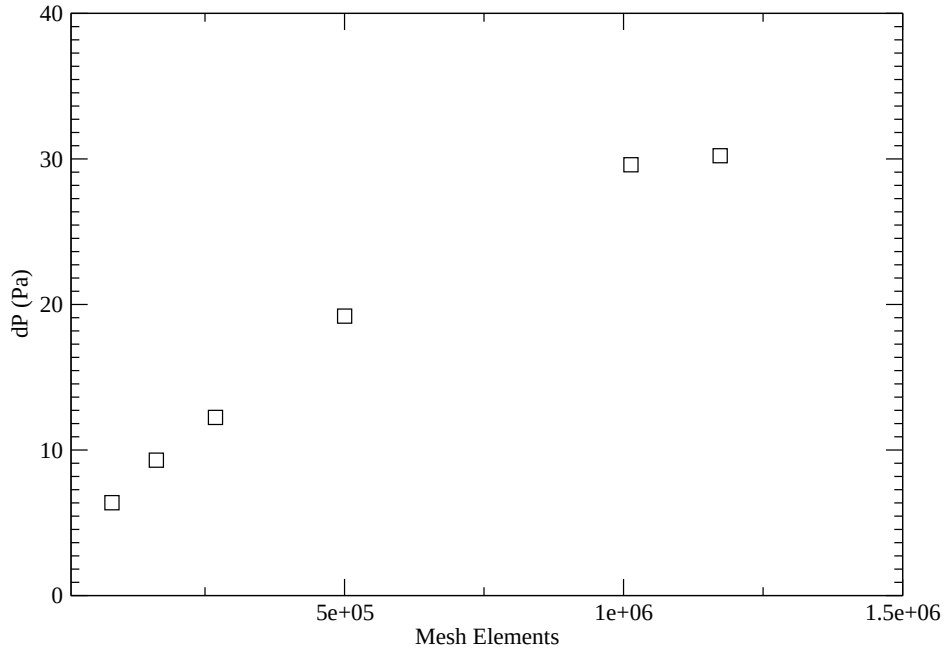

Figure 4.6: Grid convergence study

ement. In reality, methods for determining mesh quality are not dependant on the physical geometry of the mesh and its deviation for a 'perfect cell' but more dependant on the application. For example, laminar, steady state fluid motion down a straight pipe is unlikely to be susceptible to a degenerate mesh than an unsteady turbulent regime through a complex geometry due to the additional equations being solved. Here and in industry, CFD is used as a tool to generate a result. In industry the result is used to make money, in research it is there to widen our understanding and breadth of knowledge on the subject. It could be argued that if a realistic result for the job in question is achieved, which does not diverge and ultimately leads to a successful solution, is obtained from a skewed mesh, does the mesh skewness remain an issue? From 4.8, 4.10 it can observed that the mesh contains a few highly skewed elements. When meshing complex

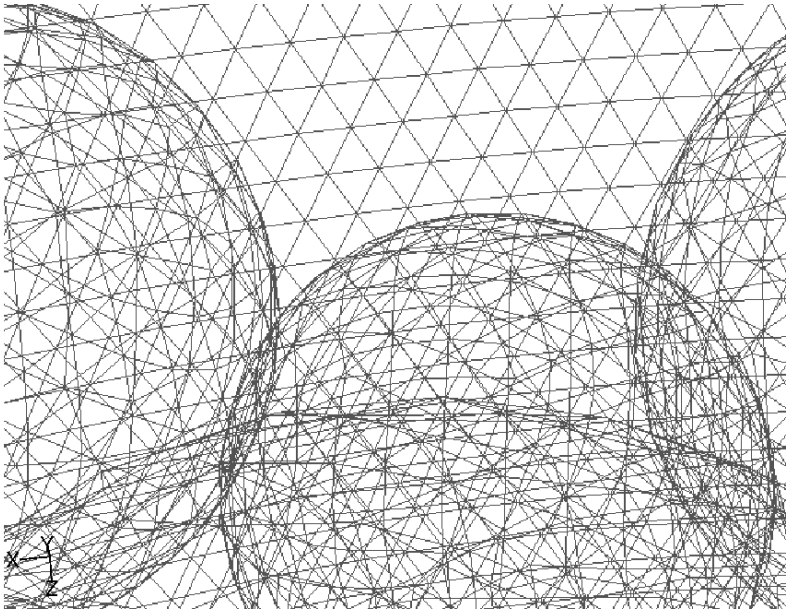

Figure 4.7: Geometry and mesh of top of bed

spherical geometries, such as this, skewed cells are often unavoidable. In the case of regular sphere packings particle distances from one another (gaps) can be set to allow a suitable size element to be fitted, such as Logtenberg & Dixon (1998) and Atmakidis & Kenig (2009). In this case distances vary quite considerably and in which case the majority of skewed elements are located in areas of particle near contact points shown as in figure 4.11. To reduce this undesirable phenomena Atmakidis & Kenig (2009) shrink each of the particles by 2% to allow for a gap between the particles to reduce the effect of mesh skewness at the particle contact points, however, due to its static instability does not replicate a real packed bed. Fluent also provides a range of features after the mesh has been produced to smooth the mesh and reduce skewness. However, in most cases this does not completely eliminate all skewed elements. Fluent provides provisions to overcome this when using the PISO solver by the addition of skewness correction and neighbour coupling. In this case the neighbour correction is set to 1 and the skewness correction to 6, to stabilise the solution.

When modelling turbulence it is imperative that the near wall region is adequately treated. This can be done in two ways, firstly the mesh is fine enough

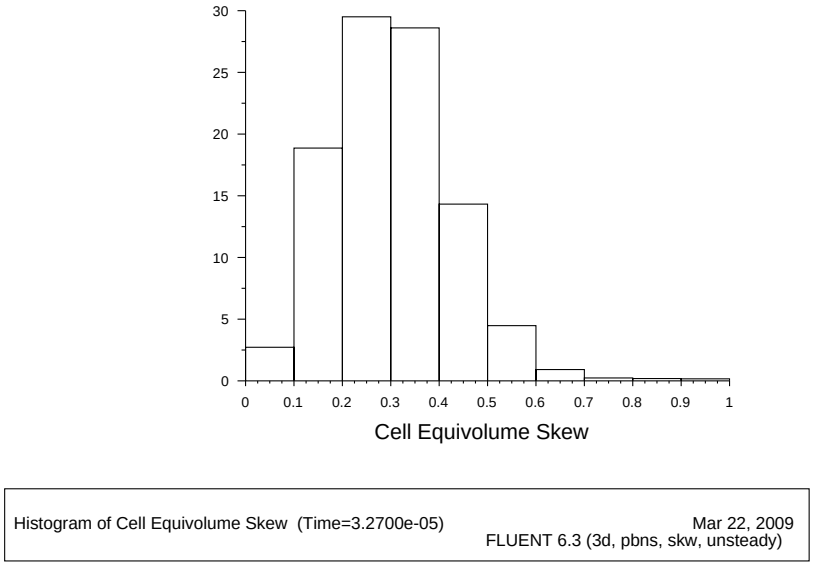

Figure 4.8: Mesh cell equivolume skew for 14mm media

to resolve the viscous sublayer and secondly, if the mesh can not be made fine enough a log law profile is assumed for cells adjacent to the boundary. We know from boundary layer theory that the flow velocity directly adjacent to a wall is zero. Away from the wall turbulent flow can be categorised into four flow regions, the viscous sub-layer where the velocity gradient is virtually linear, the buffer layer where turbulence is becoming more apparent, the transition layer where turbulence is dominant and the outer layer which is no longer effected by the presence of the wall. The law of the wall is described by

$$\frac{u}{u_\tau} = \frac{yu_\tau}{\nu} \tag{4.5}$$

where

$$u_\tau = \sqrt{\frac{\tau_0}{\rho}} \tag{4.6}$$

From empiricism, this relation is shown to describe the viscous sublayer well for $0 < yu_\tau/\mu < 5$ (Cengel & Cimbala, 2006). In many cases it is appropriate to work in a dimensionless distance in which case a value of $y+$ is introduced given

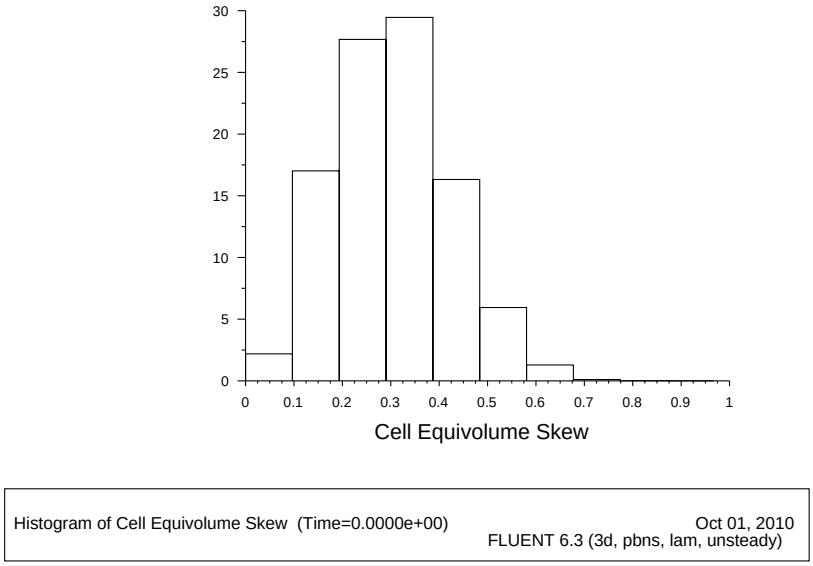

Figure 4.9: Mesh cell equivolume skew for 16mm media

as

$$y+ = \frac{yu_\tau}{nu} \tag{4.7}$$

In regard to the $k-\omega$ SST turbulence model, the mesh must be fine enough at the wall region to realistically capture the effect of the viscous sub-layer and Fluent assumes there to be a linear velocity relationship within these cells. In which case y is the distance of node contained by the cells adjacent to the wall from the wall

1.

. Appropriately the limits which are acceptable for cell size at the near wall region are the same as the limits set by empirism where $0 < y+ < 5$. When enhanced wall treatment is switched off, the wall region is treated as a log law profile for the cells adjacent to the wall and in which case appropriate $y+$ values can be in the region of $30 < y+ < 300$. If we focus our attention back to chapter 2, there has been much discussion regarding the onset of laminar and turbulent flow through packed beds. It is generally understood that there is a possibility that all three modes of flow can exist. In which case by using the SST $k-\omega$ we are

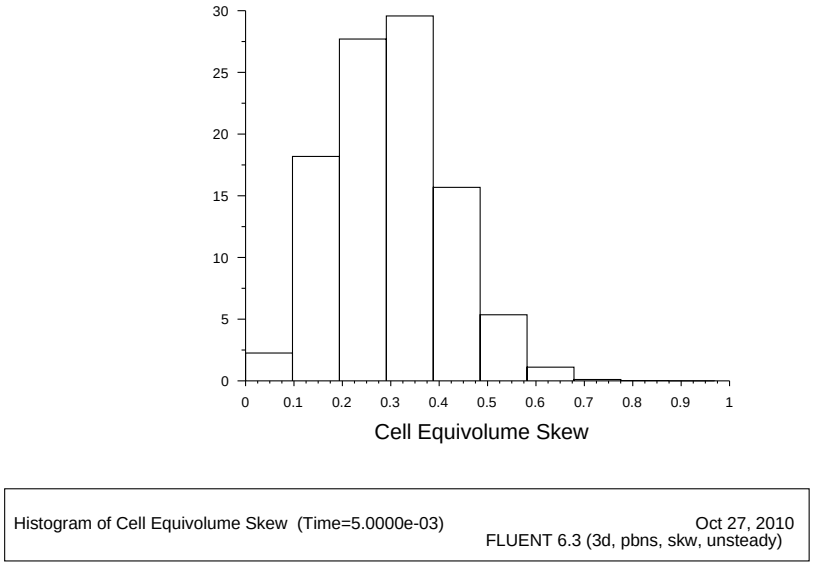

Figure 4.10: Mesh cell equivolume skew for 22mm media

resolving flow near the boundary using the $k-\omega$ model and in the free stream the $k-\varepsilon$ model, and the cells contained in the viscous sublayer are treated with a linear relationship. If we applied the standard $k-\omega$ model, without enhanced wall treatment the cells in the buffer layer ($30 < y+ < 300$) would be treated as a turbulent log law profile for the whole medium regardless of the flow regime in that particular region, possibly neglecting the strains associated with the laminar boundary layer. In addition, the spherical media at the top of the bed is being exerted to pressure drag with a degree of recirculation and separation behind each individual sphere. We can see from figures 4.12, 4.13 and 4.14 that although $y+$ is dependant on the velocity it would be difficult to argue from these values that the viscous sub-layer is not being sufficiently resolved. What is more concerning is that within literature the author has found no evidence of published $y+$ when a turbulent solver is applied to a packed bed. Again, these graphs represents a bulk quantity and in some cases it is apparent that the viscous sub-layer is not being properly resolved. Figure 4.15 depicts velocity profiles for a sphere in the near wall region. We can see the boundary layer of the sphere has merged with the wall boundary layer, most probably due to degenerate, highly skewed elements.

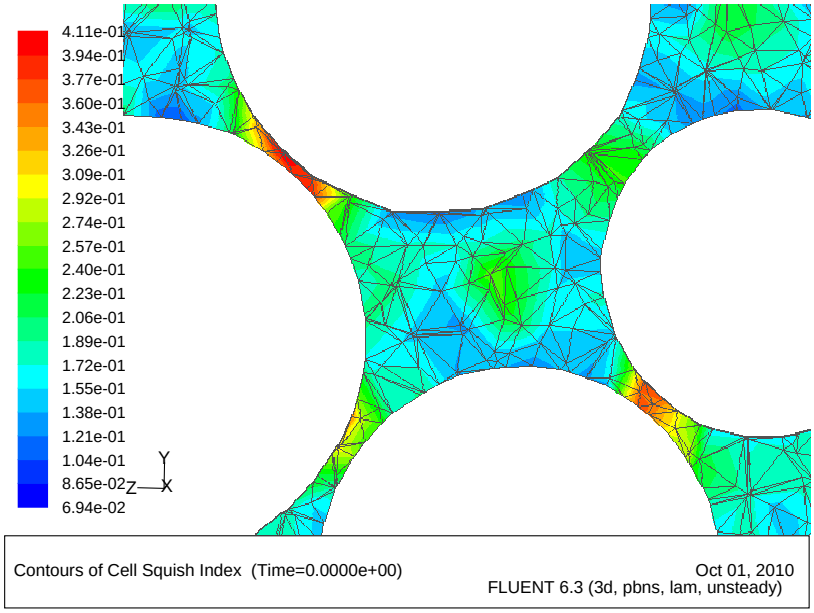

Figure 4.11: Contours of cell squish index for 16mm media

This effect is however isolated in regions of minimal flow. The only favourable result of the presence of skewed elements is that they are generally confined to the spherical contact points, which in most cases are in regions of relative flow stagnation. The likely hood of the skewness effecting the overall result is low, providing convergence criteria are met.

4.5 Computational fluid dynamics

Due to the complex geometry and uncertainty in mesh quality, the simplest combination of differencing and solvers are initially used and hence convergence is virtually guaranteed. For this work a steady state, incompressible laminar solver is used coupled with the SIMPLE algorithm and first order upwind differencing scheme, where the steady state Navier-Stokes equations are solved

$$\rho \nabla . \underline{u}\, \underline{u} = -\nabla p + \nu \nabla^2 \underline{u} \tag{4.8}$$

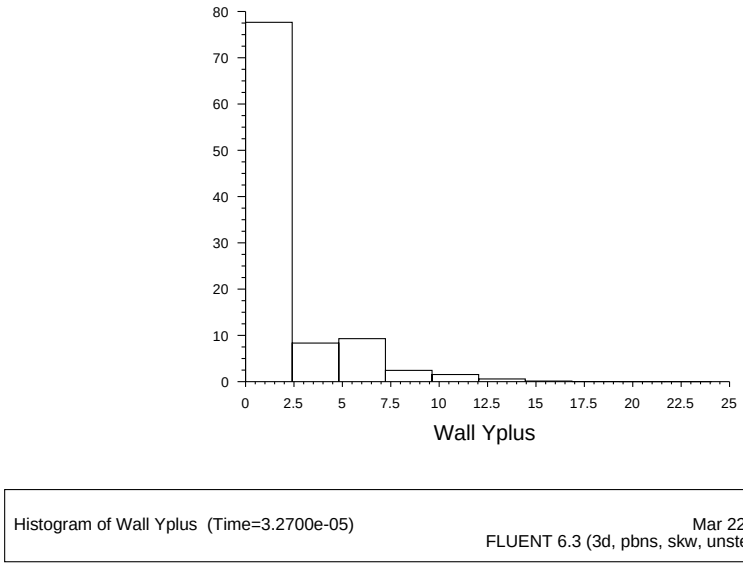

Figure 4.12: y+ values for the wall region for 14mm spheres

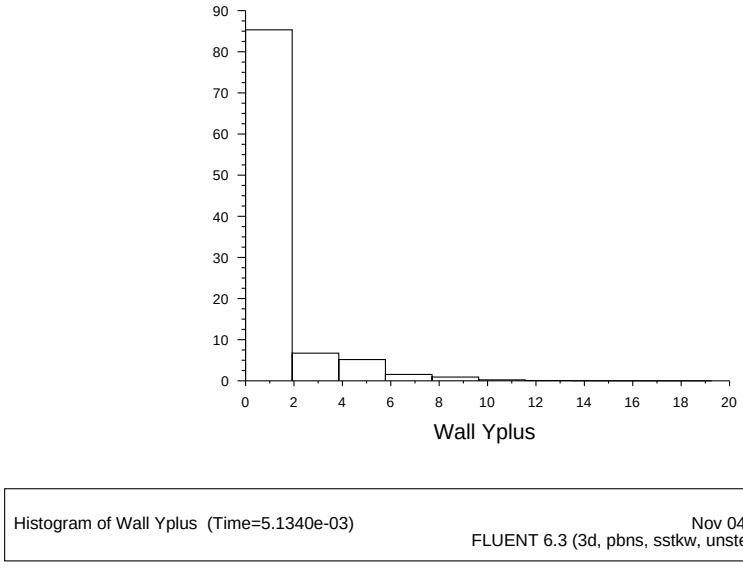

Figure 4.13: y+ values for the wall region for 16mm spheres

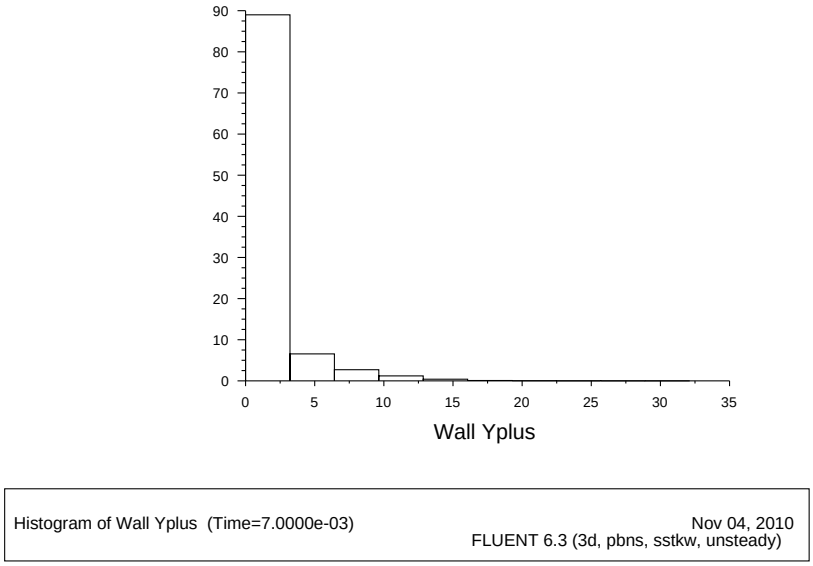

Figure 4.14: y+ values for the wall region for 22mm spheres

Although air is a compressible fluid, the flow speeds presented here are relatively low and compressibility effects are unlikely to be contributing to the behaviour of the fluid. Cengel & Cimbala (2006) suggest that compressibility effects can be neglected if the Mach number is $M < 0.3$ (around $100m/s$ in air), and the change in density ($\Delta\rho$) is less than 5%. The Mach numbers described in this work are all less than $M < 0.012$ so compressibility effects are likely to be minimal and so an incompressible solver is adopted. Once a steady state solution for the domain has been delivered and unsteady solver is used. This reduces the amount of guesswork involved in the guess and correct procedure and therefore enhances solver stability. Although the Navier-Stokes equations are in themselves deterministic, with the addition of a turbulence model and the pseudo-random instabilities of turbulence, they become deterministic chaotic and a degenerate element can cause the magnitude of chaos to increase violently. In parallel, the nature of the computational solver itself can display instabilities, forming a deterministic chaotic nature, thus it can be difficult in many cases to establish whether the instabilities are a result of turbulence, or as a result of instabilities in the solver due to mesh quality. Initially the flow is assumed to be steady state

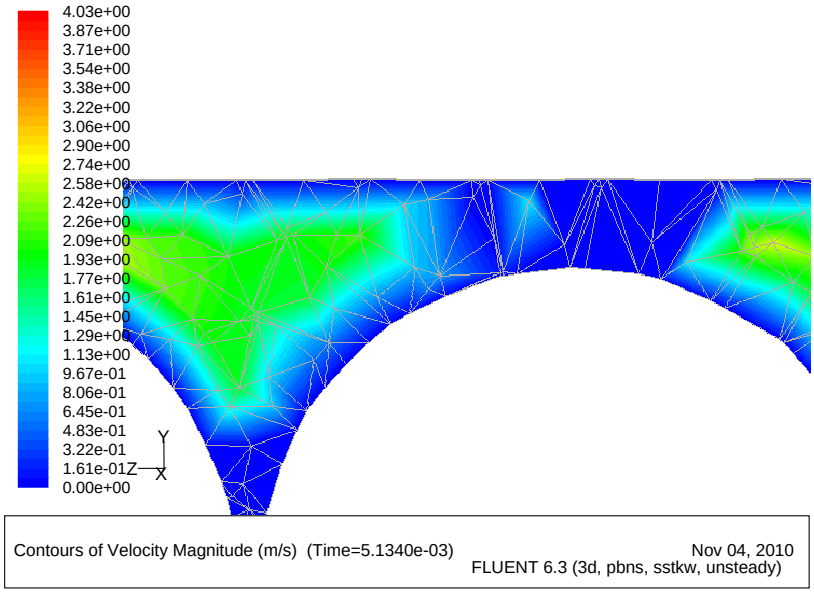

Figure 4.15: Contours of velocity at the near wall region

and the SIMPLE algorithm is chosen to deliver a solution. The PISO algorithm is often less stable in respect to the extra corrector step and highly degenerate mesh elements. However, the PISO algorithm does include a skewness correction. Once a solution has been delivered using a the SIMPLE algorithm, PISO is used to deliver the final solution.

Choosing an appropriate turbulence model to give an accurate representation of the flow can be challenging but not impossible. We already know that there is no generic turbulence model applicable for every case. The turbulence models described in chapter 3 are based around assumptions made about certain length scales and an enhanced fictitious viscosity. In this case the length scales are likely to vary considerably from the largest possible vortices based on the diameter of the header region, intermediate length scales based on the pore sizes and the smallest vortices being governed by the fluid viscosity. Generally, we base our decision on some characteristics we already know about the the flow, for example the Reynolds number, based on some scaling function of the flow geometry. Here there is an amount of uncertainty in exactly what the internal micro-structural flow is likely to be. We know from the work of Ziolkowska & Ziolkowska (1988)that

flow can be characterised as laminar ($Re_{dP} < 10$), transitional ($10 < Re_{dP} < 300$) or fully turbulent ($Re_{dP} > 300$). However, Scheidegger (1960) suggest that it is impossible to determine a realistic value for the onset of turbulence in a packed bed. In addition, the flow regime inside the bed is likely to vary considerably due to flow channelling and stagnation zones. We can however rule out certain approaches. For instance, a DNS approach is far too computationally expensive and requires more computer power which is readily available. A mixing length model is not appropriate due to the complex geometry and pore size variation. Choosing a suitable mixing length using this model would be almost impossible and coupled with its limited wall treatment would likely give a misleading result. An LES model is suitable but beyond the scope of this work. This leaves us with the two equation models. Traditionally the $k-\varepsilon$ model is regarded as the status-quo, but we know from Versteeg & Malalasekera (1995) that the $k-\varepsilon$ model produces poor results with flow with large extra strains, such as curved boundary layers (flow around spheres). In addition it is only valid for fully turbulent flows and has difficulty in modelling separated flows. However, the $k-\varepsilon$ model has been successfully used by Tóbis (2000) on a regular packing with promising results to describe turbulence in packed beds. This is most likely attributed to a regular bed having uniformity in pore size. Due to this, a suitable length scale can be determined.

The flow within the beds described in this work is likely to display, laminar, transitional and turbulent features, so here the $k-\omega$ SST model is used due to its enhanced wall treatment and the benefits of combining $k-\epsilon$ in the free stream and using $k-\omega$ in the near wall region.

Once a solution has been delivered from solution of the un-steady NSE, the full RANS equations are used with the addition of second order differencing and the SST $-\omega$ model to close the equations.

The meshes described here may my contain half a dozen severely skewed slithers which potentially can cause the solution to divergence due to the node position in relation to the face centres. This of course can be damped out to a certain extent by the adjustment of the under-relaxation factors but in many cases this is not sufficient to ensure stability. The PISO algorithm also has a

skewness correction facility, in this case set to 6, but in many cases, the elements in question are so slithered that any correction does not guarantee a convergence.

In the case of grids containing many skewed cells, many of the usual computational techniques for a successful convergence are not applicable. For example, it would be assumed that the more iterations per time-step would lead to a more accurate and stable solution. In the case of time-stepping across a highly skewed element, the more iterations per time-step increases the magnitude of error resulting which can ultimately bounce the solver into divergence away from the solution. This phenomena becomes more prevalent in higher-order differencing schemes. When an answer has been produced by a slithered element, the hope is the following cell will be of a realistic geometry and produce such an answer as to stabilise the divergence back towards delivering a solution and ultimately away from a possible divergence.

4.6 Results

Here experimental data is compared with CFD results in the form of pressure drop per unit length (Pa/m) as a function of the dimensionless Reynolds number given as

$$Re_{dp} = \frac{\rho U d_p}{\mu} \tag{4.9}$$

In many applications of fluid mechanics, it is desirable to present data in its dimensionless form. In which case here the computational and experimental results have been presented using the dimensionless pressure drop described by Eisfeld & Schnitzlein (2001) as

$$\phi = \frac{\Delta P d_p}{\rho L U^2} \tag{4.10}$$

We can see from 4.10 that the dimensionless pressure drop is sensitive to deviations in the velocity and pressure drop per unit length. Any small deviations in the velocity are magnified to a misleading extent when represented logarithmically, such as in 4.10. In this work it is also appropriate to compare the results

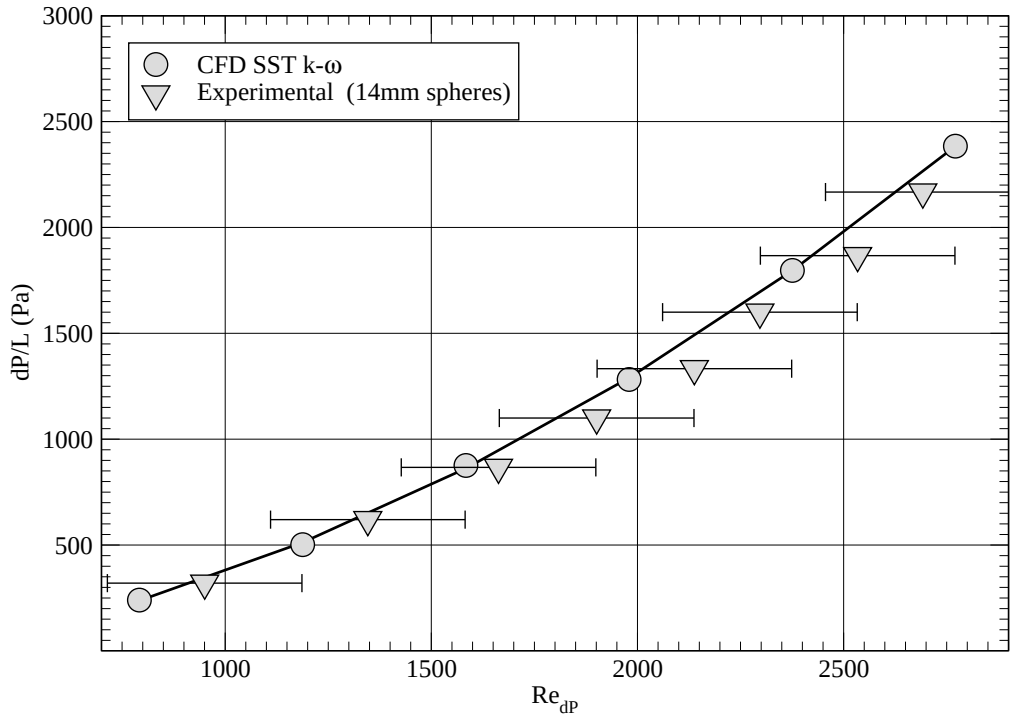

Figure 4.16: Pressure drop per unit length as a function of the particle Reynolds number (Re_{dp}) for 14mm spheres. Experimental uncertainty $\Delta Re_{dp} = \pm 236$, $\Delta(\Delta P/L) = \pm 4.167 Pa/m$

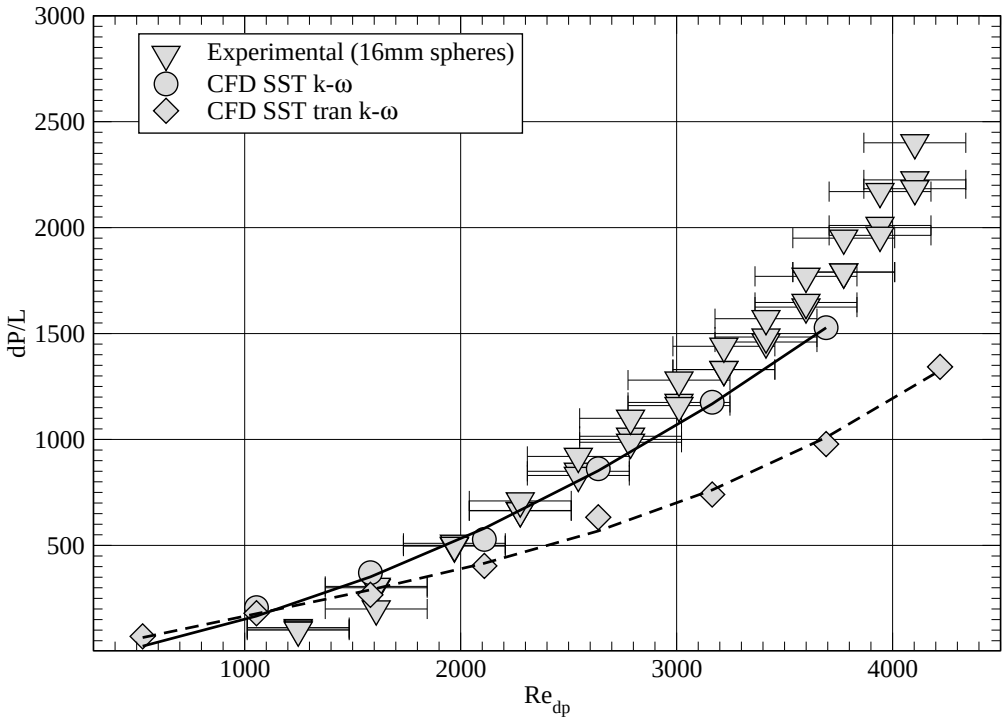

Figure 4.17: Pressure drop per unit length as a function of the particle Reynolds number (Re_{dp}) for 16mm spheres. Experimental uncertainty $\Delta Re_{dp} = \pm 236$, $\Delta(\Delta P/L) = \pm 4.167 Pa/m$

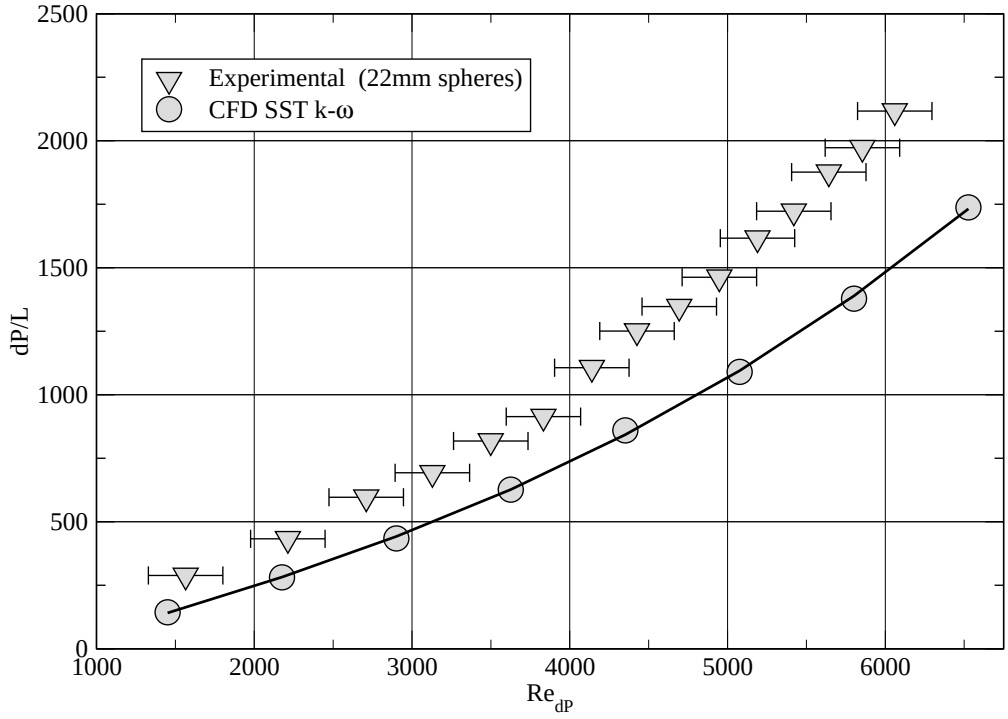

Figure 4.18: Pressure drop per unit length as a function of the particle Reynolds number (Re_{dp}) for 22mm spheres. Experimental uncertainty $\Delta Re_{dp} = \pm 236$, $\Delta(\Delta P/L) = \pm 4.167 Pa/m$

with the correlation proposed by Eisfeld & Schnitzlein (2001) to give the results some credibility. The equation for dimensionless pressured drop given by Eisfeld & Schnitzlein (2001) takes the form

$$\phi = \frac{K_1 A_W^2}{Re_{dp}} \frac{(1-\varepsilon)}{\varepsilon^3} + \frac{A_W}{B_W} \frac{1-\varepsilon}{\varepsilon^3} \tag{4.11}$$

$$A_W = 1 + \frac{2}{3(D/d_p)(1-\varepsilon)} \tag{4.12}$$

and

$$B_w = \left[k_1 \left(\frac{d_p}{D} \right)^2 + k_2 \right]^2 \tag{4.13}$$

Here the media is spherical, in which case Eisfeld & Schnitzlein (2001) give the values for the three coefficients as K_1, k_1 and k_2 as 154, 1.15 and 0.87 respectively. We know the correlation of Eisfeld & Schnitzlein (2001) is based on empirically derived coefficients, however, we can see from figure 4.19 that the spread of data between $Re' = 10 - 10,000$ is quite considerable. This may be due to effects such as turbulence effects, tortuosity (not described by any relation) or due to the heterogeneity in possible packing regimes. The most likely effect of this variation is statistical due to most research being conducted on this range of parameters. Another possible cause of the large spread of data may be due to the regressive technique; the correlation essentially gives a mean value of this data and does not correlate well with data at the extremities of this data. In addition, data sets can have identical statistical properties but can be considerably different when represented graphically. This can be explained by Ashcombe's Quartet (Ashcombe, 1973), in which four considerably different trends are presented, but results using simple statistical evaluation techniques are identical. Ashcombe emphasizes the need to graph data and not just rely on statistical analysis. This is reinforced in this work by the close trends observed when presented graphically compared to the relatively large deviations from statistical methods. For example, Eisfeld & Schnitzlein (2001) report the their models closeness in respect to the relative root mean deviation, however this only describes the models closeness in respect to the roots of all the data points and not in respect to the shape or form of the distribution. This does not describe effects such as divergence or convergence

away or towards the correlation, but describes this as an average. Results are also compared to the results of Reichelt (1972). The results of Reichelt (1972) are chosen due to their closeness in both particle diameter and porosity.

MacroPac provides the facility to evaluate porosities across the bed. Results for the various beds are shown in figure 4.20. As expected the porosity is roughly uniform across the core region but rises steeply within the near-wall region of the column where the packing is effected by the presence of the wall. A similar porosity decaying-sinusoidal distribution has been observed by du Toit (2008) from a mathematical model, and the same characteristics have previously been observed using an empirical approach (Goodling *et al.*, 1983) and MRI (Mantle *et al.*, 2001; Sederman *et al.*, 2001). Some low aspect ratio two zone correlations such as DiFelice & Gibilaro (2004) rely on two values of porosity, usually defined as wall and core porosities. Using MacroPacs function these can be determined by the averaging the values of the wall region (1 sphere radius), and the core region. However, the correlation of DiFelice & Gibilaro (2004) is fairly rudimentary and does not fit experimental data as obediently as the semi-empirical correlation of (Eisfeld & Schnitzlein, 2001).

The actual flow patterns through the beds are shown in figures 5.19. These show colour plots of velocity magnitude and turbulent kinetic energy on vertical and horizontal cutting planes through the domain. The random packing of the spheres is clearly visible; also note the practical difference between the interior of the bed and the near-wall region where the packing of the spheres is constrained by the presence of the wall. This lowers the porosity in these regions and a significant fraction of the flow is being channelled through this region. One advantage of computational simulation of the flow is the vast volume of data available for analysis; in particular here, flow velocities at every point in the bed, which are available for statistical analysis.

Figures 4.23 and 4.24 depict pressure in its dimensionless form as a function of the bed distance ratio. We can see that they loosely obey the hypothesis of Martin (1978) who defined the wall region as being one half of the particle diameter. Note the effect of the boundary layer at the near wall regions (in addition the pressure is considerably higher at the wall region indicating higher velocity and distinct flow channelling). The low pressure away from the wall

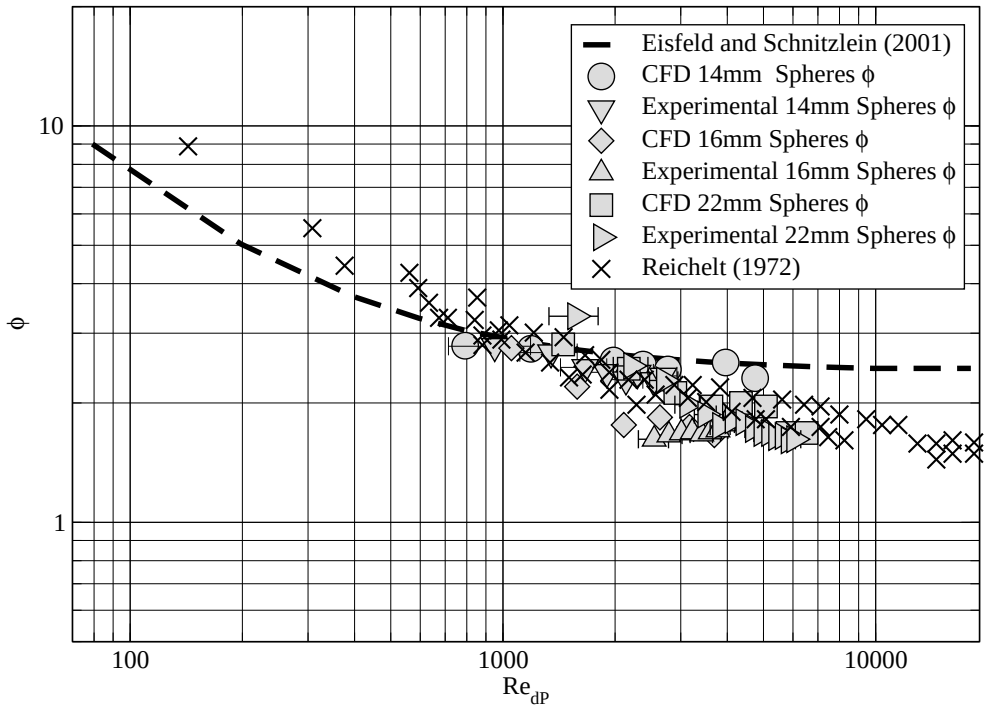

Figure 4.19: Dimensionless pressure drop (ϕ) as a function of particle Reynolds number (Re_{dp})

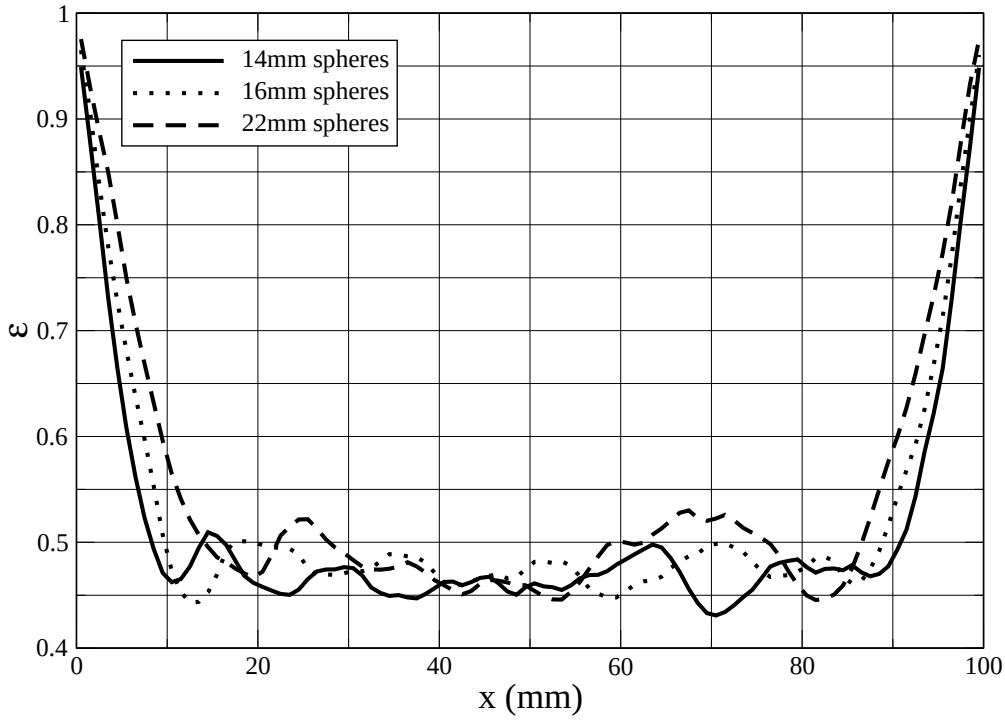

Figure 4.20: Porosity as a function of distance across the x-plane of packed bed

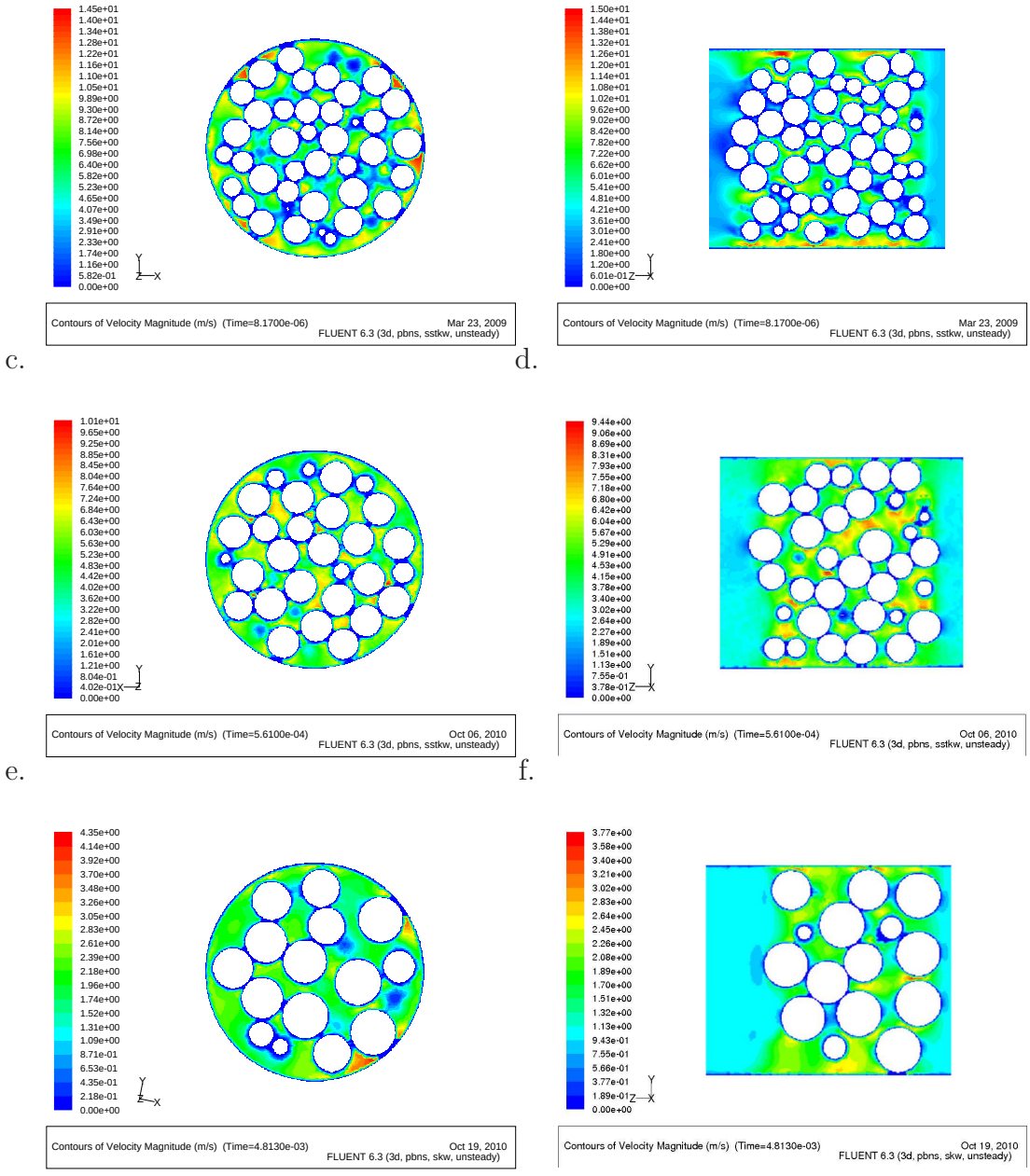

Figure 4.21: Contours of velocity magnitude for 14mm spheres (a,b), contours of velocity magnitude for 16mm spheres (c,d), contours of velocity magnitude for 22mm spheres (e, f). Fluid flow is in the $+z$ direction

a. b.

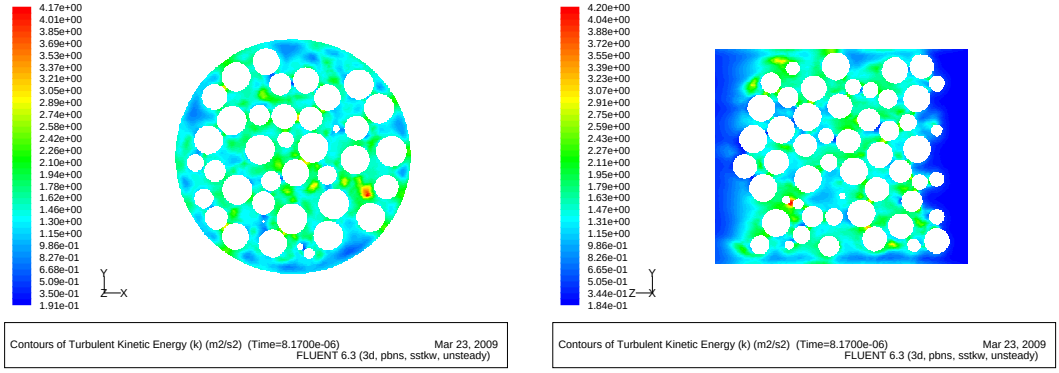

Figure 4.22: Contours of turbulent kinetic energy for 14mm spheres (a, b)

reinforces the well established theory of Stanek (1994) and Foumeny *et al.* (1993) that the inhomogeneities in the wall region cause increased flow channelling. We can also see that the size of the wall region and distinctive flow channelling is more prevalent in the 16mm media in comparison to the 14mm media. Although we are primarily interested in the drop in pressure, near-wall effects can also be seen in the structure of the flow patterns themselves. When fluid percolates through a network of channels, the pathway of mainstream velocity at a low Re takes the shortest route through the backbone of the bed (Andrade *et al.*, 1997). At higher values of Re, the pathway of mainstream velocity is dictated by the bed geometry (Andrade *et al.*, 1997). In addition, the high pressure zone at the centre of the bed is due to the high resistance to the flow caused by bed core regions lower porosity in comparison to the wall reion. Figure 5.19 a-b illustrates pathways of mainstream velocity through the bed, biased towards the wall region.

4.6.1 Uncertainty

With every experimental study there is always a certain amount of uncertainty in the approach used. This work is primarily a computational study where the experiments validate the computational data. In addition, this is uncertainty or the possibility of error in contrast to physical error. Here there are no error bars plotted for computational data, due to there being no uncertainty in the result

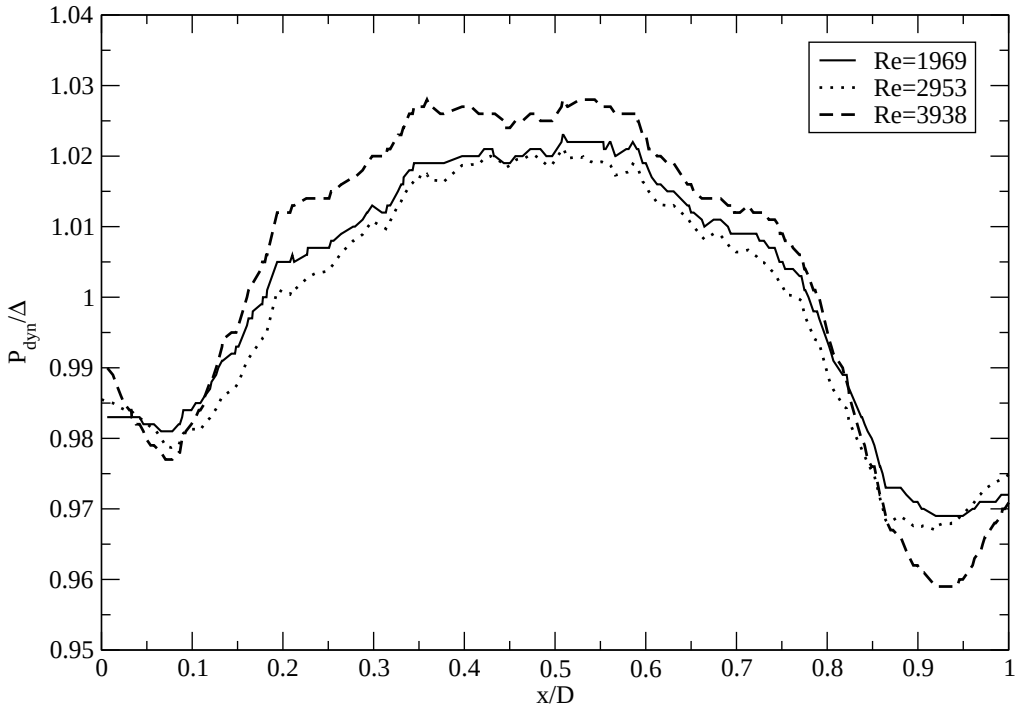

Figure 4.23: Dimensionless pressure distribution as a function of the distance ratio across the bed for 14mm media

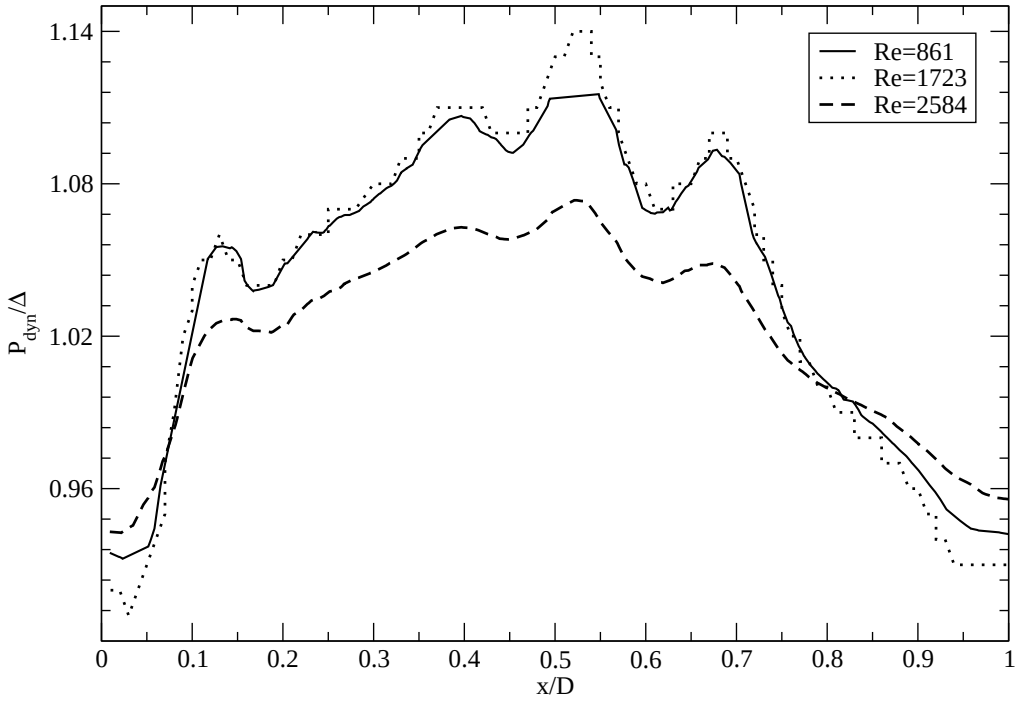

Figure 4.24: Dimensionless pressure distribution as a function of the distance ratio across the bed for 16mm media

of the mathematical approach used. However there may be uncertainty in the mathematical approach itself, in regard to the averaging procedure, in respect to a suitable length scale and the production of k. In addition the full turbulent behavior within the bed is not known and as a result assumptions have to be made when choosing a suitable turbulence model. To determine the uncertainty within the turbulence model would constitute an advanced numerical analysis of all the transport equations used and would be tortuous and arduous and most of all far beyond the scope of this work. None the less, the results match closely and with the 14mm and 16mm spheres fall well within the margin of uncertainty. The results produced for the 22mm holds the same quadratic trend but the magnitude of deviation is quite considerable. It is appropriate to use a statistical method to quantify the deviation in the form of the root mean square (RMS) deviation in respect to the computational compared to the experimental as well as a graphical plot. The RMS is given as

$$\sigma = \sqrt{\frac{1}{N-1}\sum_{i}^{N}\left[\frac{\Delta P/L_{EXP} - \Delta P/L_{CFD}}{\Delta P/L_{CFD}}\right]^2} \tag{4.14}$$

Here the RMS deviation (σ) is given in table 4.4. However, this statistical deviation is a bulk representation of the data and its value is heavily penalised due to the divergence in data in the higher Reynolds numbers. In which case, a windowed value is also given (σ_w) which excludes the CFD which diverges away from the experimental at the higher Reynolds numbers. This is not implemented for the $14mm$ spheres as the data does not diverge due to the relatively narrow range of data. It must also be remembered that the RMS represents the deviation of the raw data, neglecting any uncertainty (error bars) and in the case of 14mm and 16mm spheres the data falls within the margin of uncertainty.

4.7 Discussion

Results for 14mm and 16mm spheres show a strong correlation with the equivalent experimental beds with a RMS deviation of $\sigma = 0.24$ and $\sigma = 0.26$ respectively. The computational beds produced by MacroPac slightly over predict the drop in

Properties	σ	σ_w
14mm spheres	0.24	-
16mm spheres	0.26	0.13
22mm spheres	1.5	1.35

Table 4.4: Root mean square of the standard deviation of CFD compared with experimental

pressure for 14mm spheres and in turn slightly under predict the drop in pressure for 16mm beds. None the less, the results match closely.

This small discrepancy can be attributed to a number of factors. Firstly, the turbulence model is based around a mathematical assumption (a Boussinesq approximation) which may account for the slight deviation. We know from the work of Menter *et al.* (2003) that the SST $k-\omega$ model has a limiter in regard to the production of k and in which case turbulent kinetic energy may be unrealistically low in the stagnation zones. However, it can be argued that there is minimal flow in a stagnation zone, so is this continuous production of k having any effect on the drop in pressure? The model may additionally be producing unrealistic levels of k in regions of minimal turbulent activity. This is because the production of k is not a known quantity but a product of the closure equations and the guess and correct procedure. It is debatable if what we are seeing here is actual true stochastic turbulence or just bursts of un-steady flow behavior, such as the formation of vortices behind the particles which detach and are then damped out by the geometry and viscous shear. In addition the turbulence model is likely to model all unsteady behaviour as turbulence, which may give unrealistically high values of k.

Secondly, the inlet flow profile here is assumed to be flat and hence reassembling a transitional to turbulent profile, in this case more flow may be channelled through the bed centre than through the wall region which provides less resistance, resulting in a higher pressure drop. This effect of the wall has been argued extensively by Stanek (1994) Mehta & Hawley (1969) with no conclusive outcome as to the effect of the wall region. Conversely, it could be argued that the pipe Reynolds number at the bed inlet is turbulent and thus obeys a 1/7 power law

profile, which can be modelled by the plug flow assumption due to a flat profiles closeness to a 1/7 power law.

Finally, the most influential parameter is likely to be discrepancies in bed geometry, here the three beds satisfy all the dimensional properties and are considered equivalent beds, however, this does not account for bed structure, which we already know is random and disordered. Most of all the internal flow paths and geometry could be significantly different. We know that as the aspect ratio increases the variance in bed structure becomes less influential ultimately leading to a continuously packed bed. Conversely when the aspect ratio is around 0.9 there is only one packing possibility, although its polar orientation may vary. The effect of the aspect ratio on the bed structure can be seen with the 22mm bed, the aspect ratio is lower and as a result, the internal bed structure is likely to vary considerably from the experimental. It is plausible that this accounts for the large discrepancy in results ($\sigma = 1.5$).

To reinforce the data presented in this chapter, all the results presented are compared with the results of Reichelt (1972) due to the similarity of Reynolds numbers and aspects ratios. The results compare well with the results falling in the middle of the spread of data. The results are also compared with the correlation proposed by Eisfeld & Schnitzlein (2001). The discrepancy between that of the CFD, experimental results presented here and the correlation proposed by Reichelt (1972) can be attributed to the coefficients determined by Eisfeld & Schnitzlein (2001) which are taken from a large spread of 2300 data points from 24 sets of published results over a time-frame of 70 years. Figure 4.25 shows the data used to form the correlation of Eisfeld & Schnitzlein (2001), note the large spread of data in figure 4.25 at the higher range of the Reynolds numbers with $Re' = 1\times10^3 - 1\times10^6$ with almost an order of magnitude difference. This variation is most likely attributed to the wide range of shapes and sizes of particles. In addition there may be a statistical phenomena in which the majority of research has been carried out at these Reynolds numbers due to different experimental techniques and technological advances.

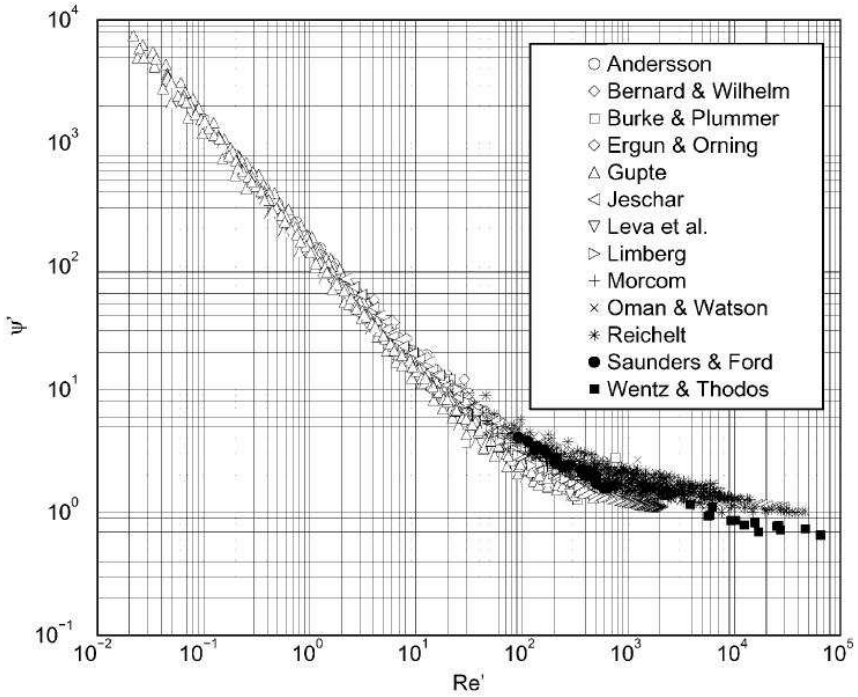

Figure 4.25: modified dimsensionless pressure drop ($\psi' = \phi' = \phi\varepsilon^3/1-\varepsilon$) as a function of the modified Reynolds number $Re' = Re_{dp}(1-\varepsilon)$ (Eisfeld & Schnitzlein, 2001)

4.8 Conclusions

This work has demonstrated the ability to construct and probe micro-structural flow through randomly packed beds using a Monte-Carlo algorithm coupled with the FV method. The macroscopic flow behaviour, i.e. the pressure drop per unit depth, was found to correlate well with experimental results in the case of 14mm and 16mm beds, but has shown significant discrepancies in exceptionally low aspect ratio beds (16mm spheres). As expected, theoretical approximations slightly over predict the pressure drop compared with computational and experimental results. This work has shown that comparing equivalent beds with computational artificial beds has shown a good correlation, but due to deviation in bed structure can cause discrepancies in the results. In which case a technique is required in which actual beds with the same structure can be compared to validate the technique.

Chapter 5

Image based meshing of 3D MRI scans of packed beds

> "Anybody who has been seriously engaged in scientific work of any kind realizes that over the entrance to the gates of the temple of science are written the words: 'Ye must have faith"'
>
> Max Planck

5.1 Introduction

Chapter 4 has demonstrated that CFD is a powerful tool for understanding the fluid flux through and pressure drop in packed beds. However, the method described in Chapter 4 is limited by the arduous task of creating the geometry and even then the quality of the mesh can be dubious. In addition, this approach generates randomly packed computational beds and compares them with equivalent beds which gives a good engineering approximation of the pressure drop, however the beds being compared are not geometrically faithful and flow distributions between the beds may vary considerably, with this effect becoming more so as the aspect ratio decreases. Due to this there is a need for computational beds to be geometrically faithful in respect to structure and flow paths as the physical beds for direct computational comparison. Chapter 4 has also highlighted robustness issues with traditional meshing software and complex geometries, so additionally

a more robust meshing technique is required to ensure computational stability and better mesh quality.

One possible method of analysing a physical bed is to use a non-invasive imaging method such as micro-CT or MRI (Manz *et al.*, 1999; Sharma *et al.*, 2001; Zhang *et al.*, 2006). This approach gives an accurate representation of complex geometries but problems arise in processing these geometries when using traditional CAD based meshing software such as Ansys Gambit. Considerable user intervention and simplification of the geometry is required to make surface creation of the flow domain possible. In this work, preliminary trials demonstrated that using traditional meshing software to create a domain was at this stage impossible due to the imperfections resulting from the scan resolution and the complexity of the MRI scan.

The work described here focuses on the use of image-based meshing software originally developed for the field of computational bio-mechanics, to create geometrically faithful geometries from 3D MRI scans of packed beds for use with computational dynamics. Disordered packed beds of cylinders ($A_{ratio} = 4.35$) and spheres ($A_{ratio} = 6.25$) are analysed in the Reynolds numbers of $Re_dp = 2 - 4735$. Suitable flow velocity inlet profiles are used to correctly reflect both fully developed laminar and turbulent flows. Where the flows are considered turbulent, the $k - omega$ SST model is used as a closure for the RANS equations. Similar work using non-invasive methods and an IBM approach has been applied to foams in the past (Tabor *et al.*, 2008) but as far as the author is aware this is the first application of these techniques to a packed bed.

Although this work is primarily a computational study, experiments were carried out on the actual scanned beds using the same approach as Chapter 4. In addition, the results are compared to the correlation of Eisfeld & Schnitzlein (2001) to describe the dimensionless pressure drop in low aspect ratio beds and the results of Reichelt (1972).

5.2 Experimental data

There is a level of uncertainty involving user inputs and estimation when using CFD. Due to this uncertainty CFD data is best reinforced with experimental data

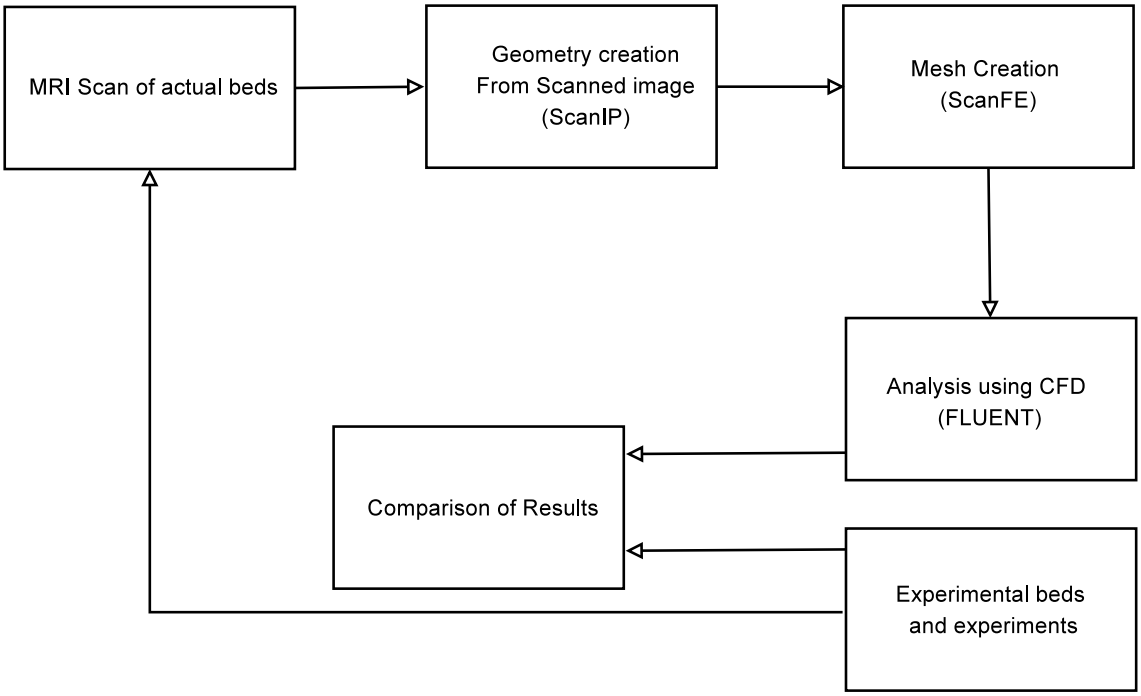

Figure 5.1: Chapter 5 methodology flow diagram

to give some validity to the solution. To this end, experimental pressure drops were measured using the experimental rig described in Baker & Tabor (2010) (Chapter 4). The rig is based on that of Tóbis (2000), with the addition of pressure taps into the bed at 0.1 m vertical intervals. Air was forced through the bed using a centrifugal pump. Volumetric flow rate Q, and hence average velocity U, was determined by measuring differential pressure (ΔP), across a plate orifice manufactured from Perspex and previously calibrated (Chapter 4). Two beds were constructed; the first used PVC rods of diameter 20 mm cut to lengths of 30 mm and packed randomly into the bed, the second consisted of 16mm marbles packed in the same way to generate a spherical disordered pack.

5.2.1 Magnetic Resonance Imaging

In this work, to generate the 3-dimensional images of the bed in order to create a mesh, MRI is used. The two packed beds were scanned using a Phillips 1.5 T whole-body MRI imager located at the Peninsula Medical School (University of Exeter), using a 2D fast spin echo (FSE) with 0.5mm^3 voxels.

The MRI scanner produces a 3-dimensional image by taking a series of slices through the bed where each slice is 0.5mm thick with each voxel contained in the slice is 1mm×1mm MRI excites hydrogen molecules within tissue, so for the scanner to distinguish between the void space and the media, the void space around the glass marbles was filled with a substance containing hydrogen molecules, in this case oil. In this case, oil was used due to its abundance and 'as an experiment' on reccomendation of the centre staff. In regard to geometric fidelity, magnetic susceptibility induced artifacts can be observed in the spherical media due to the severe susceptibility induced distortions in static magnetic field in which the sample has been placed. High resolution MRI, as used here, requires a higher B-uniformity susceptibility variation within the sample. Due to this, the cylinders were scanned using water as the void filling liquid due to their relatively close susceptibilities. Due to the need for high resolution, a small diameter coil was used. However, the length of the coil was not sufficient to capture the whole bed, so in which case the particles have effectively been cut through their cross section. A typical image produced from the cylindrical scan is shown in figure 5.2.

Image Based Meshing techniques, as described in the next section, were used to generate the geometry from this data and to create a FV mesh for the solution.

5.2.2 Porosity

One of the most influential parameters concerning the drop in pressure caused by the presence of the media is porosity. Porosity ε is defined by the ratio of the volume of voids (V_v) and the total volume (V). In this case we take the volume of voids as the mesh volume. In cases of high aspect ratios (such as a packed bed of sand) the porosity can be defined as being homogeneous with no measurable wall effect. When a bed is defined as being low aspect ratio the porosity is heterogeneous and can be broken down into two distinct regions of wall porosity and core porosity. The traditional method of measuring porosity is usually via water substitution, however this only has the ability to determine mean porosity, whereas bulk and core porosity are harder to determine and are usually calculated theoretically by approaches such as that of DiFelice & Gibilaro (2004). Alternatively, non-invasive approaches, such as MRI and CT can be used to investigate void volume and hence local porosity (Nguyen *et al.*, 2005; Wang *et al.*, 2001; Zhang *et al.*, 2006).

As described below, image based meshing techniques are used to generate body-fitted finite volume meshes from the MRI scans of the beds. Given these it is straightforward to calculate the volume of the mesh (i.e. the volume of the fluid region around the particles) and the total bed volume, and assess the porosity in this way. Both experimental and computational approaches are subject to experimental error; in particular, the start and end positions of the beds are not well defined (the thickness problem), and this is a significant issue for such a small bed (this would not be an issue for an industrial-sized bed as this would be significantly larger). Computational porosities are compared to the water displacement method to verify results. Sharma *et al.* (2001) suggest that analysis of MRI data yields consistently higher values of porosity in comparison to water substitution; however in this case the porosity determined via MRI coupled with image-based method yielded a slightly lower porosity than that from water substitution. For the cylinders the computational porosity was evaluated

Media	ε_{MRI}	ε_{EXP}	ε_{THE}
Cylinders	0.53	0.54	0.46
Spheres	0.48	0.49	0.43

Table 5.1: Porosities for cylindrical and spherical media

as $\varepsilon_{MRI} = 0.53$ against $\varepsilon_{EXP} = 0.54$ for the experimental value. For spheres $\varepsilon_{MRI} = 0.48$ against $\varepsilon_{EXP} = 0.49$. We can also compare these porosities with porosity correlations determined from empirical data such as the porosity relation defined by Jeschar (1964)

$$\varepsilon = 0.375 + \frac{0.34}{d_p/D} \tag{5.1}$$

Table 5.1 shows the porosities determined from MRI/IBM, water substitution and the empirical correlation proposed by Jeschar (1964). We can see that the correlation proposed by Jeschar (1964) under predicts the the cylindrical media quite considerably ($\Delta\varepsilon = 0.08 - 0.09$). Firstly, the correlation is based on spherical media, in addition we know that cylindrical media is highly disordered and depending on the orientation of the particles and density of the packing the porosity can vary considerably. As the reader might expect, the values for spheres show a closer agreement ($\Delta\varepsilon = 0.05 - 0.06$), but again the correlation makes no allowance for the density of the packing. Furthermore, the two porosities calculated from MRI and from the water substitution are on the same bed, where as the model proposed by Jeschar (1964) is produced from a regression analysis of many experimental beds. We can see from figure 5.7 that the MRI/IBM method does not retain perfect geometric faithfulness and modifies the geometry to suit the mesh. Further more, the water substitution method has uncertainties in regard to wetting, bed start/finish and entrapped air. All three methods have their associated uncertainties and considering the closeness of MRI with the time honoured water substitution method and the same bed, we can assume the value of porosity lies somewhere in the region $\varepsilon = 0.48 - 0.49$ for spheres and $\varepsilon = 0.53 - 0.54$ for cylinders.

Figure 5.2: Typical image x-axis slice produced by 3d MRI. Note the random disordered nature of the of the packed bed from the cylinders being effectively cut.ss

5.3 Image Based Meshing

In computational biomechanics (and here), a frequently encountered problem is that of defining, describing and meshing the geometry of interest. Biological geometries such as arteries or bronchial pathways tend to be complicated and difficult to describe, and also patient-specific; however the flow conditions can be very sensitive to the details of the geometry (Collins *et al.*, 2007) as with flow through porous media. Due to this there is a significant interest in techniques for automatically generating geometries and meshes from medical scans such as MRI scans, which inherently provide 3d geometric information. This is known as Image Based Meshing, or IBM. The fundamental problem of generating a mesh for a complex, unknown geometry based on a 3d scan occurs in a number of other areas of engineering (Tabor *et al.*, 2007) and in particular is the problem we face when trying to construct a geometrically accurate representation of the packed beds.

There are two general approaches to IBM in existence. One is to generate

bounding surfaces from the 3d scans, generally by employing some form of edge detection algorithm. The resulting surfaces (generally saved as STL files) can then be used by standard automatic mesh generation software to create the volumetric mesh. This works for topologically simple geometries, however applied to highly complex and multiply connected domains such as are the case for packed beds, the surface description will be exceedingly complex and meshing is likely to fail. Even when successful, when computational meshes are created using a traditional Delaunay-triangulation approach the meshes often contain large numbers of highly skewed elements and even non-positive volumes primarily around the areas of particle contact points.

The alternative is to combine the geometric detection and mesh creation stages in a single process, an approach which is used in the software ScanIP/ScanFE (Simpleware Ltd, Exeter, UK) used in this work. The process of generating a mesh involves first segmenting the different volumes of interest (VOI) from the 3D data. Both semi-automated and manual techniques are available within ScanIP, as well as a range of alternative image processing packages, to provide segmented masks. Techniques include noise filters, three dimensional threshold tools through to bitmap painting. These VOI are then simultaneously meshed based on an isotropic grid intersected by interfaces defining the boundaries. A base Cartesian mesh of the whole volume defined by the sampling rate is truncated at boundary interfaces based on cutting planes defined by interpolation points. Smooth boundaries are obtained by adjusting the interpolation points in one, or a combination, of two ways: by setting points to reflect partial volumes or by applying a multiple material anti-aliasing scheme. The process results in either a mixed tetrahedral/hexahedral mesh or can be converted to a pure tetrahedral mesh and incorporates an adaptive meshing scheme. An adaptive meshing scheme is available which preserves the topology but reduces the mesh density where possible towards the interior of the mesh by agglomerating hexes into larger hexes and generating transitional tetrahedral cells. The approach is fully automated and robust, creating smooth meshes with low element distortions regardless of the complexity of the segmented data. This software was originally developed for FE analysis of bones, for both stress and vibration analysis (Johnson &

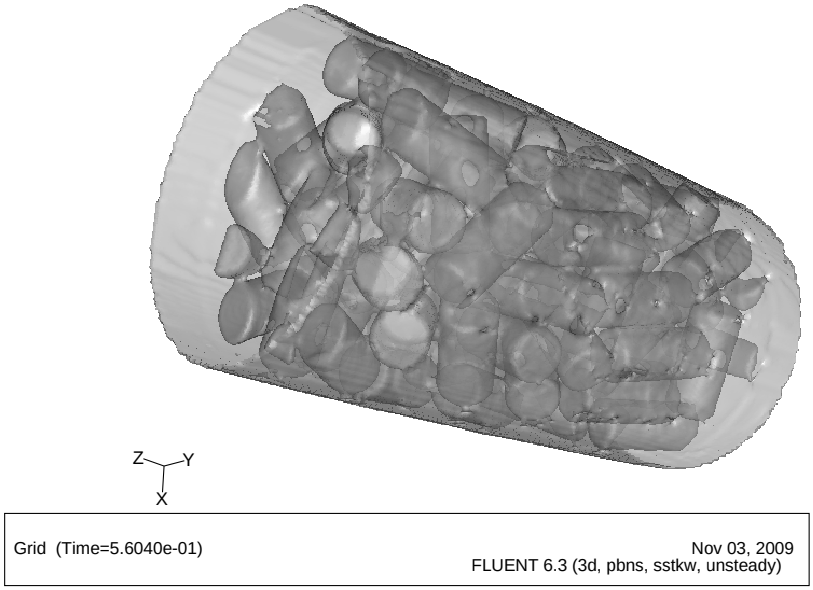

Figure 5.3: Computational domain for cylindrical media generated from MRI and IBM

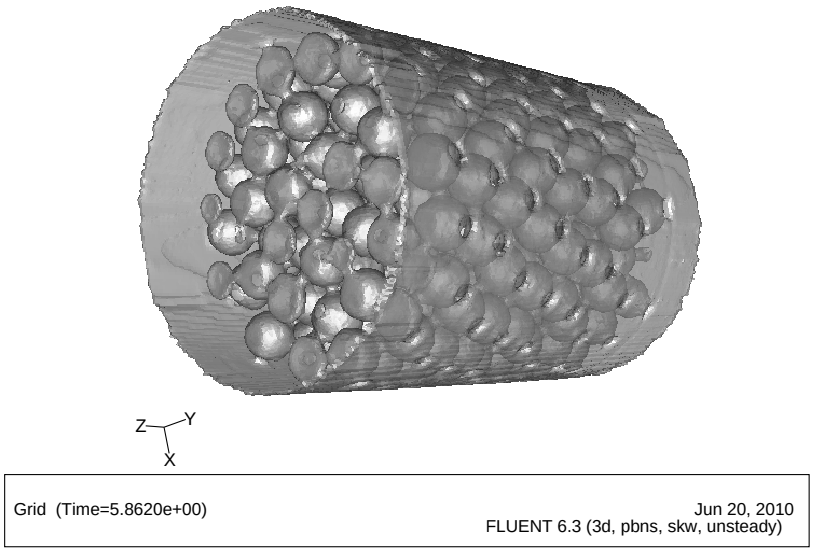

Figure 5.4: Computational domain for spherical media generated from MRI and IBM

Young, 2005; Zunarelli & Young, 1999). Since FE and FV meshes are conjugate structures, the same techniques can be used to output a FV mesh (cell/face representation, rather than point/edge representation). From this method, surface models suitable for rapid prototyping can also be generated which are exact representations of the meshed domains. Amongst other things this also allows experimental tests to be carried out to provide experimental corroboration of numerical results, demonstrated in the following chapter.

The quality of the scans is such that the MRI data is virtually binary, with the majority of voxels taking values 0 and 255 and virtually nothing in between. Thus segmenting the data is very straightforward. Although ScanIP provides various filters, such as Gaussian and noise reduction, to reduce noise in the image, the binary characteristic of the data meant that no preprocessing of the image stack was necessary, and the flow domain mask was easily segmented as the inverse of the bed particles (the white areas in figure 5.2; a typical MRI slice through the x-axis of the bed). The scan is of course not perfect, but represents a pixelation of the true geometry. This is particularly the case where the cylinders touch; two spheres touch at a mathematical point, but this has to be represented by at least a single voxel, and often the scanned elements are seen to merge, as can be seen in figure 5.5. This same phenomena can also be observed in the work of Johns *et al.* (2000) where particles merge together at the contact points.

These contact points form the major constraint when constructing a suitable mesh of minimal skewness. Thus, the IBM approach gains its robustness from increasing the size of the contact points in the voxelising process, reducing the need to create skewed elements inter-particulate contact region. The practical effect of this is to increase the volume of space occupied by the bed particles and reduce the porosity, as described above.

Figure 5.8 shows contours of cell squish index. This clearly shows the necking of the particles, which is an effect of the MRI resolution. Image-based meshing, due to its voxelisation approach also causes particle necking, but the magnitude of this is less apparent than the necking phenomena caused by the MRI scan resolution. In this case the particles have already been 'necked' by the MRI scan, so to speak. In comparison to the Delaunay algorithm used by Gambit and demonstrates in the previous chapter, the cell squish at the particles is quite

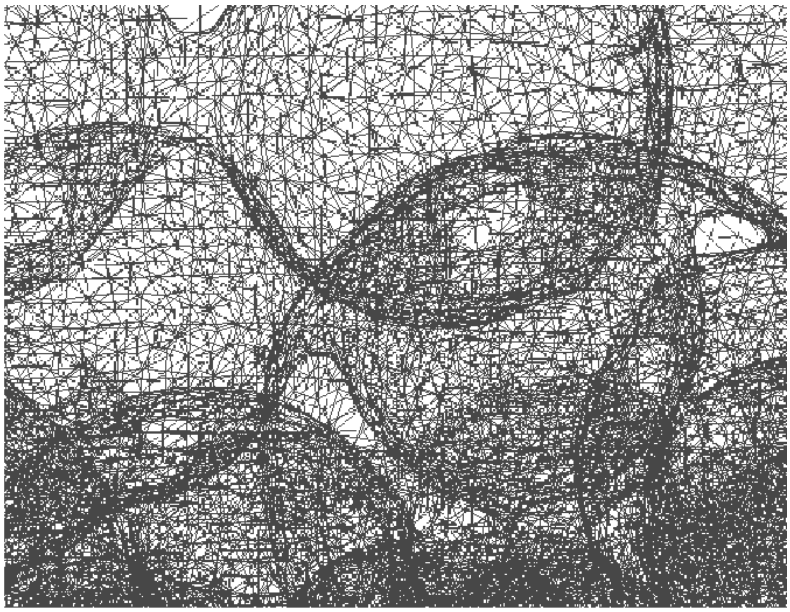

Figure 5.5: Mesh produced using IBM from MRI data

considerably less than the Delaunay approach and note the highly structured mesh in the void volume. Many of the problems encountered when trying to create a mesh from an MRI scan using traditional Delaunay triangulation are due to the added compexity produced by the scan resolution such as additional voids and inclusions (Figure 5.8).

ScanIP also provides facilities whereby the segmented mask can be dilated or eroded by a pixel or a fraction of a pixel, resulting in smaller or larger bed particles and higher or lower porosity. However the overall porosity was close enough to the experimentally-determined value and so this was not thought necessary.

We know that in the FV technique the domain has to be discretized into discrete volumes (tetrahedral, hexahedral etc) thus making meshing a rounded and spherical surfaces smoothly, virtually impossible without an infinitely small mesh or a higher order cells with curved faces, (such as NURBS patches). Figures 5.9 and 5.10 depict cell volumes for both cylindrical media and spherical media respectively. We can see that the cell volume distribution for cylinders has a wider range of volumes reflecting both the disordered pack and the larger voids (reflecting the porosity). Various algorithms also exist which offer improved tetra-

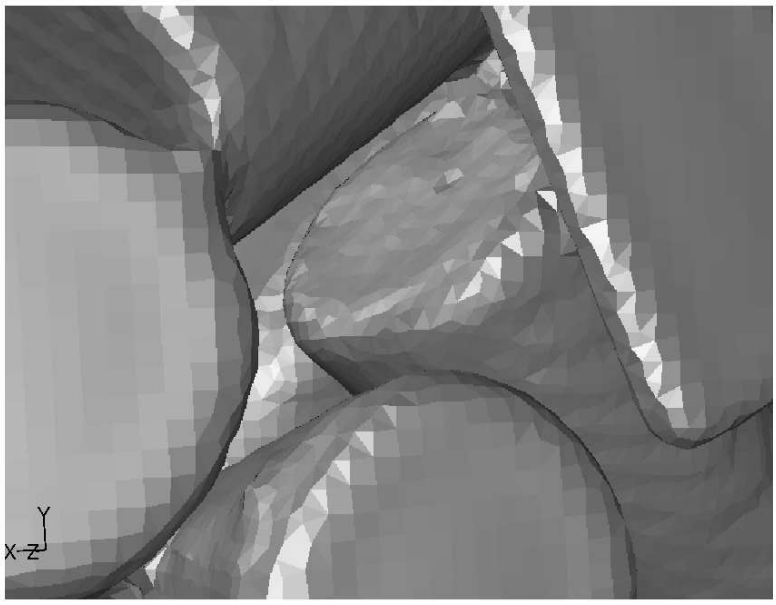

Figure 5.6: Close up of particle contact points for cylindrical media

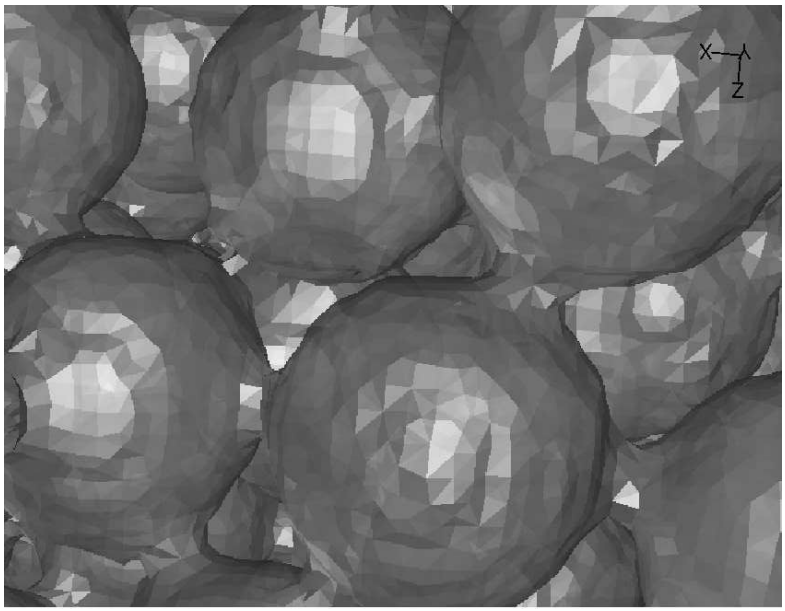

Figure 5.7: Close up of particle contact points for spherical media

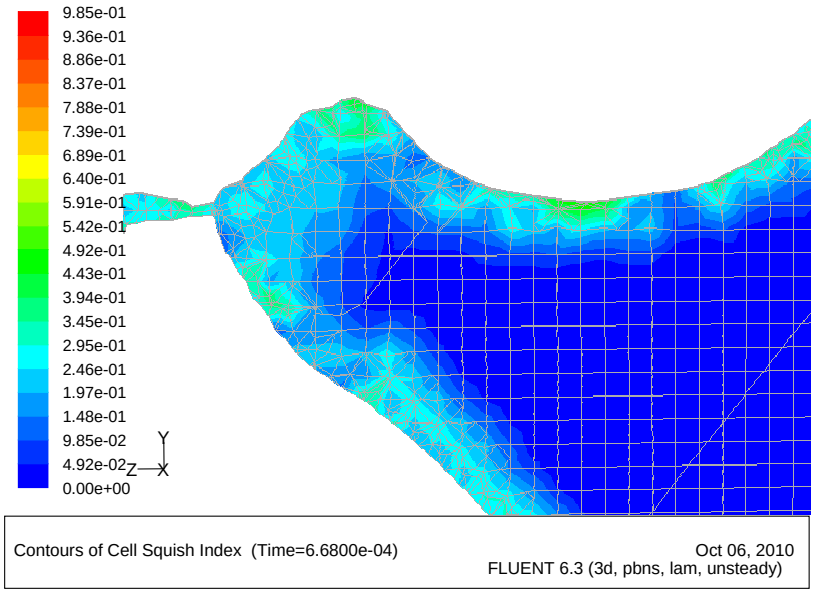

Figure 5.8: Contours of cell squish index for cylindrical media. Note the structured grid in the free-stream.

Property	Cylinders	Spheres
Max Cell vol	$1.54 \times 10^{-9}\text{m}^3$	$5.32 \times 10^{-12}\text{m}^3$
Min Cell vol	$6.66 \times 10^{-17}\text{m}^3$	$1.65 \times 10^{-12}\text{m}^3$
Max face area	$2.51 \times 10^{-6}\text{m}^2$	$1.34 \times 10^{-6}\text{m}^2$
Min face area	$1.53 \times 10^{-11}\text{m}^2$	$2.05 \times 10^{-8}\text{m}^2$
Overall Mesh Volume	$1.02 \times 10^{-3}\text{m}^3$	$7.92 \times 10^{-4}\text{m}^3$

Table 5.2: Bed mesh data

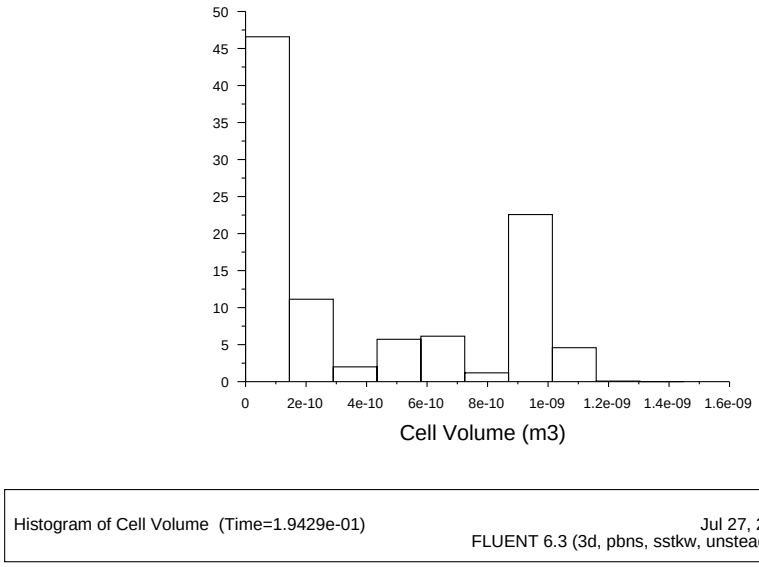

Figure 5.9: Mesh element volume distribution for cylinders

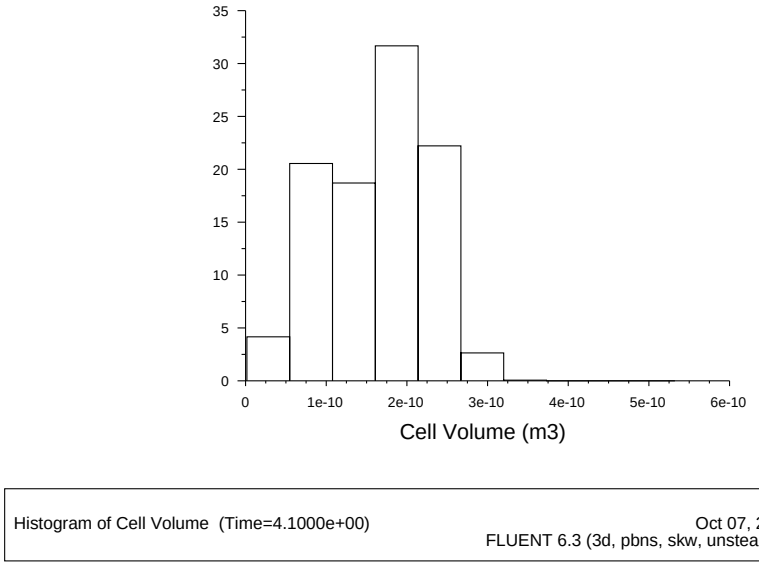

Figure 5.10: Mesh element volume distribution for spheres

hedral/hex mesh regimes (Alliez *et al.*, 2005; Leland *et al.*, 1998). In the case of coarse mesh regimes this results in spherical objects being represented as geodetic spheres affecting the fluid flow at the near boundary region such as the early work of Dalman *et al.* (1986). This also introduces complications with the mesh quality in the near wall region. Additionally the adoption of the SST $k-\omega$ transitional solver for the turbulent simulations enforces restrictions on the near-wall mesh structure; in particular the laminar sub-layer has to be resolved, resulting in a limit on the size of the cells in the near-wall region. The acceptable y^+ values at the wall adjacent cell should be in the region of $0 < y^+ < 5$. This is achieved as shown in Figures 5.11 and 5.12.

In many cases of mesh quality analysis it is desirable to use a non-dimensional parameter, such as cell equivolume skew (Eq_{vol}), calculated using the volume deviation method (for tetrahedral meshes) and equiangle skew (Eq_{angle} using the using normalised angle deviation method (for mixed tet/polyhedral meshes). For this work we employ the a parameter known as the cell squish index (CSk_{index}). The cell squish index uses the dot-products (scalar products) of each vector pointing from the centroid (the node location) of the cell to each of the cell faces and the face area vector associated with each face. Figures 5.19 (a,b) present a contour plot of cell squish index of a random cluster of cylinders within the bed. As expected the plot indicates that the majority of highly skewed elements are located within the vicinity of the inter-particulate contact points where two particles meet on a curved surface. For this work the majority of highly skewed elements ($CSk_{index} > 0.4$) are converted to polyhedra using Fluent's built in algorithm. Fluent's polyhedra conversion algorithm evaluates a highly skewed tetrahedral cell, locates an edge, then agglomerates the surrounding cells neighbouring the edge and converts the adjoining cells into a polyhedron. We can see from figure 5.13 that the majority of cells fall in the range of $0 < CSk_{index} < 0.3$ indicating an acceptable mesh quality.

5.4 Computational Fluid Dynamics

As described above the range of Reynolds numbers being investigated ranges from laminar through transitional to mildy turbulent, but the disordered structure of

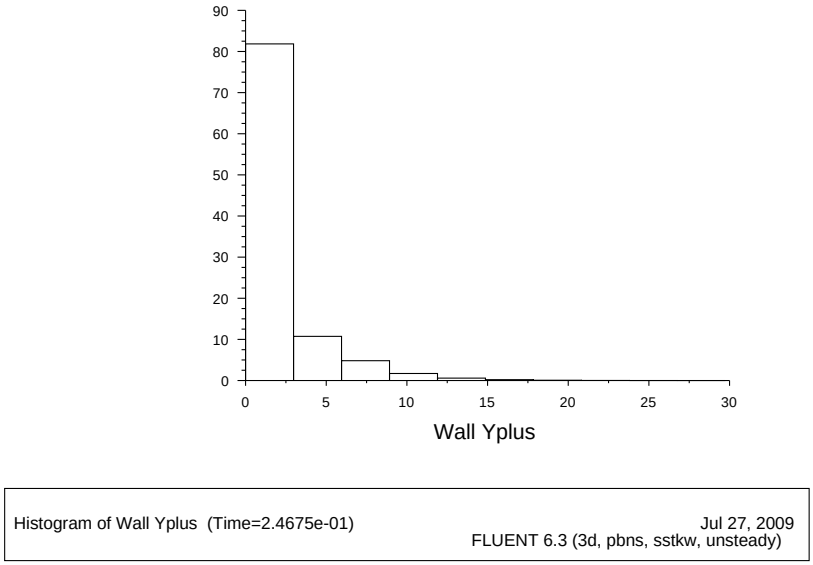

Figure 5.11: Mesh y^+ values at near-wall region for cylindrical media

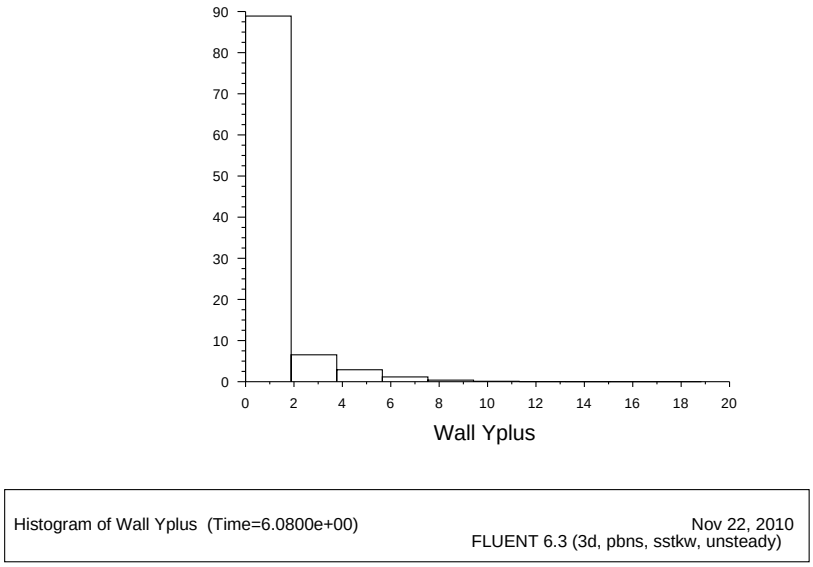

Figure 5.12: Mesh y^+ values at near-wall region for spherical media

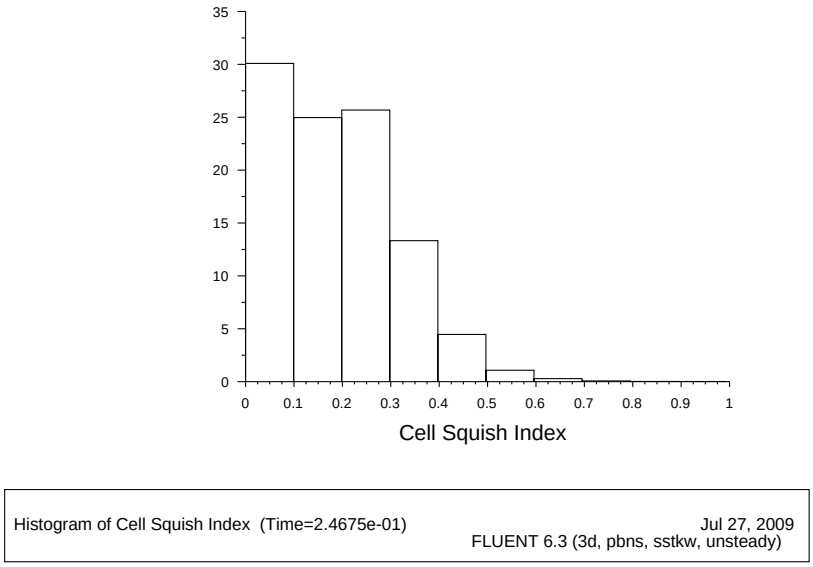

Figure 5.13: Cylinders cesh cell squish index

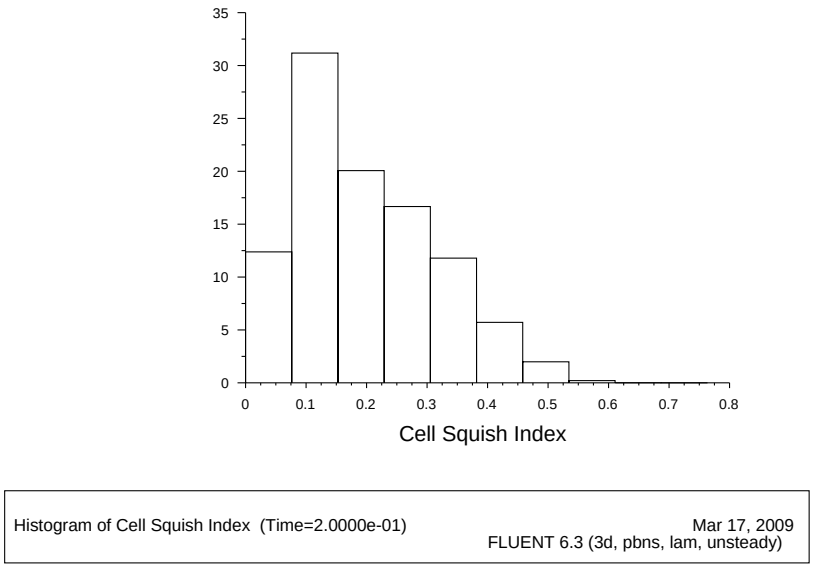

Figure 5.14: Spheres cell squish index

the bed is likely to encourage the development of disordered, stochastic flow (if not true turbulence) even for strictly laminar conditions. Conversely the requirement to resolve the structure of the bed indicates the necessity to resolve the flow with a fine mesh, so one of the main contributions of a turbulence model, that of substituting for the effect of unresolved scales, is not relevant. Accordingly, calculations were run using both laminar and turbulence modelling, and compared. For the laminar modelling, the equations being solved are standard incompressible Navier-Stokes equations. For turbulence modelling, an averaging process is applied to the equations. Here blend of both the $k-\varepsilon$ and $k-\omega$ models is used to form the $k-\omega$ SST models proposed by Menter (1993), the reader can find exact details of the PDEs in chapter 3.

For inlet pipe Reynolds numbers of $Re < 1500$ we expect a fully developed laminar flow and in which case for these cases a parabolic velocity profile is implemented by the modification of the inlet boundary conditions. For pipe inlet Reynolds number greater than $Re = 1500$ we expect the flow to transitional to mildly turbulent and in which case the inlet velocity profile is left flat.

5.5 Results

Properties	σ	σ_w
Cylinders	0.63	0.40
Spheres	0.71	0.66

Table 5.3: Root mean square of the of CFD compared with experimental

Figure 5.15 demonstrates close agreement of pressure drop per unit length for cylindrical media between the experimental results (up turned triangles) and the CFD calculations, both with and without the turbulence model switched on. Agreement between the CFD model results with and without turbulence modelling indicates that at it is plausible that at these Reynolds numbers and mesh resolution the turbulence model is having next to no effect on the pressure drop. It might be that at much higher Reynolds numbers the two sets of results

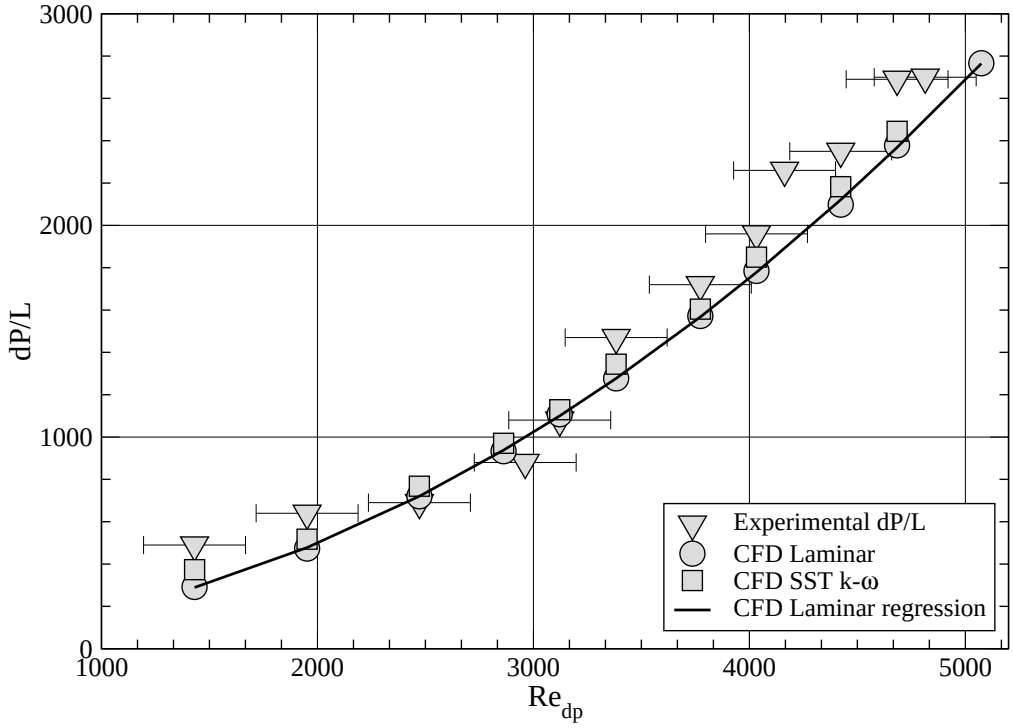

Figure 5.15: Pressure drop per unit length as a function of the particle Reynolds number for cylindrical media. Experimental uncertainty $\Delta Re_{dp} = +/- 236$, $\Delta(\Delta P/L) = \pm 4.167 Pa/m$

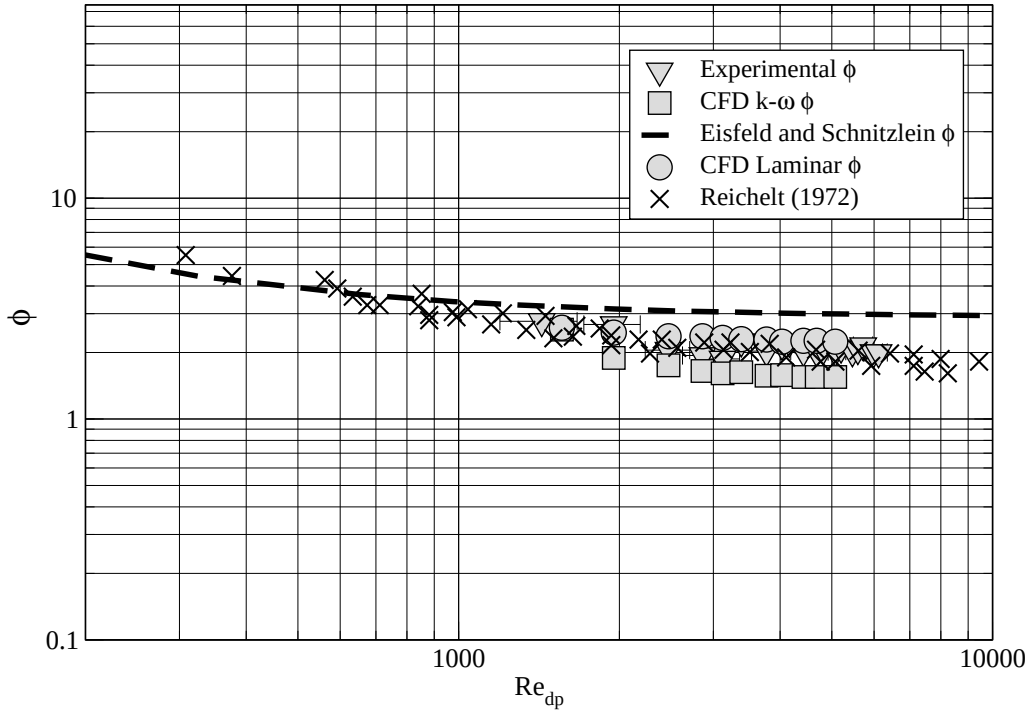

Figure 5.16: Dimensionless pressure drop per unit length as a function of the particle Reynolds number.

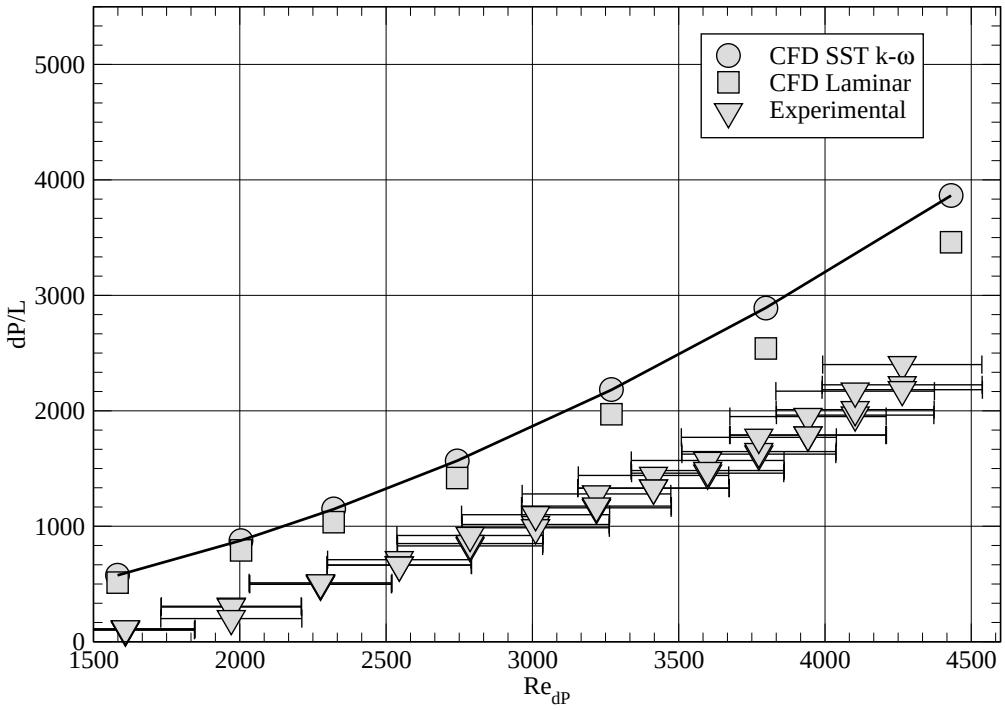

Figure 5.17: Pressure drop per unit length as a function of the particle Reynolds number for spherical media. Experimental uncertainty $\Delta Re_{dp} = \pm 236$, $\Delta(\Delta P/L) = \pm 4.167 Pa/m$

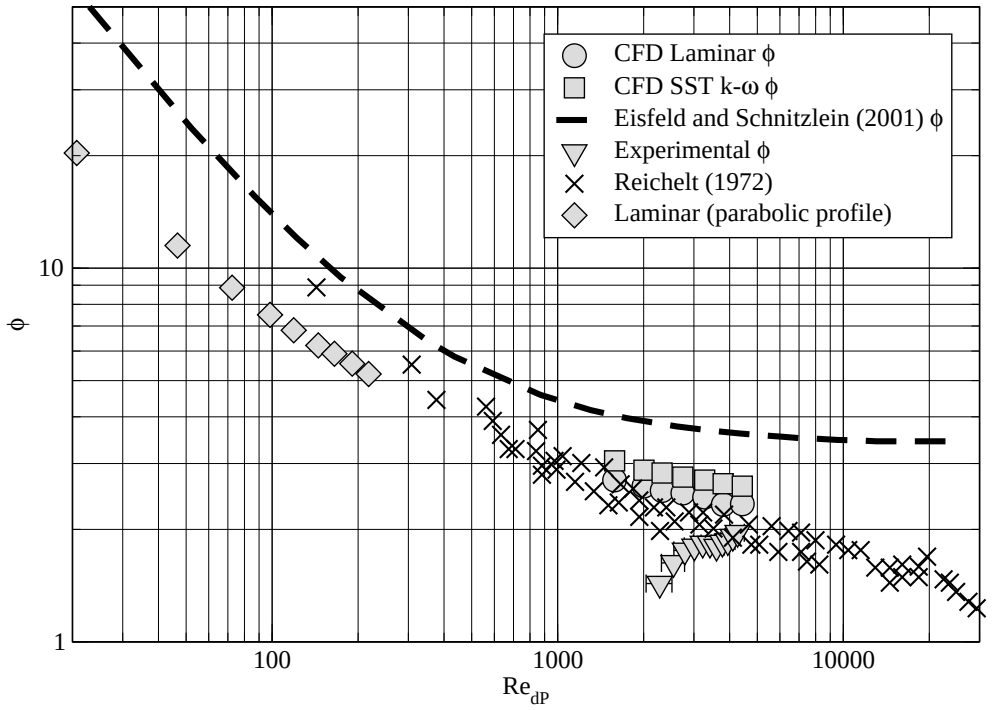

Figure 5.18: Dimensionless pressure drop per unit length as a function of the particle Reynolds number for spherical media

a. b.

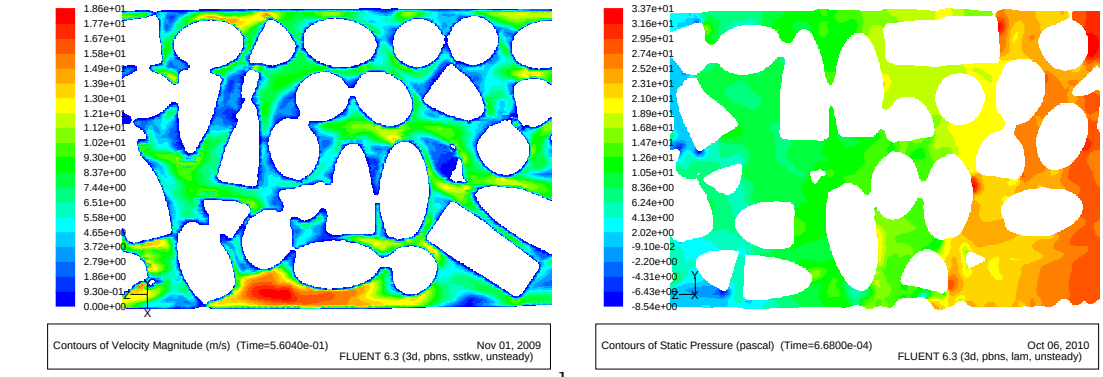

c. d.

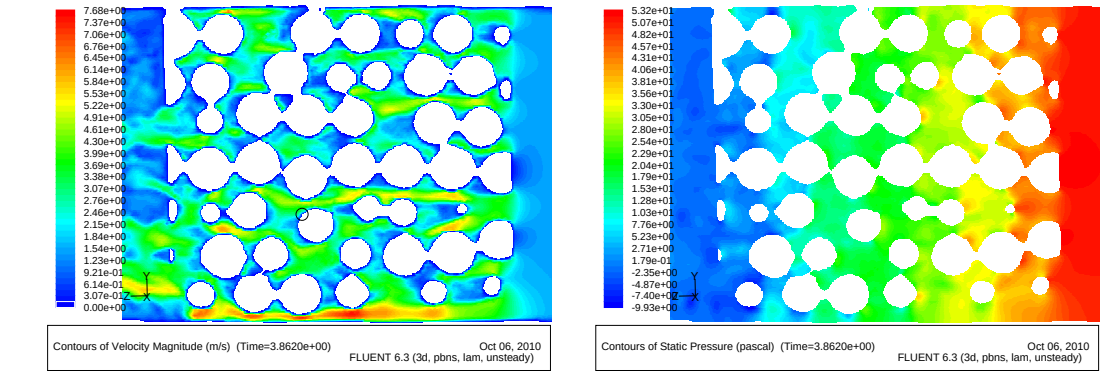

Figure 5.19: Contours of velocity magnitude and pressure for cylindrical media (a,b), contours of velocity magnitude and pressure for spherical media (c,d).

a. b.

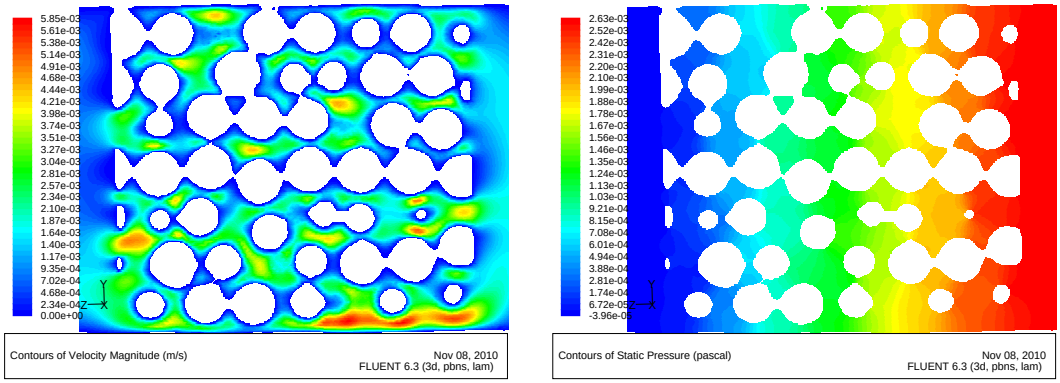

Figure 5.20: Contours of velocity magnitude (a) and pressure (b) for low Reynolds (creeping flow regime)

a. b.

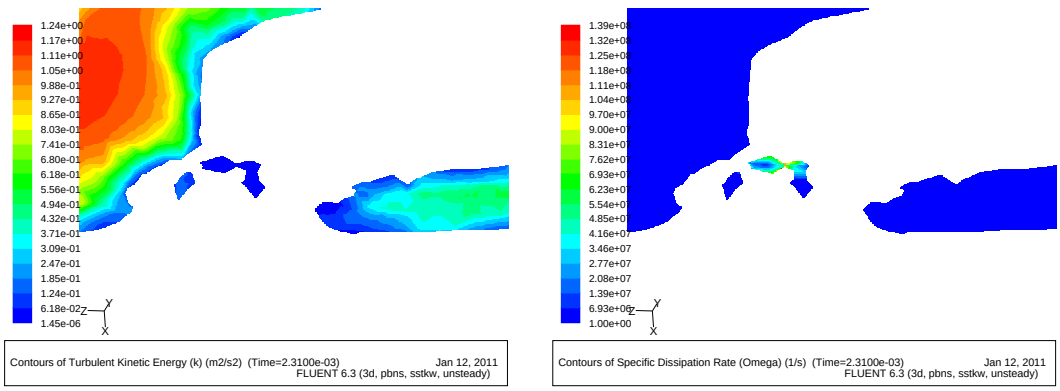

Figure 5.21: (a) Contours of turbulent kinetic energy, k. (b) Contours of turbulent frequency, ω.

might diverge further, but it seems plausible that for these Reynolds numbers the mesh resolution is high enough to explicitly resolve most of the smaller scale flow structures which are a constant as a product of the viscosity. Figure 5.16 compares our experimental and computational results for cylindrical media with the empirical correlation of Eisfeld & Schnitzlein (2001) and the empirical data of Reichelt (1972). Agreement is close although the empirical correlation slightly under-predicts the dimensionless pressure drop diverging as the Reynolds number increases. The reader is reminded that the correlation of Eisfeld & Schnitzlein (2001) is based on an amalgam of a range of experimental data representing several different geometries, whilst our experiments were performed as far as technically feasible on the exact geometry used for the CFD. Figure 5.17 shows pressure drop per unit length as a function of the particle Reynolds number for spherical media. The graph shows that the CFD data over-predicts the pressure drop per unit length and the effect becoming more apparent as the Reynolds number increases. Results for experimental values of dimensionless pressure drop for the spherical media is plotted in 5.18. Note the unusual trend where the dimensionless pressure drop for the experimental data (up-turned triangles) appears to increase as a function of the Reynolds number. This is due to the equation being heavily dependent on the velocity, in addition the logarithmic compression has graphically skewed the data misleadingly in which case the reader should refer to 5.17. The correlation of Eisfeld & Schnitzlein (2001) over-predicts the dimensionless pressure drop considerably, although the data does show a reasonable agreement with the data of Reichelt (1972).

With cylindrical packed beds (Figure 5.15) the geometry is significantly more disordered than it is the case for spherical particles (Figure 5.17), in which case pressure drop can vary significantly with each individual pack rendering it difficult to derive a single formula encompassing each individual case. Where as with spheres, the packing can less disorded and fairly regular and in which case there is less variation in packing with each individual pack. This is demonstrated in the following thought experiment. Imagine a bed of cylinders with a length to diameter ratio of 2, packed into a domain where the cylinders are of vertical orientation and a pressure drop measurement is taken across the medium. If we then take the same number of cylinders and pack them in a horizontal orientation

(as one might stack logs), the pressure drop would be considerably higher. When the cylinders are stacked vertically there is less resistance to the flow compared with a horizontal orientation. What this is saying is the tortuosity is greater when stacked in a horizontal fashion but all the dimensional properties such as porosity, particle geometry etc are the same. In which case, to provide a sensible mathematical explanation for the pressure drop due to this a effect a value of tortuosity must be determined. Here we are back to a common problem addressed in this thesis. There is no direct line of sight into the core of the bed, in addition we do not know which way the flow path is likely to go and there is no mathematical model to describe the random orientation of cylindrical particles.

One of the main sources of discrepancy between the CFD and experiment, more so with the spherical particles (Figure 5.17), can be attributed to the accuracy of reproduction of the geometry through the IBM/MRI process, in particular the effect on the mesh of the necking of the media at the inter-particulate contact points. With bed particles possessing one or more curved faces, when two or more of these objects touch, the contact point becomes infinitely small. This cannot be resolved by the MRI scan, instead the contact regions are represented by one or more contact voxels leading to a merging of the particles in this region. In addition, the thresholding tolerances in the IBM approach may also add or take away voxels in this region. This is demonstrated by the discrepancy in experimental and CFD in figure 5.17. The spheres have considerably more contacts than the cylinders (up to 12). In addition the aspect ratio is higher and in which case there are more contacts with other particles and more contact points with the wall. A contact point with a sphere or other curved surface is infinitesimally small, in which case this has to be represented by the smallest voxel possible (the scan resolution). This coupled with magnetic susceptibility induced artifacts can lead to considerable distortion at the contact points. As a result of these two characteristics, the number of undesired voxels is affecting the porosity to such an extent that it is disturbing the flow patterns through the bed resulting in a quite considerate discrepancy in the pressure drop between CFD and experimental.

A more prominent effect on the pressure drop is due to the limitations of the MRI coil, some of the particles have been effectively cut through their cross section in the computational models. As a result of this the flow impinging on

the spherical media is effectively striking the flat side of a hemisphere. We know from simple fluid mechanics that the drag coefficient caused by the flat side of a hemisphere ($C_D = 1.2$) is considerably larger than a sphere ($Re < 2 \times 10^5$,$C_D = 0.5$). The magnitude of this effect is less apparent with the cylindrical media, this is most probably due to the pack being naturally more disorderly than the spherical media with larger voids. The effect of the flat surfaces at the bed entry is less apparent in the very low Reynolds creeping regime (Stokes flow), where viscous drag is dominant over pressure drag and the shape does not have a major influence on the drag coefficient (Cengel & Cimbala, 2006). In this case drag coefficients caused by a sphere or hemisphere are functions of the Reynolds number and are given as $C_D = 24/Re$ and $22/Re$ respectively. We can see the difference in drag coefficients is only marginal between a sphere and a hemisphere. In addition some of the extra pressure drop caused by the flats of the hemispheres at the bed entry may be ameliorated to some extent by the hemispheres at the bed exit having a lower drag coefficient ($C_d = 0.4$) than if the space was occupied by a whole sphere. The effect of the small variation of the particle drag coefficient due to the particle geometry may also account for the relatively narrow variation of data observed at the lowered Reynolds regime presented by Eisfeld & Schnitzlein (2001).

The effect of MRI/IBM approach regarding geometric faithfulness is apparent not only visually, but also the discrepancy between experimental porosity and the porosity derived from the computational mesh of cylinders is $\Delta\varepsilon = 0.01$, in conparison to the case of the spheres where the difference in porosity is $\Delta\varepsilon = 0.01$. However, in this case the porosity is not giving a realistic value of the difference in geometry. Due to the scan resolution and tolerances in the IBM approach, voxels are not only added in some places but may be taken away in others again losing fidelity and causing fissures, but also giving a deceiving effect of compensation. Should the scan be carried out with a higher resolution, one would expect a reduction in the inter-particle contact region. Alternatively, a bed produced with a lower aspect ratio would also yield the same effect. A related issue is the mesh quality; the distance between surfaces in the region near the contact point results in poor cell quality. This is to some extent ameliorated by the finite resolution of the contact points alluded to earlier; a conventional meshing strategy based on

CAD realisations of the particles (which can represent the true curvature of the particles, which thus generates very fine wedges of space to be meshed close to the contact point) creates extreme problems in meshing and generates very poor mesh quality in these regions. When discretized, the size of the contact points is limited to the smallest element which is possible for the meshing software to create. Statistically, due to the geometrically complex domain, the total pressure drop is fairly insensitive to variations in mesh quality, providing the mesh has a suitable quality not to cause simulation divergence. However, when it is desired to analyse flow structure in detail, the mesh is required to be suitably fine to resolve the near wall region.

Although this chapter is primarily concerned with the problems associated with the mesh creation of packed beds, the flow heterogeneity is also of interest. Once a computational study has been run, one of the most difficult of problems to solve is post processing, in regard to interpreting a suitable visual output and the vast computational effort required due to the number cells. This is further complicated by the issue of trying to view a complex 3D domain in 2 dimensions. This problem is analogous to the problem of the almost impossible use of PIV or LDA techniques when analysing flow through packed beds due to not having a direct line of sight through the bed particles. Fluent does offer the option to make the particles translucent, however this only clutters the output and makes it difficult to draw any conclusions. The most realistic approach, and the approach we adopt here, is to cut a 2d plane through the bed in order to interpret the pressure and velocity distribution as a 2D representation, and this is shown in figure 5.19 c. and d. As expected with low aspect ratio, disordered beds, figure 5.19 (c) shows distinct pathways of mainstream velocity with a good proportion of the flow being channeled in the wall region due to the increased porosity in the region resulting in a higher interstitial velocity.

5.6 Conclusion

The work described in chapter has shown how MRI coupled with image-based meshing can be used to recreate physical experimental beds for analysis using CFD. The method has shown to be robust in regard to creating a workable

mesh of suitable quality but fidelity issues arise when MRI scanning small highly curved objects with regard to the representation of the multiple contacts points. The inclusion of the points being represented by one or more voxels, due to the vast number of contacts, statistically can affect global properties of the bed such as porosity yielding an unrealistically low value of porosity with the effect becoming more apparent as the aspect ratio increases. It is plausible that the addition of the voxels may be affecting the micro-scale flow at the contact points but not significantly changing the main flow paths having most influence on the pressure drop. The results on the whole have shown good agreement between experimental, theoretical and computational data for cylindrical media and less so for spheres. On the whole, the work has provided a valuable insight into how non-invasive methods can be coupled with the novel method of image-based meshing to replicate actual physical beds for direct comparison with CFD data.

Chapter 6

On creating geometrically faithful beds with RP

> "A fact is a simple statement that everyone believes. It is innocent, unless found guilty. A hypothesis is a novel suggestion that no one wants to believe. It is guilty, until found effective."
>
> Edward Teller

6.1 introduction

This Thesis has already demonstrated that one of the biggest hurdles to overcome when analysing a packed bed using computational fluid dynamics is re-creating an accurate computational model which is geometrically faithful to the physical bed. Previous research (Baker & Tabor, 2010) discussed in Chapter 4 has included the analysis of an equivalent beds for direct CFD comparison using a computational bed created using the packing algorithm MacroPac and the results have shown to correlate well with experimental. However, the bed has the same geometric characteristics, but the internal flow structure is likely to vary considerably. Coupled with creating the geometry is the problem of producing a workable mesh. Using traditional CAD based meshing software has shown inefficiencies when applied to complex geometries. Similar research using this approach was conducted by (Caulkin *et al.*, 2007, 2009) using digital packing algorithms and included the

code DigiPac to create computational packed beds for analysis using CFD. Direct comparison using this method yields good results in respect to global properties such as pressure drop, however it is not possible to compare the internal flow distributions using this technique.

The work described in chapter 5, reported in Baker *et al.* (2011) has presented the use of non-invasive methods (MRI) to replicate a 3-dimensional model of an experimental bed using an image based meshing technique. This method provides a geometrically faithful bed in respect to bed structure, however this method is heavily dependant on the scan resolution and aspect ratio. The method has shown that even with a relatively high scan resolution, the necking of particles can be observed at contact points affecting global properties such as porosity. However, on the beds analysed in chapter 5, it is plausible that this effect is not changing the flow paths considerably.

Up until now, this work has highlighted the problems when analysing packed beds computationally, via CFD and comparing them with actual physical experimental beds, either physical scanned beds or equivalent beds. The aim of the work reported in this chapter is to circumvent these problems by generating actual physical beds which are geometrically faithful to the computational simulations In addition to analyse the bed structure and flow paths using a novel process depicted in 6.1.

In this chapter, as in Chapter 4, computational packed beds are generated using the particle packing code, MacroPac (Monte-Carlo approach) which has shown to generate disordered beds efficiently. From MacroPac a coordinate and diameter for each particle is exported, which is then transformed into a stereolithography format (STL) using a simple C program. A bed of mixed spheres is imported into the meshing software ScanIP/ScanFE (Simpleware, Exeter UK) and a computational mesh is created. In parallel the STL created from the mesh geometry is physically recreated in ABS for experimental analysis using rapid prototyping. This ensures both the computational bed and the experimental bed are geometrically identical in all respects. As far as the author is aware this is the first packed bed manufactured for direct computational comparison using additive layer manufacturing or more specifically 3d-printing. In addition, in many published research papers (Baker & Tabor, 2010; Tóbis, 2000; Zeiser *et al.*,

2001; ?) the velocity profile is left flat to represent a fully turbulent regime. Here velocity inlet profiles are added; parabolic when the flow is assumed to be fully developed and laminar, both flat and power law profiles are when the flow is assumed fully developed turbulent and compared in detail.

6.2 Experimental method

In this work the experimental rig described in chapter 4 is used. In this instance the max velocity of the flow is required, in which case a hot wire anemometer is positioned in the centre of pipe to allow the instantaneous velocity at the crest of the profile to be measures.

6.3 Rapid Prototyping and 3DP

Here, the beds are created using rapid prototyping (RP) or more specifically three-dimensional printing (3dP). Rapid prototyping developed out of the need to create cheap and fast prototypes of components to be manufactured. Traditionally prototypes were made by hand or one off tooling was made to produce a few individual components which is expensive in respect to material and man-hours. Recently RP has developed to such an extent that is no longer limited just to prototypes, but can be used for mainstream manufacturing, particulary for creating complex components. Even today, without rapid-prototyping techniques, such as additive layer manufacturing, there is no method for constructing a completely hollow sphere in one piece.

Various rapid prototyping methods are available, the most common of which are selective laser sintering (SLS) where a high powered laser is used to fuse particles into an object replicating the computational model, deposition modelling, such as 3dP/FDM where successive layers of material are added to form the prototype, electron beam melting (EBM) where a high energy electron beam fuses parts together in an additive layer fashion. For this work we adopt a 3DP/FDM approach due to its speed of manufacture and cost relative to component quality. The model is manufactured using the thermoplastic Acrylonitrile Butadiene Styrene (ABS). The resolution used for the model is 0.1mm and this forms the

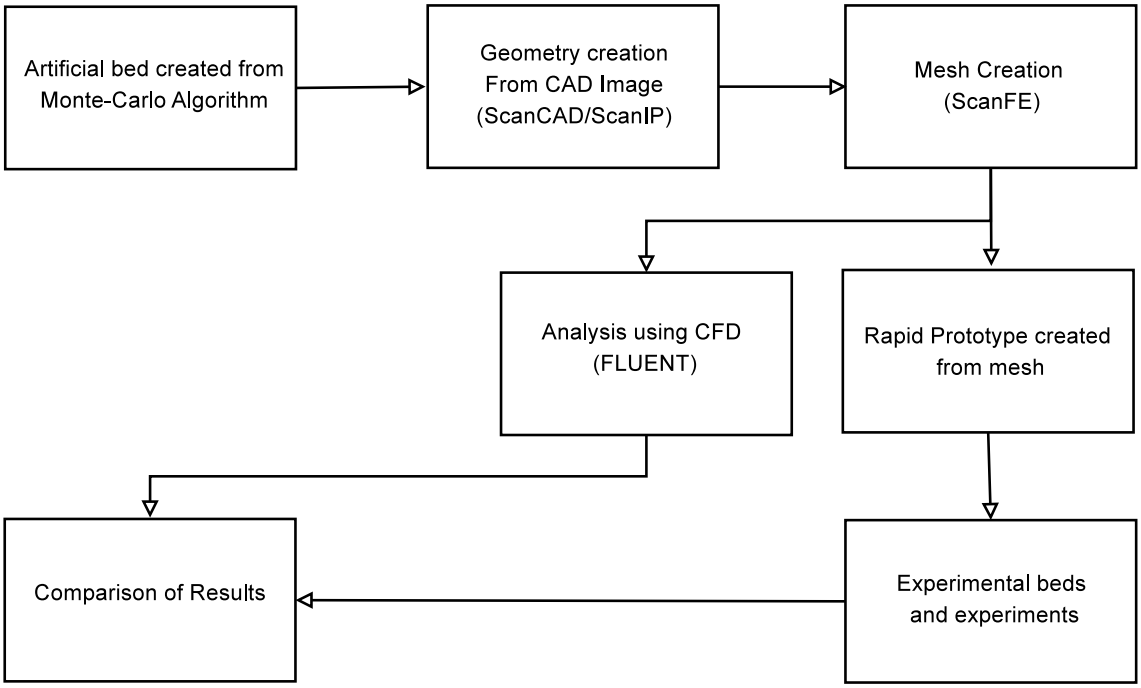

Figure 6.1: Chapter 6 methodology flow diagram

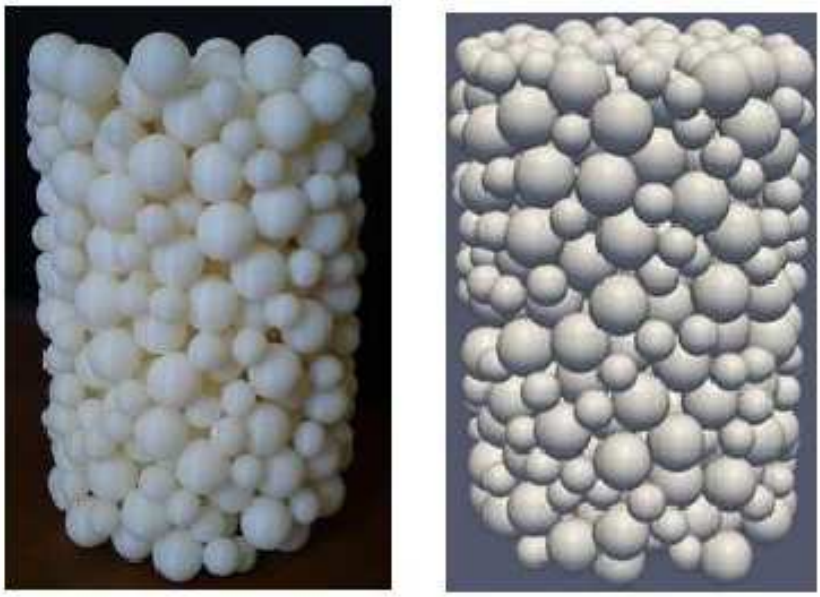

Figure 6.2: Photograph of rapid prototyped bed (Left) and computationally recreated bed (Right)

thickness of each added layer. When being constructed the ABS balls are held together with a temporary structure which is water/detergent soluble. On build completion the model is left to soak in detergent to allow the temporary structure to dissolve. We have already discussed the effect of the necking due to additional voxels of particles and the detrimental effect it has on the fidelity of the computational model. Here, the effect of the necking is used as an advantage. Without the phenomena of necking the particles the physical structure would be statically unstable. Although actual packed beds do not display particle necking, here we are interested in replication of the exact geometry with fidelity rather than reproducing a real life packed bed. This method presented is completely geometrically faithful to the mesh in respect to geometry, particle size etc. The only physical difference between the experimental bed and computational is the fine horizontal banding produced by the RP resolution. The banding is considered sufficiently small to be considered as a surface finish rather than a variance in the geometry and research has shown conflicting evidence, biased towards particle roughness having little to no effect on the overall drop in pressure. This will be discussed

in the next section.

6.4 Particle roughness

In the study of the motion of fluids the roughness of the boundary wall adjacent to the fluid can affect its behaviour. From basic fluid mechanics, in turbulent pipe flow ($Re > 4000$) the relative roughness increases the friction factor as a function of the Reynolds number and therefore cause a higher drop in pressure or head loss than a hydraulically smooth pipe. For laminar flow the friction factor is given as $f = 16/Re$ derived from the Hagen-Poisselle relationship. For laminar or turbulent flow for rough pipes, which are not hydraulically smooth, the drop in pressure or head-loss can be simply determined from the Darcy-Weisbach equation, coupled with the Moody diagram, or the Hagen-Poisselle equation. We know from literature that many of the classical correlations are based on the theoretical tubes assumption (Burke & Plummer, 1928; Carman, 1937; Ergun & Orning, 1949) and therefore should obey the same assumptions as simple pipe flow; the rougher the wall and/or longer the pipe (more tortuous in the case of packed beds) the greater the drop in pressure. Much research as been devoted to the investigation of particle roughness. Leva *et al.* (1951) and Dullien (1979) observe and increased drop in pressure due the the particle roughness, where as Fand *et al.* (1972) observe the exact opposite. Eisfeld & Schnitzlein (2001) analysed the research of Leva *et al.* (1951) and Dullien (1979) and conclude that their observations are most probably due to experimental error or a misinterpretation of data suggesting that the drop in pressure is not affected by particle roughness or at least that this parameter has an unmeasurable effect. Reinforcing the argument of Eisfeld & Schnitzlein (2001) the conflicting evidence could also be attributed to the level of the confidence involved in the studies. We know a packed bed can have the same dimensional parameters e.g porosity, particle diameter, length depth etc but can have a significantly different internal flow paths. This suggests that a bed of rough spheres cannot simply be packed and then compared to another pack of smooth spheres as the most influential parameter (the flow geometry) is being changed. In fact, to produce any credible level of confidence using this technique would require a population of hundred, if

not thousands of packed bed samples, all with the same dimensional properties. In addition, the semi-empirical correlation devised by Eisfeld & Schnitzlein (2001) includes a graph 6.3 in which over 2000 data points are plotted from various researchers. The work of Leva *et al.* (1951) is featured in figure 6.3, there is no deviation from the smooth particles of Reichelt (1972) compared to the rough particles of Leva *et al.* (1951). However, the spread of data is so vast (orders of magnitude) that any deviation due to particle friction is likely to go unnoticed and absorbed by experimental error and transient effects. In reality its is most probable that the particle friction is likely to be affecting the drop in pressure in some way, but this effect is likely to be so minimal and the effect of the geometry predominantly influential and that realistically the effect is not measurable or possible to be separated no matter how large the data set.

The advantage of the approach described in this chapter is that actual beds can be physically recreated which are identical to the computational beds. This allows only one parameter to be changed keeping the geometry faithful. We know that the resolution can produce horizontal banding (roughness height of 0.1mm) and by changing this resolution beds with the same structure and different friction heights could be analysed. With a sufficiently large data set it is possible that conclusions could be made as to the the effect of particle roughness on the overall pressure drop, providing the effect can be physically measured.

6.5 Particle size distribution

We know a packed bed of spherical particles can be made up of either uniformly sized spheres or a distribution of sizes. In this work the spheres are bi-distributed, weighted 50:50 by volume with diameters of 16mm and 10mm. Blake (1922) and Carman (1937) studied variation in particle size and suggest it can treated in the same way as different particle geometries by introducing an equivalent particle diameter. Burke & Plummer (1928) and Gupte (1970) have proved by experiment that packed beds of mixed spheres show a higher drop in pressure compared with beds of mono-sized spheres and as a result they can not simply be treated in the same way by using the equivalent diameter. A higher pressure drop due to beds containing more than one size sphere is likely to be apparent when the ratio of

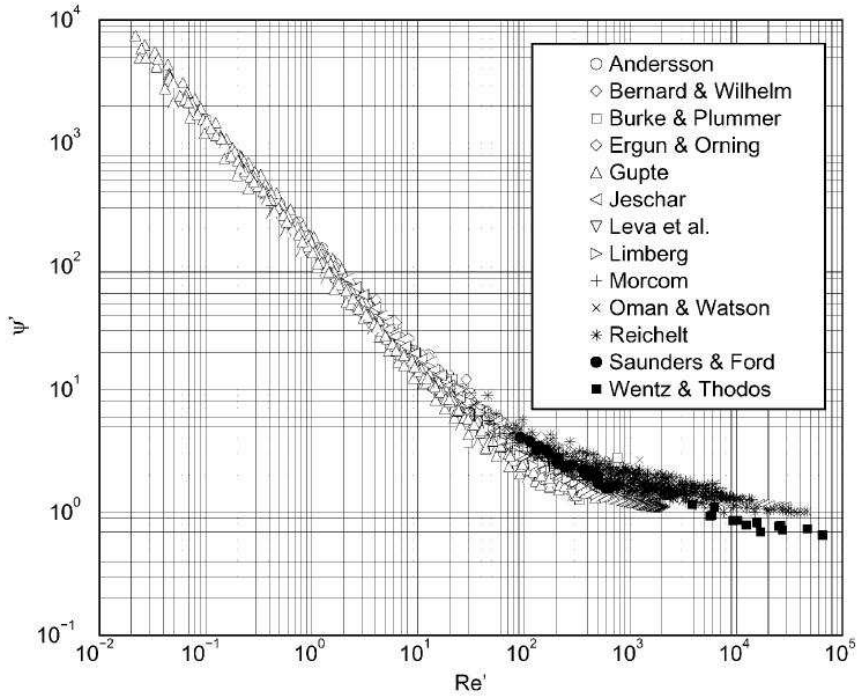

Figure 6.3: modified dimensionless pressure drop ($\psi' = \phi' = \phi\varepsilon^3/1-\varepsilon$) as a function of the modified Reynolds number $Re' = Re_{dp}(1-\varepsilon)$ (Eisfeld & Schnitzlein, 2001)

the smaller sphere to the larger sphere is such that it fits perfectly into a pore in the pseudo-close hexagonal packing formation.

6.6 Computational Domain

In order to analyse the domain using CFD a mesh is constructed using the image based meshing software ScanCAD, ScanIP and ScanFE. An STL file is created from a simple, purpose written C program from the raw coordinate data and particle diameters generated by MacroPac. The STL is then imported into ScanCAD and a workable mesh is produced in the same way as in Chapter 5. Here the mesh contains 30,443,307 mesh elements, 62,844,838 faces and 6,679,187 nodes and is probably one of the largest meshes created to analyse a packed bed. Note in passing, in this work the beds have progressed from a few hundred-thousand elements, such as chapter 4, a few million in chapter 5 and tens of millions presented in this chapter.

Properties	Max Cell vol	Min Cell vol	Max face area	Min face area	Mesh Volume
Mesh	1.71×10^{-7}	2.82×10^{-18}	5.54×10^{-5}	1.11×10^{-12}	1.35×10^{-3}

Table 6.1: Mesh data for bed of mixed spherical particles

Figure 6.5 shows the cell squish index for the computational domain for 16mm and 10mm spheres. Comparing this to the squish index presented in chapter 5, the mesh here is of considerably better quality containing a far smaller percentage of degenerate elements probably due to the small element size. This is because in chapter 5, the geometry is altered by the scan resolution and is further altered by the IBM technique. In this case, the IBM method is given a raw geometry which can be then manipulated to create a mesh.

One feature that can be argued as both an advantage and disadvantage is the relative uniformity in mesh element size. It could be suggested that in free-stream the relatively small element size is resolving the majority of the smallest turbulent structures, thus resembling a rough-pseudo-LES approach. However, it is debatable how much effect this is having on the overall solution and it will

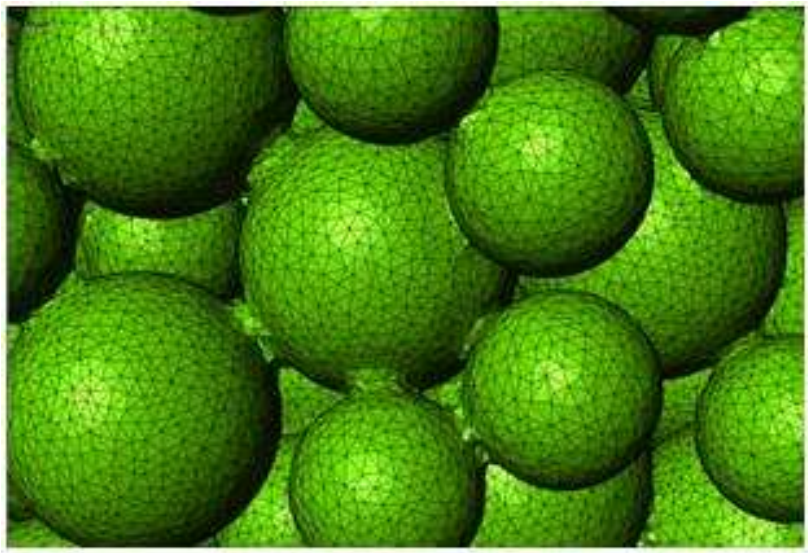

Figure 6.4: Computational domain

incur additional on-cost to computational time and efficiency. This is apparent in the header region directly before the bed, this region is solely there to carry the flow through to the media, thus is it necessary to resolve the higher frequency turbulent structures.

6.7 Computational Fluid Dynamics

In chapter 4 the $k-\omega$ SST model was shown to model pressure drop through packed bed with a good deal of accuracy compared with experimental data. However, the low Reynolds transitional $k-\omega$ model is applied and considerably under-predicts the pressure drop, with the possibility that certain turbulent effects are being neglected by the model or being over-damped or not modelled correctly. An un-steady laminar model has shown to match closely with the $k-\omega$ SST model, meaning the mesh is fine enough to describe most of the smallest turbulent structures. However, a DNS approach cannot be claimed here in respect to the differencing and a relatively low discretization scheme will not be capturing the smallest turbulent events. However, it can be argued that the presence of a

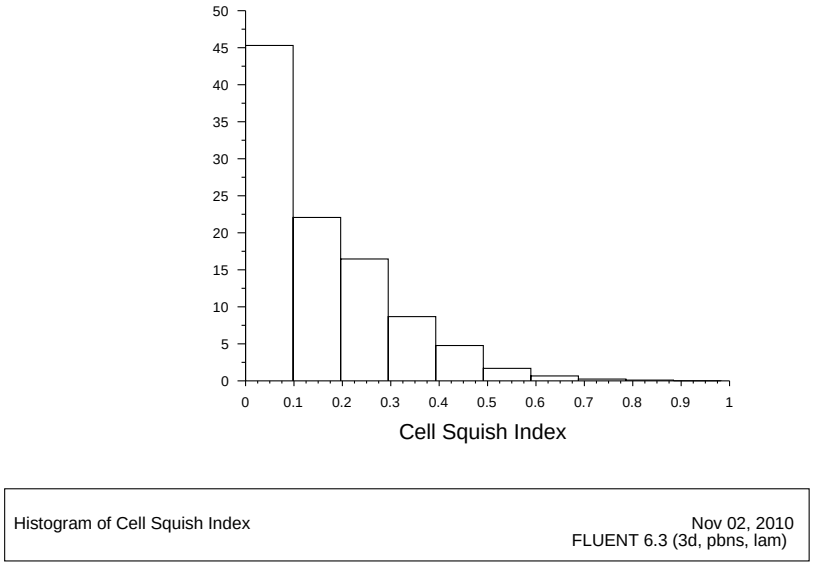

Figure 6.5: Cell squish index for computational domain

turbulence model is having a minimal effect on the solution.

Computational fluid dynamics is simply a tool for solving a second order partial differential equation. It is not intelligent nor can it give a conclusive answer as to the flow behavior, it is the interpretation of the user and their knowledge of fluid physics coupled with CFD which makes it a useful tool for research and industrial applications. Two conflicting issues arise in respect to the argument for the use of a turbulence model over an unsteady laminar model. Firstly, is the $k-\omega$ model generating turbulence that shouldn't't be there? Is it representing deterministic behaviour as true stochastic turbulence? Packed beds are less well understood than most engineering flows (jets, wakes etc) and we still cannot conclusively say whether the expected behaviour of the flow in a packed bed is laminar or turbulent at a specific Reynolds number. We cannot use CFD (with RANS or LES) to study this effect as turbulence model itself is a user input. We can use DNS to study this but for a media as complex as the media studied in this thesis the Author postulates at least another decade in computer development before this is readily available to the end user. For this work, due to the closeness of the results for the unsteady laminar model to those with the

turbulence model demonstrated in chapter 5, in this chapter an unsteady laminar solver is used without the addition of a RANS model.

The closeness of an unsteady laminar model to the RANS model can form conflicting arguments. We could argue that the mesh is fine enough to resolve the majority of the smallest turbulent scales, governed by the Kolmogorov length scale. However, a DNS approach cannot be claimed as the 2nd order upwind scheme is unlikely to capture the highest frequency turbulent events, unlike a full DNS approach requiring higher order schemes as much as 10th order. However, what we can claim is a pseudo-LES approach in which the majority of the length scales are being resolved, but not all the highest frequency turbulent events. Another argument may suggest that there is minimal transient effects as a result of the pore size and damping caused by the bed geometry and viscosity thus, the addition of a turbulence model is having little to no affect on the solution.

To study a packed bed we need a header region before the bed to set a superficial velocity and in some cases a suitable velocity profile. If a header region is not set the interstitial velocity (pore space velocity, $U_i = U_s/\varepsilon$) must be used as the velocity inlet is channelling flow directly into the pores. The header region may be turbulent, but then the presence of the medium may damp out any large turbulent structures with the possibility of flow re-laminarising. In addition there may be sudden burst of turbulence in transitional zones which are then damped out by a convergence in pore diameter. A model such as the $k-\omega$ model is likely to treat all the control volume (apart from the near wall regions) as being turbulent, what is more with enhanced wall treatment there may not be suitable $y+$ values in the pore spaces due to size restrictions. The SST $k-\omega$ model ameliorates this to some extent by treating the free stream with all the benefits of the $k-\epsilon$ model and the near wall and pore spaces with $k-\omega$.

To correctly model a fully developed flow, the flow conditions at the velocity inlet are set to an appropriate velocity inlet profile for each flow condition. We know that with laminar flow the fluid is flowing uniformly along the path-lines, viscous shear is dominant and energy is transferred across the streamlines by molecular diffusion (Cengel & Cimbala, 2006). With turbulent flow, the motion is chaotic and time dependant and the random motion of vortices transfers energy at a higher rate than molecular diffusion. In which case, turbulent flow has higher

frictional losses associated with it than laminar flow. Because of the relatively low frictional effects with laminar flow, the presence of the wall in a circular pipe forms a parabolic velocity profile relationship described by the equation 6.1.

$$U = U_0\left(1 - \frac{r^2}{R^2}\right) \tag{6.1}$$

Turbulent flow is considerably more complex and there are much higher losses in which case the profile is much fuller and decreases steeply at the wall region and is described by a 1/7 power law profile 6.2. The velocity represented in 6.2, u (U) is the some of a mean $\widehat{u}(\widehat{U}$ and a fluctuating component $u'(U')$.

$$U = U_0\left(1 - \frac{r}{R}\right)^{1/7} \tag{6.2}$$

Here the velocity at the inlet is already a time average, deduced from experimental data. In reality the 1/7 power element can be varied, a mildly transitional flow may display a 1/5 law, where as a strongly turbulent regime may be as much as 1/10. In turbulent flow, the power law profile is an average flow profile which is constantly changing due to the stochastic nature of turbulence. The experimental setup has a sufficient header region of straight smooth pipe to be considered fully developed (10D).

When presenting results with different velocity profiles an average velocity or volumetric flow rate is needed to satisfy the conservation of mass. For a flat plane profile $U = U_{avg}$, whilst for a laminar or turbulent profile the volume beneath the velocity profile needs to be obtained through integration to determine the volume flwo per unit-time, Q. In this work the plate orifice has given the volumetric flow rate Q, m^3/s and the hot-wire anemometer has given $U_{max} = U_0$. For a circular pipe

$$m = \rho U_{avg} A = \rho Q = \int_A \rho u(r) dA \tag{6.3}$$

$$U_{avg} = \frac{1}{\rho \pi R^2} \int_0^R \rho u(r) 2\pi r dr \tag{6.4}$$

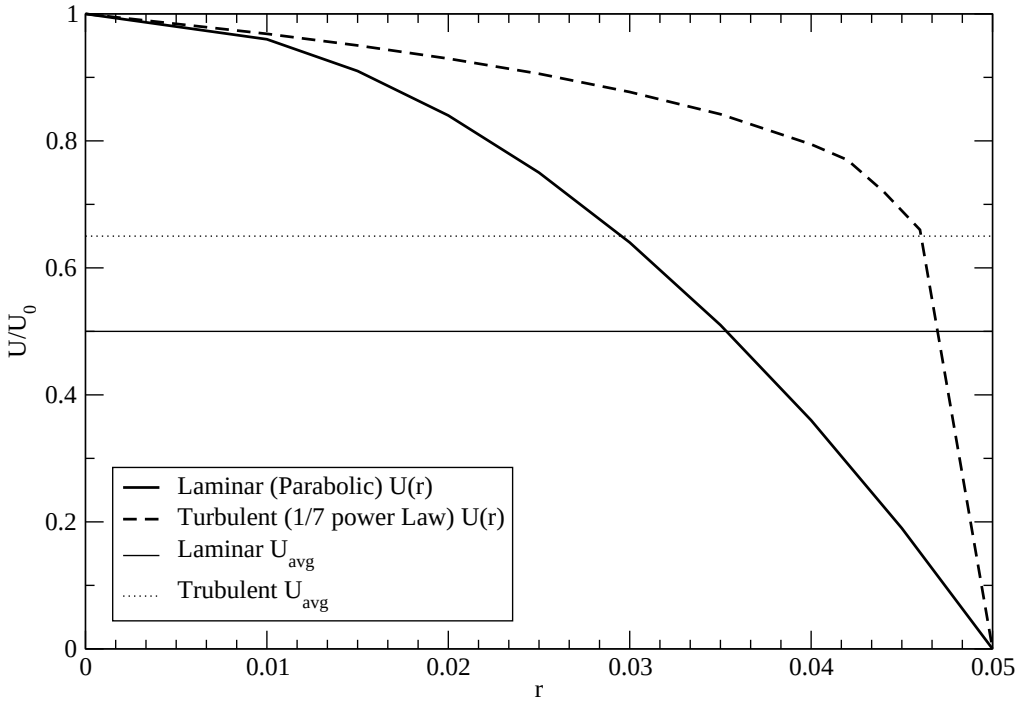

Figure 6.6: Velocity profiles for laminar and turbulent flow regimes. Dimensionless velocity ratio is plotted as a function of distance across pipe

6.8 Results

We can see from figure 6.7 that the computational data, with and without the inclusion of an appropriate profile is in close agreement with the experimental data, at low Reynolds number falling well within the margin of uncertainty and slightly under-predicting the pressure drop per unit length. The results, the same as chapters 4 and diverge away from the experimental data as the Reynolds number increases regardless of the inclusion of an appropriate profile. Results show there is little difference in the overall drop in pressure between a laminar parabolic profile, a turbulent 1/7 power law profile and a flat profile.

The RMS deviation for the experimental compared with the results obtained by CFD is $\sigma = 0.61$ for the full range of Reynolds numbers. Windowing this to lower Reynolds numbers not accounting for the deviation gives $\sigma_w = 0.06$ representing the closest agreement presented in this Thesis.

Figure 6.8 depicts the dimensionless pressure drop as a function of the volumetric flow rate, Q. We can observe from the graph that the inclusion of the different velocity profiles is having little to no effect on the global pressure drop. It is plausible the bed geometries strong influence is absorbing any effect on the pressure drop caused by the variation in the velocity profile. The respective pressure drops are also compared with the correlation proposed by Eisfeld & Schnitzlein (2001) and show promising agreement. Figure 6.9 compares the results obtained from both computational and empirical studies. In both cases they show excellent agreement with the correlation proposed by Eisfeld & Schnitzlein (2001).

Figure 6.10 shows scalar plots of velocity (Left) and pressure (Right) for parabolic, flat and 1/7 power law turbulent from top to bottom respectively. Although the data is in 2-dimensions, we can see that there is little difference between them in regard to velocity channelling or internal flow structure, reinforcing the theory that the velocity profile is having a minimal effect on the pressure drop.

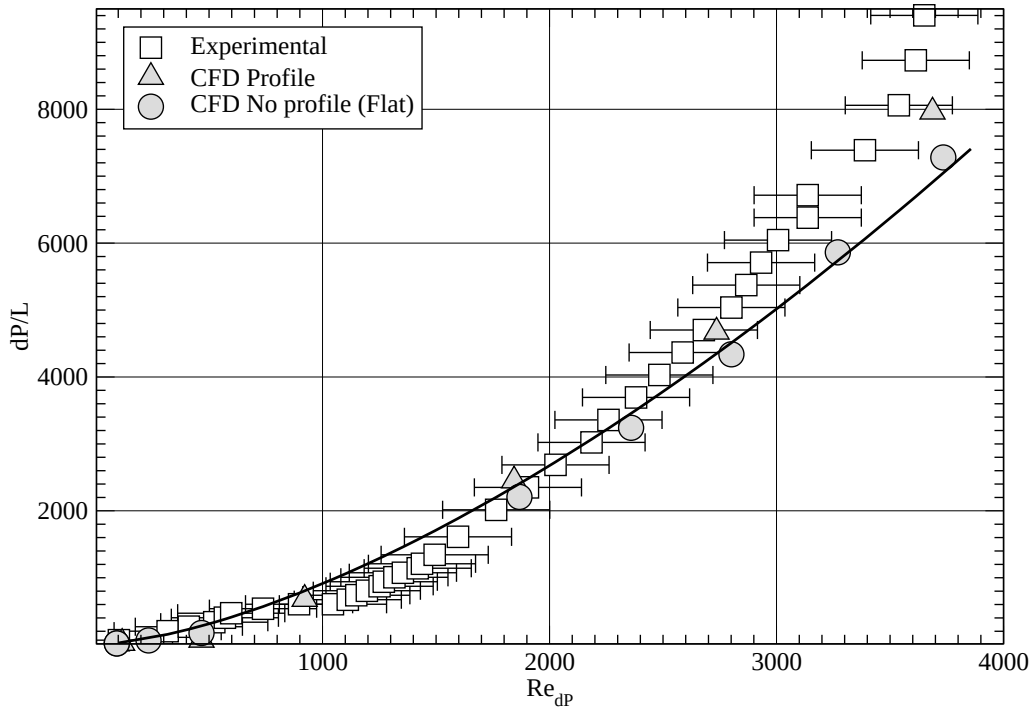

Figure 6.7: Pressure drop per unit length as a function of Reynolds number for bi-distributed spheres of 16 and 10mm

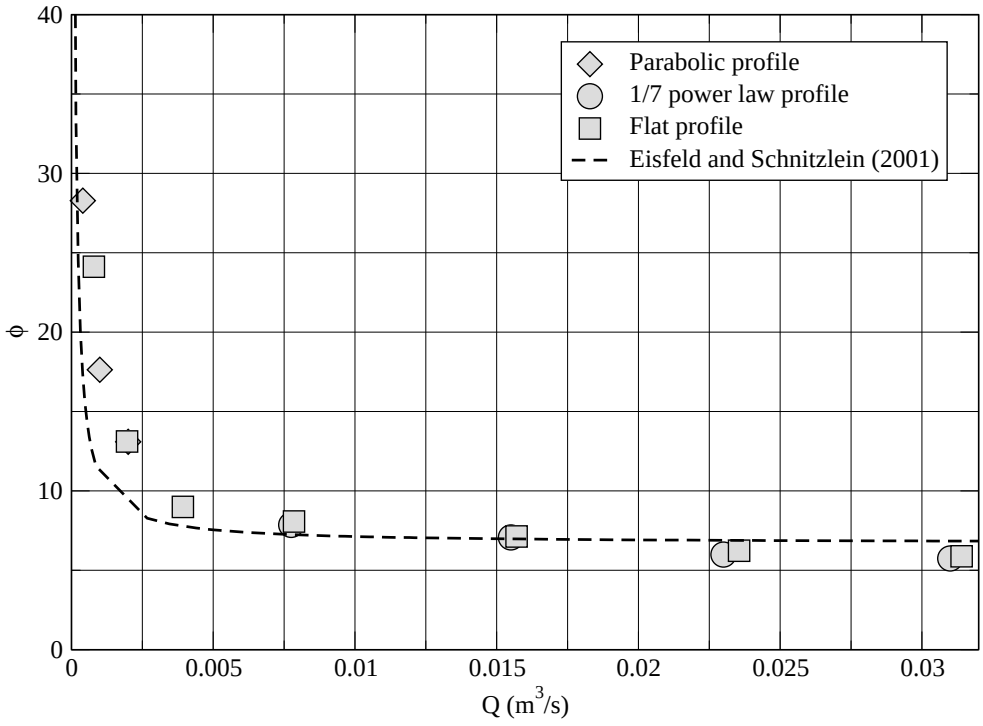

Figure 6.8: Dimensionless pressure drop as a function of volumetric flow rate for bi-distributed spheres of 16 and 10mm where $\phi = \Delta P d_p / L \rho U^2$. Note the little difference in ϕ irrespective of turbulent profile.

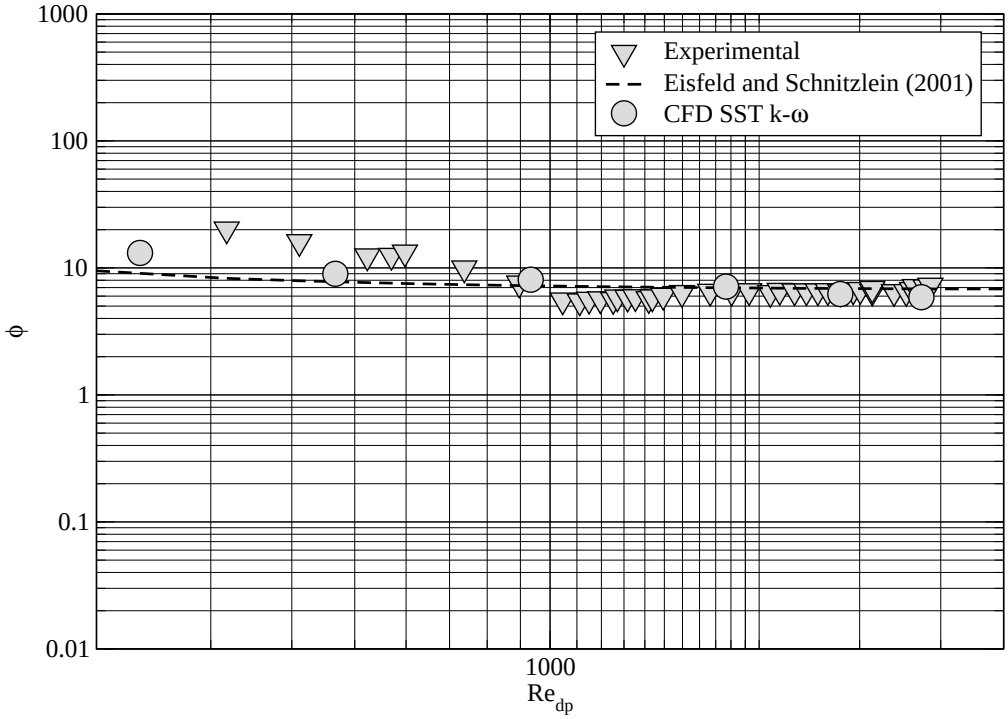

Figure 6.9: Dimensionless pressure drop as a function of Reynolds number for bi-distributed spheres of 16 and 10mm

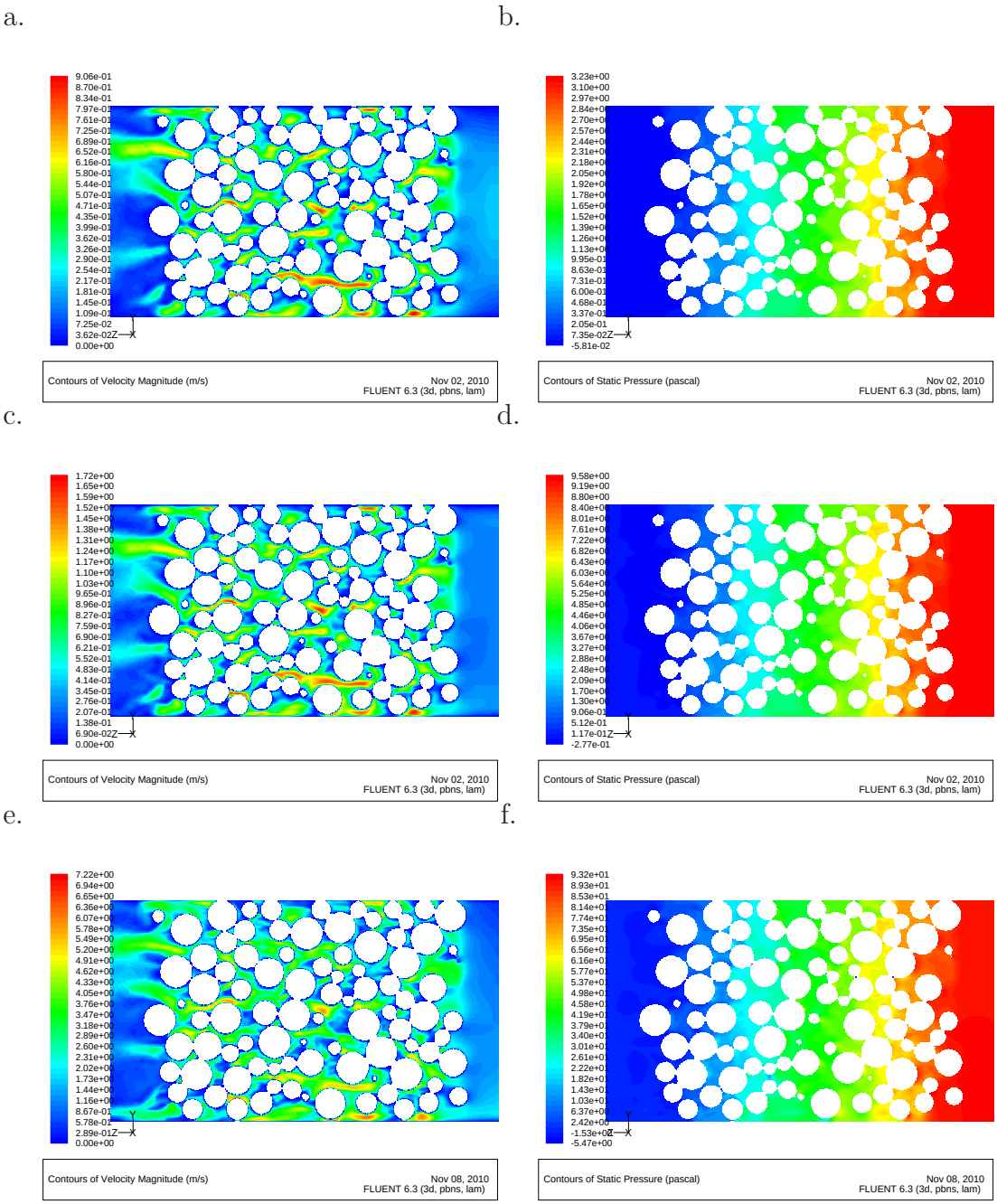

Figure 6.10: Contours of velocity magnitude (a) and pressure (b) for mixed bed of 16mm and 10mm beds of spheres with parabolic inlet profile. Contours of velocity magnitude (c) and pressure (d) for mixed bed of spheres with flat plane profile. Velocity magnitude and pressure for a 1/7 law profile a, and b, respectively

6.9 Discussion

We can see from figure 6.8, where the pressure drop per unit length is plotted as a function of volumetric flow rate that the effect of the profile is having a minimal effect and parabolic, flat and 1/7 power law show minimal difference in results. This is due to the bed geometry having a strong effect on the pressure gradient before the bed and distorting the velocity profile before the fluid reaches the media. This justifies the closeness of results to the experimental in chapters 4 and 5 without the use of a velocity profile for a fully turbulent regime. The data presented in the correlation proposed by Eisfeld & Schnitzlein (2001) does not mention the effect of the velocity profile, although there is a significant amount of empirical data to represent this, only the individual effects cannot be separated from the correlation. The effect of the profile may well account for the significant spread in the results. In addition, this is based on the assumption that the Authors of all the research papers have designed an experimental rig suitable to allow a fully developed flow to be formed before the obstruction of the media. In regard results presented here it seems plausible the effect of the velocity profile is having minimal effect on the pressure drop.

Figure 6.11 depicts velocity vectors for a random location within the bed. We can see recirculation in stagnation zones and at the rear of the spheres in the pressure drag region which normally would be averaged out by the RANS equations when a turbulence model is implemented. A similar vortex structure behind spherical media has been observed by Dalman *et al.* (1986) using a computational approach and Yevseyev *et al.* (1991) using laser doppler anemometry. Conversely, Tsotas (2002a) report no vortex shedding from the particles around particle Reynolds numbers of $Re = 4780 - 7010$ which are in the ranges analysed here. Their experimental method relies on the use of hot-wire anemometers in the void space to detect unsteady flow behaviour. However, a hot wire anemometer utilises Newton's Law of cooling and the temperature difference to determine the velocity, and it is unlikely that the response time is fast enough to capture the highest frequency turbulent events in the turbulent spectrum. In addition, the bed analysed by Tsotas (2002a) is based on a rhombahedral, structured packing and not a bi-distributed disordered pack.

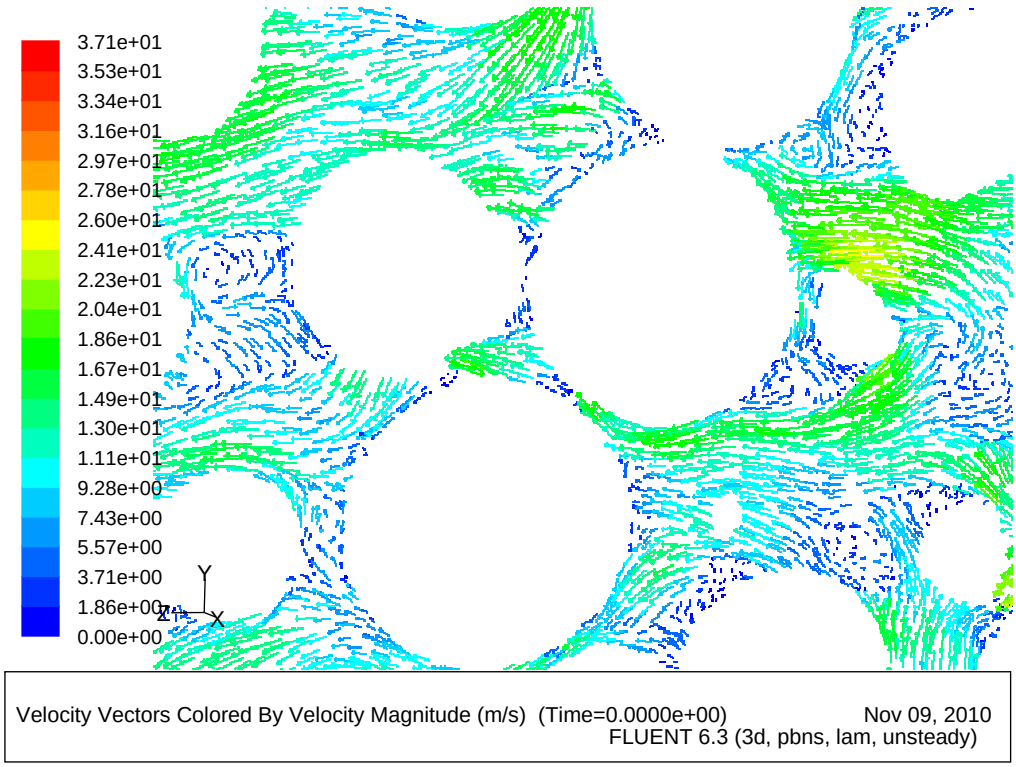

Figure 6.11: Vectors of velocity showing flow recirculation inside the bed at 3.0m/s

Behind a bluff body such as sphere or cylinder, the wake region is likely to exhibit both true stochastic turbulence and periodic deterministic vortices and recirculation at distinct frequencies. With these two effects coinciding in the same location, the two phenomena are notoriously hard to separate using empirical techniques. With the approach used in this work the velocity vectors are calculated from the cell node value in the form of a magnitude and direction. In which case it is impossible to decipher whether this is true stochastic turbulence or periodic deterministic vortex shedding from the back of the sphere. Furthermore, the skewed elements can be affecting both the magnitude and the direction of the vectors. In regard to this Thesis as a whole, skewed elements may be affecting local phenomena, such as recirculation; damping out or creating recirculation zones which should not be there, however the effect is not significant enough to be affecting global properties such as the pressure drop caused by the media. In addition, this effect is fairly localised to particle contacts which are naturally in locations of minimal fluid flux.

In all cases, with and without a suitable inlet flow profile results have shown to slightly under-predict the pressure drop with this effect becoming more apparent as the Reynolds number increases.

6.10 Conclusions

In this chapter, computationally generated packed beds (generated using MacroPac) have been meshed using IBM techniques (ScanCAD, ScanFE), to create CFD models for bi-distributed beds. At the same time, RP techniques have been used to synthesise a geometrically accurate physical bed for experimental investigation. Both experimental results carried out of the RP bed and computational results have shown to match closely, particularly at the lower Reynolds range. As the the Reynolds number increases the solver has tended to under-predict the pressure drop. The work has also investigated the application of the expected appropriate flow profiles to the computational model's boundary conditions. Results have show that that the velocity profile is having minimal effect on the pressure drop, and is heavily dependant on the flow geometry. As a whole, this work has

laid the foundations for further work into the application of rapid prototyping in manufacturing disordered structures for comparison with CFD results.

Chapter 7

Correlations and Conclusions

> "A story should have a beginning, a middle, and an end... but not necessarily in that order."
>
> Jean-Luc Godard

7.1 Introduction

This final Chapter draws on the techniques described in the previous Chapters to generate two new models to predict bed porosity and pressure drop and in addition concludes this Thesis. Drawing on the previous work, Chapters 4 and 6 have implemented the particle packing algorithm MacroPac to generate packed beds for computational fluid dynamics. MacroPac has been shown to generate computational models fast and efficiently lending itself to the production of a large data set from which bed properties can be extracted. This chapter uses this to generate a data set of randomly packed beds to which a correlation can be fitted to determine expected bed porosity as a function of aspect ratio. This correlation is then compared to other empirical correlations in the literature (Beavers *et al.*, 1973; de Klerk, 2003; Dixon, 1988; Jeschar, 1964; Zou & Yu, 1995). The computational and empirical methods used in this Thesis have generated a large data set, such that a regression can be constructed to describe the dimensionless pressure drop for the window of Reynolds numbers and aspect ratios studied. Referring back to chapters 2, 4 and 5, realistically, there is no single formulation which can

describe the dimensionless pressure drop for every single case due to the tortuosity and packing type not being taken into account. It could be argued that the correlation proposed by Eisfeld & Schnitzlein (2001) accounts for all these effects by the large range of empirical data used to fit the regression, however these terms cannot be separated from the data, nor are any values given. Rather than a 'one size fits all approach', it is more suitable to window the data to specific Reynolds number and suitable aspect ratios. The regressions described here do not replace or provide the accuracy of empirical and computational methods, but provide an alternative in the form of a 'good engineering approximation' for the described Reynolds numbers and aspect ratios. The computational methods described in this Thesis can model pressure drop with a good degree of accuracy, however, there is still not enough computer power available to the average Engineer to perform these computer simulations in a suitable time frame. An empirical calculation can take a matter of minutes, where as CFD simulation of a flow domain as complex as the media described in this thesis takes several hours or even days.

7.2 Porosity

The bulk average porosity, or just the bed porosity is a global quantity which heavily affects the passage of fluid through a packed bed. Determining a realistic value of porosity can be challenging due to the associated uncertainties with most well established techniques. One of the simplest approaches is to fill the voids with a known amount of water representing the void volume, V_v (Leva *et al.*, 1951). A similar technique is to remove the bed particles and add them to a measuring cylinder with a known volume of water and measure the fluid's rise due to Archimedes' 'Eureka' theory, as applied by Giese *et al.* (1998). However, this group of techniques is susceptible to entrapped bubbles around the media and is limited to non-absorbent particles. The effect of the bubbles can be considerably reduced, with the use of a surfactant coupled with a vacuum chamber or the use of mercury due to its non-wetting properties. However, mercury has its own disadvantages in very being dense and viscous, such to an extent that often smaller particle pores or gaps are not filled by the liquid. Additionally, mercury

is included in the RoHS directive (Risk of Hazardous Substances) due to its cumulative toxicity and poses a significant risk to health from continuous exposure. Although the smallest pores are not likely to be filled by the mercury, it is arguable the effect is not likely to be effecting the pressure drop or flow pathways considerably. This is reinforced by the fact that the primary cause of pressure drop is governed by the bed geometry and not so much by the particle roughness or micro-scale geometry. Other empirical methods include the use of wax to fill the voids and the mechanical removal of layers of a known thickness for weighing (Gotz *et al.*, 2002) which is time consuming and cumbersome and most of all destructive. However this technique can be useful in determining local porosity, a feature not provided by water substitution due to its global technique. The technique suffers similar viscosity associated complications as mercury porosimetry and the same argument can be applied.

Non-invasive methods, such as MRI, XRM (X-ray microtomography) and CT provide an approach which allow the probing of a packed beds internal microstructure, as demonstrated in Chapter 5. M.C.Thadani & Peebles (1966) have shown how a packed bed of plastic spheres fixed in a matrix can be segmented and each segment radio-graphed and local porosities determined from the photometric reading of the radiograph emulsion point densities. Their results show that the porosity as a function of particle centroid distance from the wall exhibits a decaying sinusoidal trend. MRI techniques are valuable for determining a bed's complex flow paths, but with high resolution MRI, magnetic susceptibility induced artifacts can cause particle necking. This phenomena makes little difference in a very low aspect ratio bed ($A_{ratio} < 5$), but as the aspect ratio increases the more particles equates to more contact points resulting in an a wildly inaccurate value of porosity. If the scan resolution is not sufficiently smaller than an individual particle it is likely that most of the voids will not be detected at all.

The disadvantage of all these techniques is the arduous task of completing the experiments and the associated expense in regard to setup cost and man-hours, thus limiting these techniques for research purposes. A good quick engineering approximation for average or bulk bed porosity is best served by a single empirically derived correlation. Correlations exist to predict a value for bed porosity

in regular and irregular packings and are given as porosity as a function of the dimensionless aspect ratio, such as the empirical correlation proposed by Jeschar (1964)

$$\varepsilon = 0.375 + 0.34\frac{d_p}{D} \tag{7.1}$$

Dixon (1988) proposed a similar equation to form what is considered 'the standard' correlation for the porosity as a function of aspect ratio for a packed bed given as

$$\varepsilon = 0.4 + 0.05\frac{d_p}{D} + 0.412\left(\frac{d_p}{D}\right)^2 \tag{7.2}$$

de Klerk (2003) proposed the following equation to describe the porosity as a function of aspect ratio

$$\varepsilon = 0.41 + 0.35e^{0.39D/d_p} \tag{7.3}$$

whilst another correlation is proposed by Zou & Yu (1995)

$$\varepsilon = 0.4 + 0.001\left[e\left(\frac{10.686}{(D/d_p)}\right) - 1\right] \tag{7.4}$$

The porosity correlations are shown in 7.1. We can see from figure 7.1 that the exponentially based correlation of Zou & Yu (1995)never reaches zero, in which case this correlation diverges away from the correlations of Dixon (1988); Jeschar (1964) and de Klerk (2003) steeply at low aspect ratios. This may not be as misleading as first assumed. If we consider a spherical bed with an aspect ratio of one, a single sphere is likely to completely block the pipe, in which case no flow can pass through. This may not be the case with a particle with an equivalent diameter of one. A sphere can completely block a pipe, but it is still porous in regard to the $\varepsilon = V_v/V$ relation although no fluid can pass. The correlations of Dixon (1988); Jeschar (1964) and de Klerk (2003) will still give a value of porosity when the aspect ratio is one and be used in conjunction with and equation such as Eisfeld & Schnitzlein (2001) which will still give a value of pressure drop, which we know is not possible. In the case of very low aspect ratio beds, the pressure drop should not be quantified by the porosity but more the area available to the flow around the sphere.

Beavers *et al.* (1973) proposed a model for bulk porosity introducing

$$\varepsilon = \varepsilon_\infty \left[1 + 2\frac{d_p}{D}\left(\frac{\varepsilon_w}{\varepsilon_\infty}\right)\right] \tag{7.5}$$

Choi *et al.* (2008) suggest that the correlation of Beavers *et al.* (1973) is more accurate for predicting bulk porosity than the equations of Zou & Yu (1995).

Here MacroPac is used simply a tool for for implementing a Monte-Carlo method and generating random disordered beds. It is used for analysing the porosity for different beds and therefore creating a data set for an appropriate regression analysis to be performed. MacroPac determines the porosity in two ways, either with a voxel approximation or a sphere slice approximation. With the voxel approximation, the bed is discretized into a lattice of voxels in which a voxel either lies inside a particle, or outside a particle. From the ratio of those that lie within a particle to those which lie outside, an approximation of porosity can be determined. The sphere slice approximation determines the porosity by taking slices through the spheres and calculates sphere volume within the sliced region. Intelligensys quote 'In systems consisting entirely of spheres, the results returned will be 100 % correct' or at least to the specific bed. On this basis this is the chosen method for this work.

In this case MacroPac is set to take a value of porosity from a control volume excluding particles at the extreme ends of the bed. This is achieved by setting the two boundaries in the z-axis to 'soft' enabling more spheres to be packed into the volume, enabling a value of porosity to be taken from the core of the bed. The soft function allows a particle to marginally overlap or stretch the confining geometry to allow more particle to be packed. If this is not applied, MacroPac will fill the control volume with the maximum amount of spheres possible. Figure 7.1 shows the data produced by MacroPac fitted with a regression and compared with other previous research. The regression gives the function

$$\varepsilon = 0.6\left(\frac{D}{d_p}\right)^{-0.16} \tag{7.6}$$

resulting in a coefficient of determination of $R^2 = 0.82$

This graph shows that porosity data produced by MacroPac is in good agreement with previous research and the correlations proposed by Jeschar (1964) and

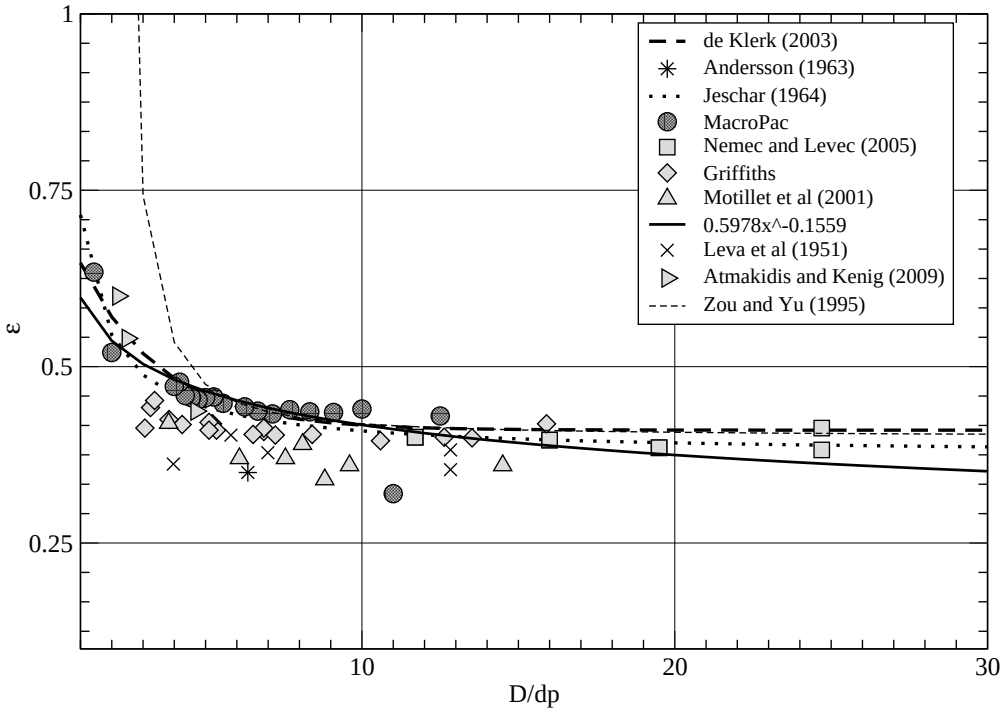

Figure 7.1: Porosity correlations as a function of aspect ratio compared with experimental data

de Klerk (2003). We can see from figure 7.1 that the correlation proposed by Zou & Yu (1995) fits the data well at aspect ratios of $A_{ratio} > 5$ but below this value diverges steeply away from previous research and proposed correlations. Where as the correlations proposed here and the correlations of Zou & Yu (1995) diverge steeply away at low aspect ratios due to the use of an exponential function.

7.2.1 Local Porosity

Figure 7.2 shows height averaged porosity (ε) as a function of the dimensionless distance ratio (x/d_p) for a range of low aspect ratio beds. The bed is created using MacroPac with a bed diameter of 100mm and a length of 250mm. The porosity is calculated using the sphere slice method using a 2d slice taken across the centre of the bed from top to bottom.

The plot displays homogeneity in the results resembling under-damped oscillation, where the first peak is a mean representative of the centroids of the spheres adjacent to the bed wall. If we interpret the extents of the wall region as the linear porosity region from the wall to the edge of the first particle then this proves the assumption which was made by Martin (1978). However, in a fluids based interpretation the wall region penetrates further into the bed and only stops when the fluid flow through the core region is no longer affected by the wall. In beds of very low aspect ratios the wall region is likely to be dominant through the whole bed. In a high aspect ratio, continuously packed bed, the wall region has no noticeable effect.

On question that can be raised when determining a low aspect ratio packed bed porosity is when does the bed finish? Here the argument is presented that the spheres at the most extreme point of the bed are only half packed and are in contact with the spheres directly below them, in which case the bed would finish at their centroids an in the case of water substitution this would be the fill level. This is fine providing each of the sphere centroids are level, such as for a regular cubic pack, this would suggest in a random arrangement that the water would be filled to the mean centre line of all the most extreme spheres. This raises the issue how this would be determined? Similarly, this argument could be applied to the base of the bed. However, the first row of spheres has an impact on the

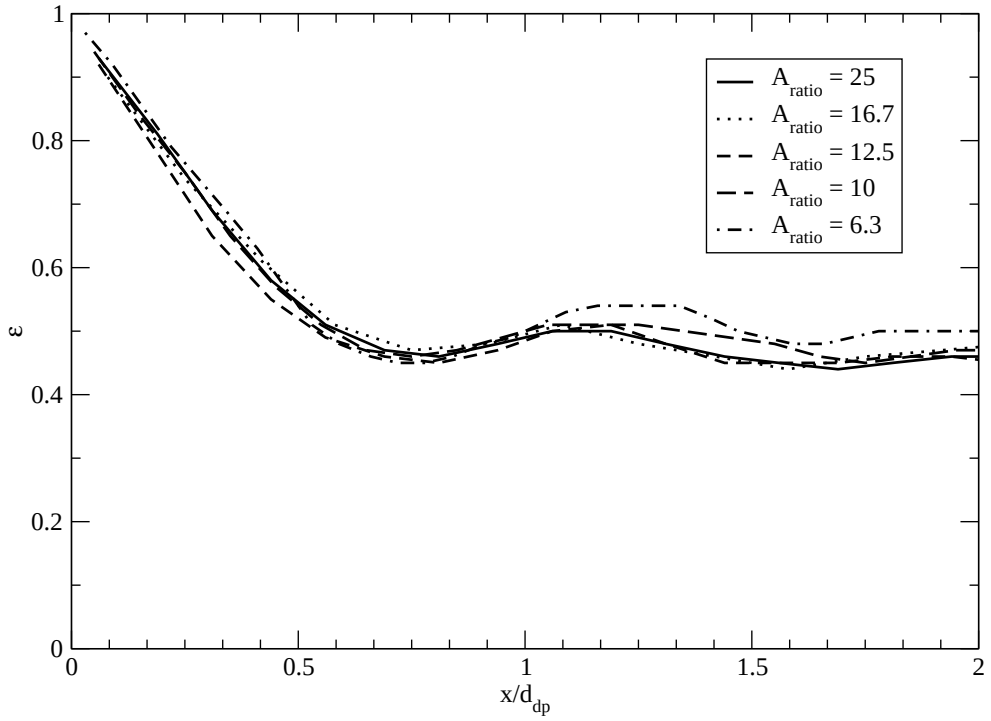

Figure 7.2: Bed porosity as a function of distance from wall (x) non-dimensionalised using the particle diameter (d_p)

bed due to their aerodynamic properties in regard to flow channelling and drag. If these spheres were in fact hemispheres with the flat end leading, this would result in considerably more pressure drag resulting in a higher drop in pressure.

Figure 7.3 shows the standard deviation of porosity from a data set of over 250 beds generated using MacroPac. We can see that the highest standard deviation is in the region of $4 < A_{ratio} < 6$. With an aspect ratio less than 4 there are fewer packing possibilities or at least the structure is the same but may vary radially. Where the aspect ratio is greater than 6 ($A_{ratio} > 6$) the bed will start to become more homogeneous.

7.3 The dimensionless pressure drop model

We have discussed correlations which have been devised to predict pressure drop through packed beds and porous mediums, such as work of Darcy (1856). Some of these are purely theoretical models, based on Hagen-Poiselle flow (theoretical tubes) (Carman, 1937; Ergun & Orning, 1949), some are empirical or semi-empirical (Eisfeld & Schnitzlein, 2001). The work of Eisfeld & Schnitzlein (2001) is considered to be one of the most promising correlations devised from adjusting the coefficients of (Reichelt, 1972) with a regression of over 2300 data points from 13 difference academic sources. Although a considerable population has been analysed every data point in the work of Eisfeld & Schnitzlein (2001) is empirically derived from physical experiments. Although it would be hard to question the simplicity, accuracy and reliability of a fluid manometer, the work of Eisfeld & Schnitzlein (2001) is somewhat limited by the range of techniques for acquiring the pressure drop. This raises the question, that with the rapid progression of computational techniques and the speed and simplicity, are empirical methods the most accurate? And should we now be reinforcing empirical measurements with computational ones in contrast to traditionally reinforcing computational approaches with empiricism?

We know that there is no individual correlation that can model pressure drop in a packed bed for every case with sufficient accuracy. Even though this is well understood, the large range of both experimental and computational data

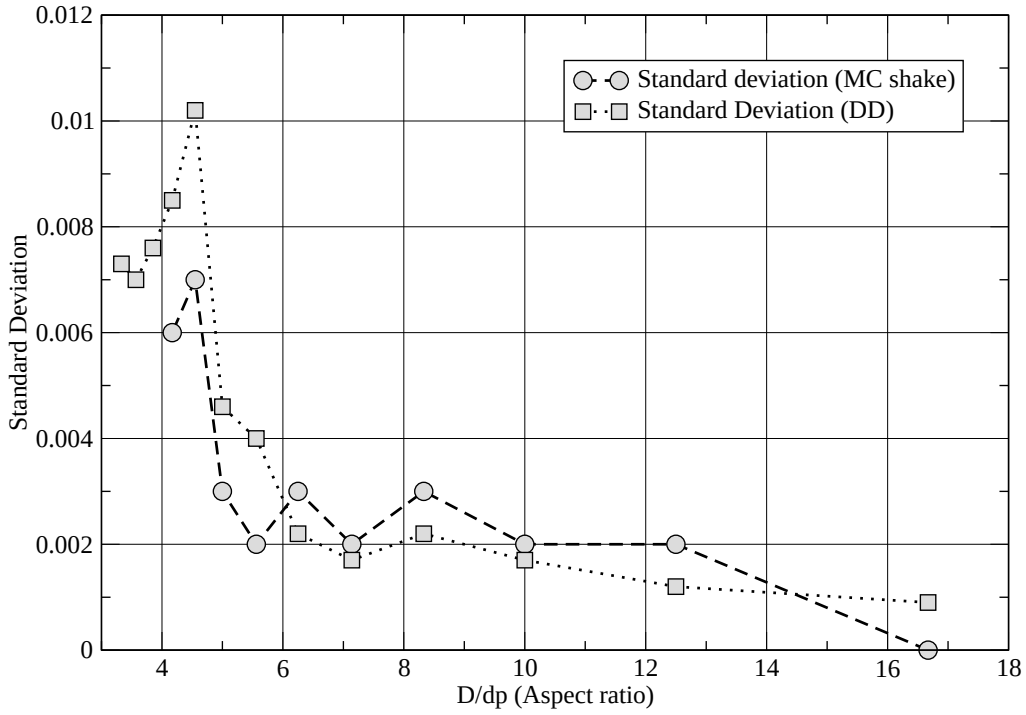

Figure 7.3: Standard deviation of porosity for packed beds

obtained in the previous chapters, means that it would be a waste not to derive some sort of correlation and compare it to the experimental data of other researchers.

Here the data is presented in the form of a modified dimensionless pressure drop (modified friction factor) as defined by Eisfeld & Schnitzlein (2001); Ergun (1952) as

$$\phi' = \frac{\phi\varepsilon^3}{(1-\varepsilon)} \tag{7.7}$$

This is necessary when comparing bed of different porosities as the dimensionless pressure drop and particle Reynolds number do not take into account the bed porosity. Figure 7.4 shows all the data presented in this thesis as modified dimensionless pressure drop as a function of the particle Reynolds number. A least squares regression is fitted to figure 7.4 to give

$$f(x) = 15.4Re_{dp}^{-0.332} \tag{7.8}$$

and hence becomes

$$\frac{\phi\varepsilon^3}{(1-\varepsilon)} = 15.4\left[Re'_{dp}(1-\varepsilon)\right]^{-0.332} \tag{7.9}$$

where 15.4 is an empirical coefficient of some other variables. Substituting in the particle Reynolds number, given as

$$Re_{dp} = \frac{\rho U d_p}{\mu} \tag{7.10}$$

yields

$$\frac{\phi\varepsilon^3}{(1-\varepsilon)} = 15.4\left[\frac{\rho U d_p}{\mu}(1-\varepsilon)\right]^{-0.332} \tag{7.11}$$

re-arranging for ϕ

$$\phi = 15.4\left[\frac{\rho U d_p}{\mu}(1-\varepsilon)\right]^{-0.332}\frac{(1-\varepsilon)}{\varepsilon^3} \tag{7.12}$$

We know from previous correlations that pressure drop through any packed bed is heavily dependant on the porosity. In addition we know dimensionless pressure

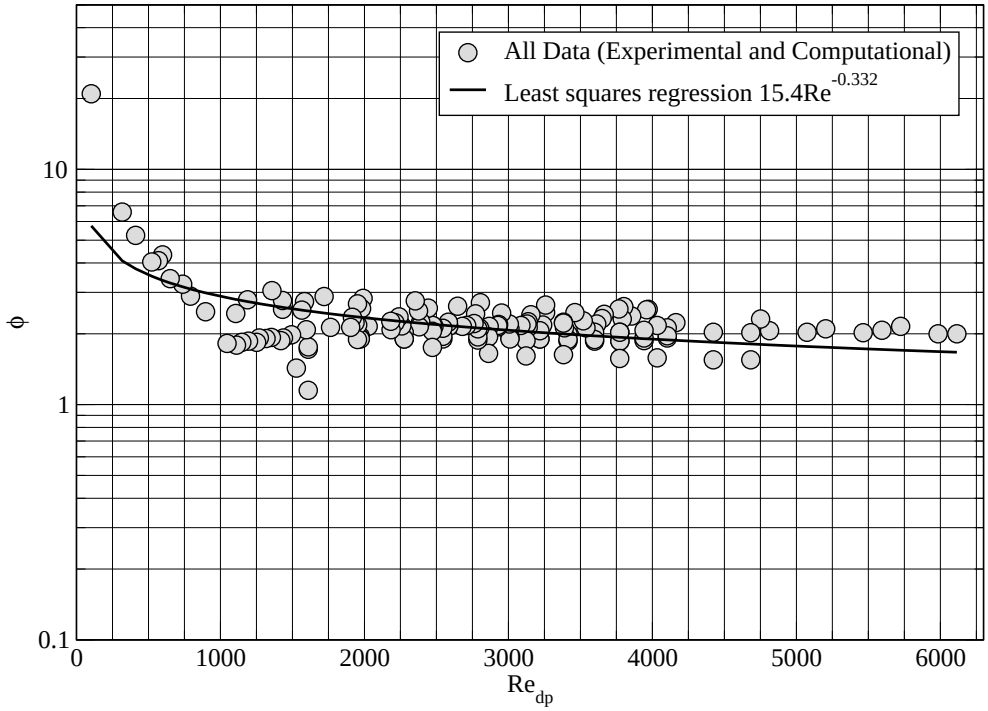

Figure 7.4: All dimensionless pressure drop data presented in this thesis as a function of particle Reynolds number

drop is given in the form

$$\phi = \frac{\Delta P d_p}{L \rho U^2} \tag{7.13}$$

re-arranging for $\Delta P/L$

$$\frac{\Delta P}{L} = \frac{\rho U^2 \phi}{d_p} \tag{7.14}$$

substituting for ϕ gives

$$\frac{\Delta P}{L} = 15.4 \left[\frac{\rho U d_p}{\mu} (1 - \varepsilon) \right]^{-0.332} \frac{\rho U^2 (1 - \varepsilon)}{\varepsilon^3 d_p} \tag{7.15}$$

We also have the result that the porosity can be defined as

$$\varepsilon = 0.6 \left(\frac{D}{d_p} \right)^{-0.16} \tag{7.16}$$

which can be used to define porosity in the equation without relying on an experimental value, which in some cases can be limiting and time consuming.

Here we do not necessarily expect the previous data to fit with absolute precision as we know that there is no formulation that can describe every individual case. Moreover, much of the data in this regression is formed around pseudo-packed beds with issues in respect to geometric fidelity regarding contact points. We also know that the described equations do not take into account bed tortuosity and therefore neglects the heterogeneous flow paths through the bed. The proposed correlation to describe dimensionless pressure drop is plotted alongside the correlation of Eisfeld & Schnitzlein (2001) selected because of its applicability to wide ranges of Reynolds numbers and aspect ratios. In addition the correlation is plotted alongside the experimental data of Reichelt (1972) due to closeness of aspect ratios studies ($3.32 < A_{ratio} < 14.32$) and encompassing a suitable range of Reynolds numbers ($74 < Re < 5463$).

Results are shown to match closely with both the correlation of Eisfeld & Schnitzlein (2001) and the experimental data of Reichelt (1972). The results deviate as a function of the Reynolds number diverging away from the correlation of Eisfeld & Schnitzlein (2001). It is plausible that this is due to the vast range of Reynolds numbers the correlation of Eisfeld & Schnitzlein (2001) has been fitted

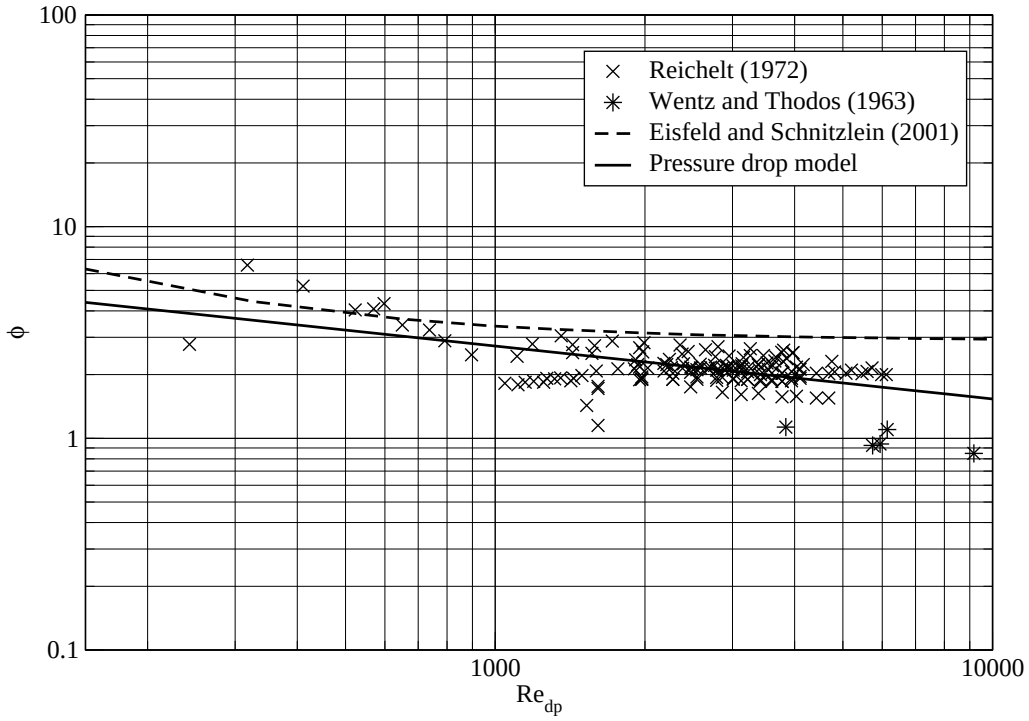

Figure 7.5: Proposed dimensionless pressure drop model compared with the experimental data of Reichelt (1972)

to and the fairly narrow specific range fitted in this study ($102 < Re_{dp} < 6114$).

7.4 Conclusions

This Thesis has investigated traditional and novel methods for generating random disordered beds for analysis using computational fluid dynamics. Chapter 4 has demonstrated how a Monte-Carlo algorithm employed by the code MacroPac can be used to generate coordinate locations for random-disordered beds of particles. This coupled with traditional CAD based geometry definition and meshing has been shown to replicate beds of spheres with a good deal of accuracy. However, the technique is not robust, and creating a suitable domain for analysis can often be tortuous and time consuming with considerable user intervention. Once a workable mesh has been created it is often of dubious quality containing a number of highly degenerate elements ultimately compromising the computational stability. Fluent has shown to ameliorate the the skewness phenomena to an extent, by a skewness correction from the PISO algorithm and by converting skewed elements to polyhedra, but does not completely eliminate the problem. Including the skewness correction in the PISO loop increases the computational run-time considerably as the correction is applied to all elements whether they are degenerate or not. Despite all the disadvantages of this approach, such as meshing robustness, the method still provides us with good results in most cases when comparing the computational data with the experimental equivalent beds. Both computational and empirical results compare well with the correlation of Eisfeld & Schnitzlein (2001) and have paved the way for the creation of more advanced meshing algorithms which can deal with highly complex curved geometries.

Chapter 5 has demonstrated that actual physical packed beds can be recreated with some accuracy using non-invasive methods (MRI) coupled with image based meshing. The image based meshing technique makes the replication of the complex geometries for analysis considerably more viable without considerable user intervention and tortuosity associated with traditional CAD based approaches. Unlike the CAD based approach the technique allows robust meshing with considerably fewer degenerate elements, without major simplification of the geometry. This method has shown to replicate the beds with a good degree of accuracy,

but is heavily limited by the scan resolution and the presence of magnetic susceptibility induced artifacts causing particles to neck at the contact points. The voxelisation used in the image based meshing approach also causes slight particle necking, but this affect is so minimal it is absorbed by the necking caused by the relatively coarse scan resolution. The effect of the necking phenomena, compared to representing the contact points using highly degenerate elements (Chapter 4) is arguable. Even so, it is possible that these effects are having a minimal effect on the pressure drop as the phenomena is fairly limited to areas of relative flow stagnation, thus it may be compromising the local flow phenomena. Considering these effects both experimental and computational results compare well with each other and show good agreement with the correlation of Eisfeld & Schnitzlein (2001) and Reichelt (1972).

Considering the phenomena discovered in Chapters 4 and 5 concerning the creation of a geometrically faithful geometry and robustness issues, Chapter 6 has shown how 100% geometrically faithful beds can be created using a blend of methods described in Chapters 4 and 5. MacroPac is used to generate a random coordinate location for each particle. A tertiary program written in C is used to create an STL file of spheres from the coordinate locations. Image based meshing has been shown to be robust in meshing highly curved, disordered geometries and in this case is used to recreate the geometry from the STL using ScanCAD, ScanIP and ScanFE. The slight necking phenomena associated with the image based meshing approach is used as an advantage to produce a statically stable structure suitable for manufacture using rapid prototyping. CFD results compared with empirical data have shown to be the most accurate of all the results presented in this thesis and compare well with the correlation of Eisfeld & Schnitzlein (2001).

With the three computational processes and methodologies described in Chapters 4, 5 and 6 a significant data set has been produced of over 200 data points to describe dimensionless pressure drop. In all cases the results obtained using CFD have shown to diverge away from the experimental as a function of the Reynolds number as the pressure drop increases. A reasonable assumption could be to assume that this is an effect of geometric fidelity issues, but this phenomena can still be observed when a geometrically faithful bed is analysed, which leads to the

assumption the uncertainty is systematic. The experimental method has been proved and unchanged for decades and is based on the successful experiments of Tóbis (2000) so is an unlikely candidate for the cause of the uncertainty. In addition, experimental uncertainty is likely to offset the data in contrast to affecting the gradient of pressure drop per unit length, $\Delta P/L$. The most likely cause of this uncertainty is from the computational modelling. We know that most complications arise due to turbulence and how it is modelled. We also that most turbulence models are grossly simplified and based on dimensional assumptions. In the work the k-ω SST model was used to model turbulence. It is a relatively low Reynolds turbulence model which benefits from the treating the free-stream flow as a standard k-ε and near wall region as k-ω. We have discussed in Chapter 2 the difficulties of modelling turbulence reinforced by George. E. Box's quote "All turbulence models are wrong", so we must ask ourselves the question 'is the k-ω model giving a realistic representation of the turbulence effects?'. The k-ω SST model has damping in place to restrict the production of turbulent kinetic energy which may be causing the results to diverge. In addition, the effect of skewed elements and the node location in regard to the face centres can cause unrealistic face values in regard to magnitude and direction which may damp out some of the turbulent effects. Furthermore, the RANS modelling technique treats all unsteady behavior as turbulence, we know that deterministic unsteady phenomena can occur behind bluff bodies end up being modelled as if they were true stochastic turbulence. In regard to the k-ω SST model itself, it relies on an array of empirical coefficients which were determined in on a variety of flows, not inclusive of geometries as complex as packed beds.

Turbulence models usually have simplifying assumptions (based on Reynolds number, lenght scales, geometry etc) and we have discussed that 'there is no generic turbulence model' that can be successfully applied to every case. Due to this, it is usually paramount that the most appropriate turbulence model is applied to each specific case in order to yield best results. To date, there is no credible turbulence model specific to packed beds. This is most probably due to the random unstructured nature of packed beds and the varying length scales and reynolds numbers that can be observed. However, in the case of random unstructured, highly tortuous geometries such as packed beds, it is likely that

the turbulence itself is having little effect on the desired studied property, $\Delta P/L$. In which case, packed beds are relatively insensitive to the choice of turbulence model and in many cases it may be advantageous to ommit the turbulence model all together.

There is conflicting evidence regarding the effect of particle roughness and this is suggested by Eisfeld & Schnitzlein (2001) to most likely to be attributed to a 'misinterpretation of data'. We know that the internal structure of the packed bed is the most important factor which concerns pressure drop. To recreate an exact empirical geometry every time is virtually impossible even with the same parameters of porosity, aspect ratio, bed length. This effect is probably what lead researchers to find conflicting evidence for and against the effect of particle roughness. However, this still does not answer the question 'Does particle roughness have an effect on the pressure drop'. With the technique described in this thesis using additive layer manufacturing (Chapter 6), further work could include the creation of maybe ten or so beds of the same parameters, but with different particle roughness to be analysed using traditional empirical methods and in parallel analysed using CFD. As a result of this it is hoped that the conflicting evidence regarding particle roughness can be resolved and put the minds of many researchers (many posthumously) at rest.

This work has shown that the FV technique is both robust and accurate in determining pressure drop through a packed bed. Results in all studies have correlated well with both the formulas of Eisfeld & Schnitzlein (2001) and empirical data from previous researchers. The technique has shown to have an advantage over empiricism in respect to cost, man hours and the amount of data which can be extracted.

Using all the dimensionless pressure drop data produced in this work a semi-empirical formula has been produced from computational and empirical studies. It is shown to correlate well with the correlation proposed by Eisfeld & Schnitzlein (2001) and data of Reichelt (1972). Further work may include the use of genetic algorithms applied to the data set to tease out relationships regarding the geometric parameter of most influence.

Are we at the stage where we should be comparing empirical data to computational in contrast to computational with empirism? Is empiricism dead? Will

'wind tunnels become cabinets for computers'? Although the Author is not an empirical purest, we are still decades away from being able to realistically model a complete stochastic turbulent flow, in a complex media. With todays computer limitations, coupled with uncertainties associated with turbulence and complex geometric domains, computational data is still best reinforced with empiricism.

Calis *et al.* (2001) anticipated that within five years packed beds containing a few hundred particles would be considered a 'standard' problem in terms of memory and calculation time requirements. Here it has been demonstrated that the memory and calculation time are now not the issue but more so, how these beds of particles can be accurately replicated in the form of a computational domain. With the postulation of Calis *et al.* (2001) satisfied, computers are becoming ever increasingly powerful, we anticipate that within a few more years it is likely that much larger beds of more than a thousand particles could be analysed in this way.

References

Al-Jahmany, Y.Y., Brenner, G. & Brunn, P.O. (2009). Simulation of the flow in a packed-bed with and without a static mixer by using cfd technique. *World Academy of Science, Engineering and Technology*, **53**, 875–880. 59

Alliez, P., Cohen-Steiner, D., Yvinec, M. & Desbrun, M. (2005). Variational tetrahedral meshing. *ACM Transactions on Graphics (Special issue on proceedings of SIGGRAPH)*, **24**, 617 – 625. 136

Andrade, J.S., Almeida, M.P., Filho, J.M., Havlin, S. & Stanley, B.S.H.E. (1997). Fluid flow through porous media: the role of stagnant zones. *Phys.Rev.Lett.*, **79**, 3901 – 3904. 114

Antiga, L., Ene-Iordache, B., Caverni, L., Cornalba, G.P. & Remuzzi, A. (2002). Geometric reconstruction for computational mesh generation of arterial bifurcations from ct angiography. *Computerized Medical Imaging and Graphics*, **26**, 227 – 235. 62

Aris, R. (1957). On shape factors for irregular particles - i the steady state problem. diffusion and reaction. *Chemical Engineering Science*, **16**, 262 – 268. 11

Ashcombe, F. (1973). Graphs in statistical analysis. *American Statistician*, **27**, 17 – 21. 109

Aste, T., Saadatfar, M., Sakellariou, A. & Senden, T.J. (2004). Investigating the geometric structure of disordered sphere packing. *Physica. A*, **339**, 16 – 23. 52

Atmakidis, T. & Kenig, E.Y. (2009). Cfd-based analysis of of the wall effect on the pressure drop in packed beds with moderate tube/particle diamter ratios in the laminar flow region. *Chem.Eng.J*, **155**, 404 – 410. 50, 51, 85, 89, 96

Azzam, M.I.S. & Dullien, F.A.C. (1976). Calculation of permeability of porous media from the navier-stokes equations. *Ind.Eng.Chem.Fund*, **15**, 281 – 285. 72

Baker, M.J. & Tabor, G.R. (2010). Computational analysis of transitional airflow through packed columns of spheres using the finite volume technique. *Computers and Chemical Engineering*, **34**, 878 – 885. 47, 84, 125, 151, 152

Baker, M.J., Young, P.G. & Tabor, G.R. (2011). Imaged based meshing of packed beds of cylinders at low aspect ratios using 3d mri coupled with computational fluid dynamics. 152

Bear, J. (1972). *Dynamics of Fluids in Porous Media*. American Elsevier Publishing Company. 25

Beavers, G.S., Sparrow, E.M. & Rodenz, D.E. (1973). Influence of bed size on the flow characteristics and porosity of randomly packed beds of spheres. *Trans. ASME J. Appl. Mech*, **30**. 174, 177, 178

Bird, R.B., Stewart, W.E. & Lightfoot, E.N. (1960). *Transport phenomena*. Wiley. 33, 34

Blake, F.C. (1922). The resistance of packing to fluid flow. *Transactions of American Istitute of Chemical Engineers*, **14**, 415 – 421. 32, 33, 34, 157

Bousinesq, J. (1877). Essai sur la theorie des eaux courantys. *Mem.Pres. par div savants l'academie Sci., Paris*, **23**, 1 – 680. 77

Bradshaw, P. (1994). Turbulence: the chief outsatnding difficulty with our subject. *Exp.Fluids*, **16**, 203 – 216. 72

Brinkman, H.C. (1947). A calculation of viscous force exerted by a flowing fluid on a dense swarm of particles. *Appl.Sci.Res*, **1**, 27 – 33. 32

Burke, S.P. & Plummer, W.B. (1928). ?? *Industrial Engineering Chemistry*, **20**. 34, 35, 36, 156, 157

Calis, H.P.A., Nijenhuis, J., Paikert, B.C., Dautzenberg, F.M. & van den Bleek, C.M. (2001). Cfd modelling and experimental validation of pressure drop and flow profile in a novel structured catalytic reactor packing. *Chem.Eng.Sci.*, **56**, 1713 – 1720. 22, 48, 192

Callaghan., P. (1994). *Principles of Nuclear Magnetic Resonance Microscopy*. Oxford University Press, Oxford. 52

Carman, P.C. (1937). Fluid flow through a granular bed. *Trans.Inst.Chem.Eng.London*, **15**, 150 – 156. 33, 34, 35, 156, 157, 182

Carman, P.C. (1938). ?? *Journal of Society of Chemical Industry*, **57**, 225. 33, 51

Caulkin, R., Ahmad, A., Fairweather, M., Jia, X. & Williams, R. (2007). An investigation of sphere packed shell-side columns using a digital packing algorythm. *Computers and Chemical Engineering*, **31**, 1715 – 1724. 49, 151

Caulkin, R., Jia, X., Fairwather, M. & Williams, R. (2008). Lattic approaches to packed column simulations. *Particuology*, **6**, 404 – 411. 49

Caulkin, R., Ahmed, A., Fairweather, M., Jia, X. & Williams, R.A. (2009). Digital preditions of complex cylinder packed columns. *Computers and Chemical Engineering*, **33**, 10 – 21. 151

Cavendish, J.C., Field, D.A. & Fry, W.H. (1985). An approach to automatic three-dimnesional finite element generation. *Int.J.Numer.Methods Eng*, **21**, 329 – 347. 68

Cebral, J.R. & Loehner, R. (2001). From medical images to anotomically accurate finite element grids. *Int.J.Numer.Methods.Eng*, **51**, 986 – 1008. 62

Cengel, Y.A. & Cimbala, J.M. (2006). *Fluid Mechanics; Fundamentals and Applications*. McGraw Hill. 22, 67, 71, 73, 87, 97, 102, 148, 162

Choi, Y.S., Kim, S.J. & Kim, D. (2008). A semi-empirical correlation for pressure drop in packed beds of spherical particles. *Transp Porous Med*. 35, 36, 38, 178

Clough, R.W. (1960). The finite element method in plane stress analysis. In *A.S.C.E. Structural Division, Pittsburgh, Pennsylvania*. 58

Collins, T.P., Tabor, G.R. & Young, P.G. (2007). A computational fluid dynamics study of inspiratory flow in orotracheal geometries. *Med.Biol.Eng.Comput*, **45**, 829 – 836. 128

Courant, R. (1943). Variational methods for the solution of problems of equilibrium and virbations. *American Mathematical Society*, **49**, 1 – 23. 58

Dalman, M.T., Merkin, J.H. & McGreavy, C. (1986). Fluid flow and heat transfer past two spheres in a cylindrical tube. *Computers and fluids*, **14**, 267 – 281. 13, 42, 43, 85, 89, 136, 170

Darcy, H. (1856). Determination des lois d'ecoulement de l'eau travers le sable. *In Les Fontaines Publiques de la Ville de Dijon*, **85**, 590 – 594. 31, 32, 182

de Klerk, A. (2003). Voidage variation in packed beds at small column to particle diameter ratios. *AICheJ*, **49**, 2022 – 2029. 16, 174, 177, 180

Delaunay, B. (1934). Sur la sphere vide, izvestia akademii nauk sssr. *Otdelenie Matematicheskikh i Estestvennykh Nauk*, **7**, 793 – 800. 63

Delele, M.A., Tijskens, E., Atalay, Y.T., Ho, Q.T., Ramon, H., Nicolai, B.M. & Verboven, P. (2008). Combined discrete element cfd modelling of airflow through random stacking of horticulatural products in vented boxes. *Journal of Food Engineering*, **89**, 33 – 41. 13, 42

Derx, O.R. & Dixon, A.G. (1996). Determination of the fixed bed wall heat transfer coefficient using computational fluid dynamics. *Heat Transfer Part A*, **29**, 777 – 749. 43

DiFelice, R. & Gibilaro, L.G. (2004). Wall effects for the pressure drop in fixed beds. *Chem.Eng.Sci.*, **59**, 3037 – 3040. 110, 126

Dixon, A.G. (1988). Correlations for the wall and particle shape effects on fixed bed voidage. *Canadian Chemical Engineering*, **66**, 705 – 708. 16, 174, 177

Dixon, A.G. & Nijemeisland, M. (2002). Cfd as a design tool for fixed bed reactors. *Ind.Eng.Chem.Res*, **40**, 5246 – 5254. 43

Douglas, J.F., Gasiorek, J.M., Swaffield, J.A. & Jack, L.B. (2005). *Fluid Mechanics*. Pearson, Prentice Hall. 71

Drazin, P. & Riley, N. (2006). The navier-stokes equations; a classification of flows and exact solutions. *London Mathemitical Society Lecture Note Series*, **334**, 1 – 19. 70, 71

du Toit, C.G. (2008). Radial variation in porosity in annular packed beds. *Nuclear Engineering and Design*, **238**, 3073 – 3079. 110

Dullen, F.A.L. (1992). *Porous Media: Fluid Transport and Pore Structur*. Academic Press inc. 31

Dullien, F.A.L. (1979). *Porous Media: Fluid Transport and Flow Structure*. Academic Press, New York. 156

Eisfeld, B. & Schnitzlein, K. (2001). The influence of confining walls on the pressure drop in packed beds. *Chem.Eng.Sci.*, **56**, 4321 – 4329. iii, viii, x, 6, 8, 25, 28, 37, 38, 47, 54, 85, 105, 109, 110, 119, 120, 123, 146, 148, 156, 157, 158, 165, 170, 175, 177, 182, 184, 186, 188, 189, 191

Ergun, S. (1952). Flow through packed columns. *Chem.Eng.Prog.*, **48**, 89. 34, 35, 38, 51, 184

Ergun, S. & Orning, A. (1949). Fluid flow through randomly packed columns and fluidised beds. *Ind.Eng.Chem*, **41**, 1179 – 1184. 36, 156, 182

Evans, K.E. (1988). The packing of thick fibres. *J.Phys.D:Appl.Phys.*, **22**, 354 – 360. 49

Fand, R.M., Kim, B.Y.K., Lam, A.C.C. & Phan, R.T. (1972). Druckverlust in kugelschttungen. *Brennstoff-Warme-Kraft*, **24**, 233–236. 156

Ferziger, J.H. & Perić, M. (1996). *Computational Methods for Fluid Dynamics*. Springer. 72, 73

Foscolo, P.U., Gibalaro, L.G. & Waldron, S.P. (1983). A unified model to for particulate expansion of fluidized beds and flow in fixed porous media. *Chem.Eng.Sci*, **38**, 1251 – 1260. 38

Foumeny, E.A., Benyahia, F., Castro, J.A.A., Moallemi, H.A. & Roshani, S. (1993). Correlations of pressure drop in packed beds taking into account the effect of confining wall. *Int.J.Heat Mass Trans*, **36**, 536–540. 18, 28, 35, 38, 45, 114

Freund, H., Bauer, J. & Zeiser, T. (2005). Detailed simulation of transport processes in fixed beds. *Ind.Eng. Chem. Res*, **44**, 6423 – 6434. 45

Fried, E. & Idelchik, I.E. (1989). *Flow resistance: Adesign guide for Engineers*. Hemisphere Pub. Corp. 38

Gibilaro, R.D.F.L.D. (2004). Wall effects for the pressure drop in packed beds. *Chemical Engineering Science*, **59**, 3037 – 3040. 36

Giese, M., Rottschaffer, K. & Vortmeyer, D. (1998). Measured and modeled superficial flow profiles in packed beds with liquid flow. *AIChEJ*, **44**, 484 – 491. 23, 175

Goodling, J.S., Vacheon, R.I., Stelpfug, W.S. & Ling, S.J. (1983). Radial porosity distributions in cylindrical beds packed with spheres. *Powder Technology*, **35**, 23 – 29. 110

Gotz, J., Zick, K. & heinen adn T. Konig, C. (2002). Visualisation of flow processes in packed beds with nmr imaging: Determination of the local porosity, velocity vector and local dispersion coefficients. *Chemical Engineering and Processing*, **41**, 611 – 629. 23, 176

Guardo, A. (2007). *Computational Fluid Dynamics Studies in Heat and Mass Transfer Phenomena in Packed beds Reaction and Extraction Equipment: Special attention to supercritical Fluids Technology*. Ph.D. thesis, Universitat Politecnica de Catalunya. 45, 52, 57, 58, 85

Guardo, A., Coussirat, M., Larrayoz, M., Recasens, F. & Egusquiza, E. (2007). Influence of the turbulence model in cfd modeling of wall-to-fluid heat transfer in packed beds. *Chem.Eng.Sci*, **60**. 44, 45

Gunjal, P.R., Ranade, V.V. & Chaudhari, R.V. (2005). Computational study of a single-phase flow in packed beds of spheres. *A.I.Ch.E Journal*, **20**, 365–378. 48

Gupte, A. (1970). *Experimentelle Untersuchung der Einflsse von Porositt und Korngrenverteilung im Widerstandsgesetz der Porenstrmung*. Ph.D. thesis, Universitat of Karlshruhe. 157

Handley, D. & Heggs, P.J. (1968). Momentum and heat transfer in regularly shaped packing. *Trans. Inst. Chem. Eng*, **46**, 251 – 264. 35, 38

Hassan, Y.A. (2008). Large eddy simulation in pebble bed gas cooled core reactors. 23, 47

Hassanizadeh, S.M. & Gray, W.G. (1987). High velocity flow in porous media. *Transport in Porous Media*, **2**, 521 – 531. 29

Hellström, J.G.I. & Lundström, T.S. (2006). Flow through porous media at moderate reynolds number. In *International Scientific Colloquium: Modelling for Material Processing, Riga, June 8-9*. 48, 89

Herman., G.T. (2009). *Fundamentals of computerized tomography: Image reconstruction from projection*. Springer, London. 52

Hess, J.L. & Smith, A.M.O. (1967). Calculation of potential flow about arbitrary bodies. *Progress in Aeronautics Sciences*, **8**, 1 – 138. 58

Hicks, R.E. (1970). Pressure drop in packed beds of spheres. *Industrial and Engineering Chemistry Fundamentals*, **9**, 500 – 502. 35

Jafari, A., Zamankhan, P., Mousavi, S.M. & Pietrinen, K. (2008). Modeling and cfd simulation of flow behavior and disperivity through randomly pacvked bed reactors. *Chem.Eng.J*, **155**, 476 – 482. 50, 85

Jeschar, R. (1964). Druckverlust in mehrkornschuttungen aus kugeln. *Arch. Eisenhiitenw*, **35**, 1155 – 1159. 16, 127, 174, 177, 178

Johns, M.L., Sederman, A.J., Bramley, A.S., Gladden, L.F. & Alexander, P. (2000). Local transitions in flow phenomena through packed beds identified by mri. *AIChE Journal*, **11**, 1251 – 2161. 53, 131

Johnson, E.A.C. & Young, P.G. (2005). On the use of a patient-specific rapid prototyped model to simulate the response of the human head to impact and comparison with analytical and finite element models. *J. Biomech.*, **38**, 39 – 46. 129

Kozeny, G. & Sitzber, J. (1927). Ober kapillare Leitung das Wassers im Boden. *Akad. Wiss, Wein, Math-naturw K1.*, **136**, 271. 33, 34, 36

Kuwahara, F., Yamane, T. & Nakayama, A. (2006). Large eddy simulation of turbulent flow in porous media. *International Communications in Heat and Mass Transfer*, **33**, 411 – 418. 76

Landahl, M.T. & Mollo-Christensen, E. (1986). *Turbulence and Random Processes in Fluid Mechanics*. Cambridge University Press, Cambridge. 20, 77

Leland, R.W., Melander, D.J., Meyers, R.W., Mitchell, S.A. & Tautages, T.J. (1998). The geode algorithm: Combining hex/tet plastering, dicing and transition elements for automatic, all-hex mesh generation. In *Seventh International Meshing Roundatable (Dearborn, Mitchigan)*, 515 – 521. 136

Leva, M. (1959). *Fluidisation*. McGraw-Hill Book Company, New York. 35, 37

Leva, M., Weintraub, M., Grummer, M. & Storch, H.H. (1951). Fluid flow through packed and fluidized systems. Tech. Rep. 504, Bureau of Mines. 156, 157, 175

Lien, F.S. & Leschziner, M.A. (1994). Assessment of turbulence transport models including non-linear rng eddy viscosity formulations and second-moment closure for flow over a backward-facing step. *Computers Fluids*, **23**, 983 – 1004. 21

Lloyd, B. & Boehm, R. (1994). Flow and heat transfer around a linear array of spheres. *Numer Heat Transfer part A*, **26**, 237 – 252. 13, 43, 85

Logtenberg, S.A. & Dixon, A.G. (1998). Computational fluid dynamics of fixed bed heat transfer. *Chemical Engineering Process*, **37**, 7 – 21. 43, 85, 96

Logtenberg, S.A., Nijemeisland, M. & Dixon, A.G. (1999). Computational fluid dynamics simulations of fluid flow and heat transfer at the wall-particle contact points in a fixed bed reactor. *Chemical Engineering Science*, **54**, 2433 – 2439. 13, 43

MacDonald, T.F., El-Sayer, M.S., Mow, K. & Dullen, F.A.L. (1979). Flow through porous media: The ergun equation revisited. *Industrial and Engineering Chemistry Fundamentals*, **18**, 199–208. 35, 38

Magnico, P. (2003). Hydrodynamic and transport properties of packed beds in small tube-to-sphere diameter ratio: pore scale simulation using an eulerian and a lagrangian approach. *Chem.Eng.Sci.*, **58**, 5005 – 5024. 50

Manjhi, N., Verma, N., Salem, K. & Mewes, D. (2006). Simulation of 3d velocity and concentration profiles in a packed bed adsorber by lattice boltzmann methods. *Chem.Eng.Sci.*, **61**, 7754 – 7765. 45

Mantle, M.D., Sederman, A.J. & Gladden, L.F. (2001). Single and two-phase flow in fixed bed reactors: Mri flow visualisation and lattice-boltmann simulations. *Chemical Engineering Science*, **56**, 523 – 529. 16, 110

Manz, B., Warren, P.B. & Gladden, L.F. (1999). Flow and dispersion in porous media: Lattice boltzmann and nmr studies. *A.I.Ch.E Journal*, **45**, 1845 – 1854. 7, 53, 123

Martin, H. (1978). Low peclet number particle to fluid heat and mass transfer in packed beds. *Chem.Eng.Sci*, **33**, 913 – 919. 17, 36, 110, 180

McGraw-Hill (2003). Dictionary. 6

McGreavy, C., Foumeny, E.A. & Javed, K.H. (1986). Characterization of transport properties of for fixed beds in terms of local bed structure and flow distribution. *Chem.Eng.Sci*, **41**, 787 – 797. 22

M.C.Thadani & Peebles, F.N. (1966). Variation of local void fraction in mixed packings. randomly packed beds of equal spheres. *Ind.Eng.Process.Des.Dev*, **5**, 265 – 268. 176

Mehta, D. & Hawley, M.C. (1969). Wall effect in packed columns. *IE and C Proceedings of Design and Developement*, **8**, 280 – 282. 18, 27, 38, 118

Menter, F. (1993). Zonal two equation $k - \omega$ model for aerodynamic flows. AIAA Journal 1993-2906. 79, 80, 81, 139

Menter, F. (1994). Two-equation eddy-viscosity turbulence models for engineering applications. *AIAA Journal*, **32**, 1598 – 1605. 84

Menter, F., Kuntz, M. & Langtree, R. (2003). Ten years of industrial experience with the sst turbulence model. Turbulence, Heat and Mass Transfer 4. 80, 81, 82, 118

Middleman, S. (1998). *An introduction to fluid dynamics*. John Wiley and Sons Inc. 33

Morais, A.F., Seybold, H., Herrmann, H.J. & Andrade, J. (1970). Non-newtonian fluid flow through three-dimensional discordered porous media. *A.I.Ch.E*, **16**, 1092 – 1093. 73

Narataruksa, P., Pana-Suppamassadu, K., Kokoo, S.T.R. & Jiamrittiwong, P. (2004). Comparative study of lattice-boltzmann and finite volume methods for the simulation of laminar flow through a 4:1 planar contraction. *International Journal for Numerical Methods in Fluids*, **46**, 903–920. 46, 47

Navier, C.L. (1827). Memoire sur leslois du movement des fluides (1822). *Acad.Sci.Inst. Fance 2*, **6**, 389 – 440. 71

Neale, G. & Nader, G. (1974). Practical significance of brinkman's extension of darcy's law: coupled parallel flows within a channel and a porous medium. *Can.J.Chem.Eng*, **52**, 470 – 478. 32

Nguyen, N.L., van Buren, V., Reimert, R. & von Garnier, A. (2005). Determination of porosity and flow distribution in packed beds by magnetic resonance imaging. *Magnetic Resonance Imaging*, **23**, 395 – 396. 16, 126

Nourgaliev, R.R., Dinh, T.N., Theofanous, T.G. & Joseph, D. (2003). The lattice boltzmann equation method: theoretical interpretation, numerics and implications. *International Journal of Multiphase Flow*, **29**, 117–169. 58

O'Neill, K. & Benyahia, F. (1997). Packed bed systems: An insight into a more flexible design. In *IChemE Research Event/The Jubilee Research Event*, 1252 – 1256. 38

Pan, C., Luo, L.S. & Miller, C.T. (2006). An evaluation of lattice Boltzmann schemes for porous medium flow simulation. *Computers & Fluids*, **35**, 898 – 909. 49

Plessis, P.J.D. & Woudberg, S. (2008). Pore-scale derivation of the ergun equation to enhance its adaptability and geralization. *Chem.Eng.Sci.*, **63**, 2576–2586. 35

Poisson, S.D. (1831). Memoire sur les equations generales de l'equilibre et du movement des corps solides elastiques et des fluides. *J.Ec.Polytech*, **18**, 1 – 174. 71

Rehder, J.E. (1990). Pressure drop in air flow through beds of charcoal. *Archaeomaterials*, **4**, 105 – 109. 35

Reichelt, W. (1972). Zur berechnung des druckverlustes einphasig durchstromter kugel- und zylinderschuttengen. *Chemie-Ingenieur-Technik*, **44**, 1068 – 1071. iii, xi, 36, 37, 38, 47, 51, 85, 110, 119, 123, 146, 157, 182, 186, 187, 189, 191

Ren, X., Stapf, S. & Blumich, B. (2005). Magnetic resonance visualisation of flow and pore structure in packed beds with low aspect ratio. *Chem. Eng. Technol*, **28**, 219 – 225. 53

Reynolds, O. (1883). An experimental investigation of the circumstances which determine whether the motion of water shall be direct or sinous, and of the law of the resistance in parallel channels. *J.Phil.Soc.Trans*, 935 – 982. 19, 20, 21

Richard, P., Phillipe, P., Fabrice, B., Bourles, S., Thibault, X. & Bideau, D. (2003). Analysis by x-ray microtomography of a granular packing undergoing compaction. *Phy.Rev.E*, **68**, 0203011–1020301/4. 52

Richardson, L.F. (1910). The approximate arithmetical solution by finite differences of physical problems involving differential equations, with application of stresses in a masonary dam. *Philosophilical Transactions of the Royal Society*. 58

Ritz, W. (1910). Uber eine methode zur losung gewisser variationsprobleme der mathematischen. *Zeitschrift fur Angewandte Mathematik und Mechanik*, **35**, 1 – 61. 58

Rogers, G.F.C. & Mayhew, Y.R. (1982). *Thermodynamic and Transport Properties of Fluids: SI Units*. Oxford Basil Blackwell, Oxford. 89

Rowe, R.C., Yourk, P., Clobourn, E.A. & Roskilly, S.J. (2005). The influence of pellet size, shape and distribution on capsule filling a preliminary evaluation of three-dimensional computer simulation using a monte carlo technique. *International Journal of Pharmaceutics*, **300**, 32 – 37. 49

Rupesh, R.K. & Joshi, J.B. (2008). Cfd modelling of pressure drop and drag coefficient in fixed and expanded beds. *Chem.Eng.Res.D*, **86**, 444 – 453. 46

Saint-Venant, B. (1843). Memoire sur les dynamique des fluides. *C.R.Acad.Sci, Paris*, **18**, 1240 – 1242. 71

Scheidegger, A.E. (1960). *The Physics of Flow through Porous Media*. University of Toronto Press. 24, 104

Sederman, A.J., Alexander, P. & Gladden, L. (2001). Structure of packed beds probed by magnetic resonance imaging. *Powder Technology*, **117**, 255 – 269. 16, 110

Seidler, G.T., Martinez, G., Seeley, L.H., Kim, K.H., Behne, E.A., Zharanek, S., Chapman, B.D., Heald, S.M. & Brewe, D.L. (2000). Granule-by-granule reconstruction of a sandpile from x-ray microtomography data. *Phy.Rev.E*, **62**. 52

Sharma, S., Mantle, M.D., Gladden, L.F. & Winterbottom, J.M. (2001). Determination of bed viodage using water substitution and 3d magnetic resonance imaging, bed density and pressure drop in packed bed reactors. *Chemical Engineering Science*, **56**, 587 – 595. 7, 53, 123, 126

Shepard, M.S., Guerinoni, F., Flahery, J.E., Ludwig, R.A. & Baehmann, P.L. (1988). Finite octree mesh generation for three-dimensional flow analysis. *Numerical Grid Generation in Computational Fluid Mechanics*, **88**, 708 – 718. 63

Sissom, L.E. & Pitts, D.R. (1972). *Elements of Transport Phenomena*. McGraw-Hill, Kogakush Japan. 10

Speziale, C.G. (1991). Analytical methods for the development of reynolds-stress closures in turbulence. *Ann.Rev.Fluid Mech.*, **23**, 107 – 157. 73

Stanek, V. (1994). *Fixed bed operations - Flow distribution and efficiency*. Ellis Horwood, London. 18, 28, 114, 118

Stokes, G.G. (1845). The theories of the internal friction of fluids in motion, and of the equilibrium and mtion of elastic solids. *Trans. Cambridge Philos.Soc*, **8**, 287 – 305. 71

Stokes, G.G. (1846). Reports on recent researches in hydrodynamics. *Rep.Br.Assoc*, **8**, 1 – 20. 71

Stokes, G.G. (1880). Reports on recent researches in hydrodynamics. *Math.Phys. Papers*, **1**, 156 – 187. 71

Strigle, R.F. (1994). *Packed Tower Design and Applications: Random and Structured Packings*. Gulf Publishing Company; Houston. 33, 34

Succi, S. (2001). *The lattice-Boltzmann equation for fluid dynamics and beyond*. Oxford Science Publications, Oxford. 58

Suekane, T., Yokouchi, Y. & Hirai, S. (2003). Internal flow structures in simple packed beds of spheres. *AIChE J*, **49**, 10 – 17. 45

Sullivan, S.P., Sani, F.M., Johns, M.L. & Gladden, L.F. (2005). Simulation of packed bed reactors using lattice boltmann methods. *Chemical Engineering Science*, **60**, 3405 – 3418. 7, 53

S.V.Patankar & D.B.Spalding (1972). A calculation procedure for heat, mass and momentum transfer in 3-d parabolic flow. *Int.J.Heat.Mass.Transfer*, **15**, 1787. 69

Tabor, G., Young, P.G., Beresford-West, T. & Benattayallah, A. (2007). Mesh construction from medical imaging for multiphysics simulation : Heat transfer and fluid flow in complex geometries. *Eng. App.Comp.Fluid Mech*, **2**, 126 – 135. 52, 128

Tabor, G.R., Yeo, O., Young, P.G. & Laity, P. (2008). Cfd simulation of flow through an open-cell foam. *Int.J.Mod.Phys.C.*, **19**, 703 – 715. 50, 52, 123

Taskin, M.E. (2007). *CFD simulation of transport and reaction in cylindrical catalyst particles*. Ph.D. thesis, Worchester Polytechnic Institute, USA. 42, 59

Tennekes, H. & Lumley, H.L. (1972). *A First Course in Turbulence*. MIT Press. 72

Thom, A. (1933). The flow past circular cylinders at low speeds. *Proc. Royal Society*, **141**, 651 – 666. 58

Tóbis, J. (2000). Influence of bed geometry on its frictional resistance under turbulent flow conditions. *Chem.Eng.Sci.*, **55**, 5359 – 5366. 48, 85, 89, 104, 125, 152, 190

Tobís, J. (2008). A hybrid method of turbulent flow modelling in packings of complex geometry. *Chem.Eng.Sci.*, **63**, 2670 – 2681. 45

Tsotas, E. (2002a). Fluid flow in packed beds. *Chemical Engineering Science*, **20**, 237–246. 24, 170

Tsotas, E. (2002b). The influence of confining walls on the pressure drop in packed beds. *Chemical Engineering Science Letter*, **57**, 1827–1827. 37

van Phai, N. (1982). Automatic mesh generation with tetrahedron elements. *Int.J.Numer.Methods Eng*, **18**, 237 – 289. 62

Versteeg, H.K. & Malalasekera, W. (1995). *An introduction to Computational Fluid Dynamics : The Finite Volume Method*. Longman Scientific & Technical. 70, 78, 79, 104

Vidal, D., Roy, R. & Bertrand, F. (2010). On improving the performance of large parallel lattice boltzman flow simulations in hetrogeous porous media. *Computers and Fluids*, **39**, 324 – 337. 58, 59

Wagstaff, J.B. & Nirmaier, E.A. (1995). Airflow in beds of granular solids. *Industrial and Engineering Chemistry*, **47**, 1129 – 1135. 37

Wang, Z., Afacan, A., Nandakumar, K. & Chuang, K.T. (2001). Porosity distribution in random packed columns by gamma ray tomography. *Chemical Engineering and Processing*, **40**, 209 – 219. 126

Whitaker, S. (1996). The forcheimer equation: A theoretical development. *Transport in Porous Media*, **25**, 27 – 61. 72

White, F. (2003). *Fluid Mechanics*. McGraw Hill. 22

Wilcox, D.C. (1993). Turbulence modelling for cfd. DCW Industries Inc. La Canada, California. 80

Yevseyev, A.R., Nakoryakov, V.E. & Romanov, N.N. (1991). Experimental investigation of a turbulent filtration flow. *Int.J.Multiphase Flow*, **17**, 103 – 118. 22, 23, 170

Young, P., Beresford-West, T. & Murphy, F. (2008). Imaged based meshing and its role within computational biomechnics. In *International Biomechanics conference, University of Ottawa*. 62, 63, 64, 68

Zamankhan, P., Tynjala, T., jr, W.P., Zamankhan, P. & Sarkomaa, P. (1999). Stress fluctuations in continously sheared dense granular materials. *Phys.Rev.E*, **60**, 7149 – 7156. 50

Zavoronkov, N.M., Aerov, M.E. & Umnik, N.N. (1979). Hydraulic resistance and density of packing of a granular bed. *J.Phys.Chem*, **23**, 342 – 361. 51

Zeiser, T., P. Lammersa, E.K., Lia, Y.W., Bernsdorfc, J. & Brennera, G. (2001). Cfd-calculation of flow, dispersion and reaction in a catalyst filled tube by the lattice boltzmann method. *Chem.Eng.Sci*, **56**. 49, 152

Zeiser, T., Steven, M., Freund, H., Lammers, P., Brenner, G., Dusrt, F. & Bernsdorf, J. (2002). Analysis of the flow field and pressure drop in fixed-bed reactors with the help of Lattice Boltzmann simulations. *Phil.Trans.Roy.Soc.A: Physical and Engineering Sciences*, **360**, 507 – 520. 49

Zhang, W., Thompson, K.E., Reed, A.H. & Beenken, L. (2006). Relationship between packing structure and porosity in fixed beds of equilateral cylindrical particles. *Chem.Eng.Sci*, **61**, 8060 – 8074. 7, 54, 123, 126

Ziolkowska, I. & Ziolkowska, D. (1988). Fluid flow inside packed beds. *Chemical Engineering Process*, **23**, 137 – 164. 23, 24, 103

Zou, R.P. & Yu, A.B. (1995). The packing of spheres in a cylindrical container: the thickness effect. *Chem.Eng.Sci.*, **50**, 1504 – 1507. 16, 174, 177, 178, 180

Zunarelli, L. & Young, P.G. (1999). Analytical and numerical modelling of head injury mechanisms. Simulation and Modelling Techniques Applied to Medicine, Institute of Physics, November 2-3, London. 131